THE UNIVERSITY OF CHICAGO

UNCONVENTIONAL CONDENSATION PHENOMENA FROM SUPERCONDUCTORS TO POLARITONS

A DISSERTATION SUBMITTED TO
THE FACULTY OF THE DIVISION OF THE PHYSICAL SCIENCES
IN CANDIDACY FOR THE DEGREE OF
DOCTOR OF PHILOSOPHY

DEPARTMENT OF PHYSICS

BY
ALEX EDELMAN

CHICAGO, ILLINOIS
JUNE 2022

In memory of Krystyna Konopka

TABLE OF CONTENTS

LIST OF FIGURES

ACKNOWLEDGMENTS

I am grateful for their help in bringing this work to its conclusion to the members of my committee: Woowon Kang, Jon Simon, and Liantao Wang.

I am honored to have been part of the community of the University of Chicago Physics Department and the James Franck Institute.

It is largely thanks to Brenda Thomas that I was able to do anything at all.

For their mentorship as I got off the ground I thank Richard Brierley and Ryo Hanai.

I owe an enormous debt of gratitude to Peter Littlewood for his infinite patience, support, enthusiasm, encouragement, and belief in me.

Finally I thank my family and friends.

ABSTRACT

Systems with strongly interacting constituents can acquire macroscopic coherence and develop collective excitations at new energy scales that would be difficult to foresee from the microscopic ingredients. Bose-Einstein condensation and superconductivity are two paradigmatic examples of this kind of emergence. In this thesis I consider how these phenomena change in the presence of a cavity, broadly construed as some kind of field that is capable of mediating long-range forces across the system. I focus specifically on two examples: a kind of polariton in which strongly-interacting excitons on a lattice couple to photon field in a physical cavity, and forms a supersolid state in which the condensate coexists with spatial order; and superconductivity in strontium titanate, considered as a case in which the collective motions of the electron fluid and the lattice, respectively plasmons and optic phonons, hybridize to produce superconductivity mediated by long-range forces.

CHAPTER 1

INTRODUCTION

1.1 Introduction to this Thesis

This thesis contains a slightly diverse collection of works that are thematically unified by examining condensation in a few slightly peculiar models. In particular, while condensation phenomena have long been well-understood in terms of local interaction, here I will ask what changes in the presence of long-ranged forces. I broadly refer to this as cavity physics, since in some cases the long-ranged forces are mediated by coupling to a physical cavity while in others the model merely looks similar and the physical implications are similar. My aim in this thesis is not to reproduce the techniques and concepts that may be found in standard textbooks, but to focus on aspects of prior work that are more obscure or difficult to track down. The work is organized as follows.

This chapter, an extended version of a chapter written for (N Proukakis and Littlewood [2017]), introduces condensation phenomena in the context of a crossover from weak to strong coupling, and also serves as an introduction to both polaritons and superconductors, the systems I will deal with in later chapters. I argue here that the properties of a condensate are best deduced from its dynamics, and in the remainder of the thesis I will follow that philosophy.

Chapter 2 is an expanded version of a paper that twists the usual polariton problem by introducing strong interactions that allow the system to exhibit spatial order, including in the presence of a condensate. The model may be relevant to understanding recent experiments on polaritons in a Moiré lattice.

Chapter 3 is an expanded version of a paper that deals with a model of $SrTiO_3$ (STO), an enigmatic unconventional superconductor. This model is the starting point for many calculations of the superconducting properties of the material but I analyze its normal state

predictions and find that they are severely at odds with what can be observed experimentally.

Chapter 4 is based on unpublished work that examines the superconducting properties of this model, and variations, in more detail. As the philosophy in this introduction suggests, I find that the superconducting phase diagram alone is not a good guide to the adequacy of the theory. The work in this chapter should be regarded as laying the foundations for a more sophisticated calculation in the future.

I conclude by returning to the philosophy of cavity physics.

1.2 Introduction to the BEC-BCS Crossover

A system of two kinds of fermion with an attraction between them will spontaneously order, pairing off its constituents and further conspiring to keep the pairs in phase; it is phase coherence that is characteristic of the superconductive broken symmetry. In a dilute system pairing occurs independently of the onset of phase coherence, whereas in the conventional weakly coupled superconductors pairing and phase coherence appear coincidently. The two limits of weak coupling BCS and strong coupling BEC have long been discussed as limits of a single theory (Randeria [1995]), but it is only in the last decade that there are physical systems which can reliably span the space: conventional superconductors, cold atoms, and exciton-polaritons.

1.3 Generic Crossover Physics

1.3.1 The Vanilla Theory

Why should a crossover occur between two states of matter with substantially different phenomenology, and what are the universal parameters which could describe it without recourse to detailed materials properties? We begin heuristically with a trial wave function in the Bose or BEC limit of strong interactions or low densities, and motivate additional

formalism as we develop an understanding for a generic fermionic system.

The ground state of a weakly interacting Bose gas is well-described by a condensate wave function $|\Psi\rangle = \mathcal{N} e^{\lambda b_0^\dagger}|0\rangle$ where $b_0^\dagger$ creates a boson in its lowest-energy state, λ is a variational parameter that describes the condensate amplitude, $|0\rangle$ is the vacuum for the bosons, and $\mathcal{N}$ is a normalization constant. To generalise the condensate to a limit of paired fermion states, we write the "bosonic" creation operator in terms of fermion operators $c_k^{(\dagger)}$:

$$b_0^\dagger = \begin{cases} \sum_{\mathbf{k}} \phi(\mathbf{k}) c_{\mathbf{k}\uparrow}^\dagger c_{-\mathbf{k}\downarrow}^\dagger, & \text{Cooper Pairs} \\ \sum_{\mathbf{k}} \phi(\mathbf{k}) c_{\alpha\mathbf{k}}^\dagger c_{\beta\mathbf{k}}, & \text{Excitons} \\ \sum_{\mathbf{k}} \phi(\mathbf{k}) c_{\alpha\mathbf{k}+\mathbf{Q}/2}^\dagger c_{\beta\mathbf{k}-\mathbf{Q}/2}, & \text{Charge Density Waves (CDW)} \\ \dots & \end{cases} \tag{1.1}$$

where $\phi(k)$ is a so far unspecified internal wave function for the fermion pairs, $|0\rangle$ should now be understood as the Fermi sea, and of course the bosonic character is corrupted. For superconductivity we have particle-particle pairing, and for excitons and CDWs one has particle and hole paired in different electronic bands α, β. In what follows we will use the traditional example of Cooper pairs in a superconductor, but the same analysis qualitatively applies to any system of fermions with a pairing interaction. Expanding the condensate wave function using (1.1) and applying the anticommutation relations we obtain

$$|\Psi\rangle = \prod_{\mathbf{k}} (u_{\mathbf{k}} + v_{\mathbf{k}} c_{\mathbf{k}\uparrow}^\dagger c_{-\mathbf{k}\downarrow}^\dagger) \tag{1.2}$$

where one recovers the Bardeen-Cooper-Schrieffer (BCS) variational wave function proposed to explain superconductivity at weak interactions and high densities, with $\phi(\mathbf{k}) = v_{\mathbf{k}}/\lambda u_{\mathbf{k}}$ and we normalize so that $|u|^2 + |v|^2 = 1$. There is no distinction between the BCS and BEC limits except in the form of the wavefunction; for BEC, one expects $\phi(\mathbf{k})$ to be the

wavefunction of a single bound pair, but in the context of this theory, it is a *variational function*.

To be concrete, we follow the traditional route to minimize the free energy $F = \langle \hat{H} - \mu \hat{N} \rangle$ of a model Hamiltonian, subject to the constraint $N = \langle \hat{N} \rangle$.

$$\hat{H} - \mu \hat{N} = \sum_{\mathbf{k}\sigma} c^\dagger_{\mathbf{k}\sigma} \varepsilon_{\mathbf{k}} c_{\mathbf{k}\sigma} + \sum_{\mathbf{k}\mathbf{k}'} c^\dagger_{\mathbf{k}\uparrow} c^\dagger_{-\mathbf{k}\downarrow} V_{\mathbf{k}\mathbf{k}'} c_{\mathbf{k}'\downarrow} c_{-\mathbf{k}'\uparrow} \tag{1.3}$$

where σ, σ' are spin indices, $\varepsilon_{\mathbf{k}} = \hbar^2 \mathbf{k}^2 / 2m$ is the single-particle energy, and $V_{\mathbf{k}\mathbf{k}'}$ is an (attractive) interaction strength. This yields

$$\Delta_{\mathbf{k}} = -\sum_{\mathbf{k}'} V_{\mathbf{k}\mathbf{k}'} \frac{\Delta_{\mathbf{k}'}}{2E_{\mathbf{k}'}} \qquad N = \sum_{\mathbf{k}'} \left(1 - \frac{\xi_{\mathbf{k}'}}{E_{\mathbf{k}'}} \right) \tag{1.4}$$

known respectively as the gap and number equations, where $E_{\mathbf{k}} = \sqrt{\xi^2_{\mathbf{k}} + \Delta^2_{\mathbf{k}}}$, $\xi_{\mathbf{k}} = \varepsilon_{\mathbf{k}} - \mu$ and the variational parameters in the wave function are given by $v_{\mathbf{k}} = (1 - \xi_{\mathbf{k}}/E_{\mathbf{k}})/2$ and the normalization condition $|v_{\mathbf{k}}|^2 + |u_{\mathbf{k}}|^2 = 1$. $\Delta_{\mathbf{k}} \equiv \Delta$, assumed to be uniform, is the condensate order parameter (Alloing et al. [2014]).

It is clear from intensively rescaling (1.4) that the crossover is controlled by the particle number density n and the interaction strength. We shall parameterize the former by the Fermi momentum $k_F = (3\pi^2 n)^{1/3}$ (in 3 dimensions). Parameterizing the interaction is more subtle, physically because an arbitrary $V_{\mathbf{k}\mathbf{k}'}$ can encode a great deal of structure absent some simplifying assumptions, and technically because (1.3) must be understood as a low-energy approximation which may contain unregularized divergences. We will remedy the technical issue first by working within the so-called T-matrix approximation, replacing the bare interaction with an effective two-particle vertex given by the solution of the diagrams in Figure 1.1 (Randeria et al. [1989]). Carrying out this procedure also naturally clarifies the physical issue, distilling the interaction to a small set of relevant parameters. (As we

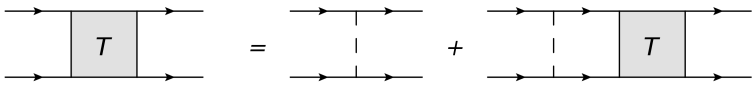

Figure 1.1: Ladder digrams for the T-matrix approximation

shall see, there is often little hope for a detailed microscopic understanding of the pairing interaction in a particular experimental realization, while it is possible to control a_S.) For instance, an attractive point-contact interaction of strength g is reduced to a scattering length a_S:[1]).

$$\frac{m}{4\pi a_S} = \frac{1}{g} + \sum_{\mathbf{k}}^{\Lambda} \frac{1}{2\varepsilon_{\mathbf{k}}} \tag{1.5}$$

where the cutoff Λ can be taken to ∞ in a controlled fashion.

A clarification is in order: in the so-called zero-range approximation, where the interaction potential does not vary over any length scale, it is always possible to parameterize it only by a_S, as can be seen from solving the Schrödinger equation directly, and no diagrammatic techniques are necessary. The utility of the T-matrix technique and its extensions is in the ability to systematically incorporate more interactions with more physical content.

The entire crossover for this vanilla theory - three dimensional, isotropic, and s-wave - will depend only on a single dimensionless parameter $\eta = 1/k_F a_S$ (Leggett [1980]). In Figure 1.2 we plot as a function of η the order parameter (identifiable with the gap in the excitation spectrum) and chemical potential obtained from solving (1.4). The chemical potential's zero crossing between its weak-coupling asymptote at the Fermi energy and its plunge downward as half the pair binding energy in the Bose limit is usually taken to demarcate the two regimes. The order parameter becomes exponentially small but remains finite deep into the

1. In two dimensions and below, scattering theory is not this simple, and in particular there exists a bound state for all purely attractive interactions. The basic principle of defining a new scale and eliminating the bare interaction through the T-matrix nevertheless still holds (Randeria et al. [1990]). In fact the crossover picture as a whole holds remarkably well, although additional transitions associated with the low-dimensional order appear, and although the control parameters of the theory are quantitatively modified compared to the 3D case (Fisher and Hohenberg [1988], Fuchs et al. [2004], Tokatly [2004]

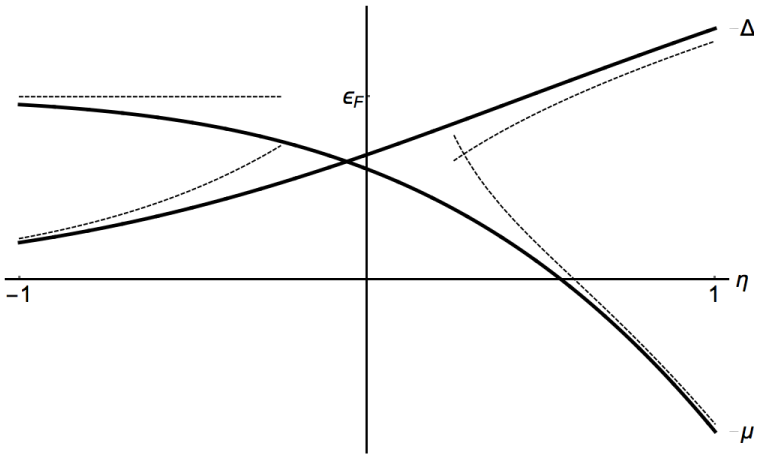

Figure 1.2: μ and Δ for the vanilla theory, as a function of the dimensionless coupling constant η. Dotted lines show approximations in the $\eta \to \pm\infty$ limits.

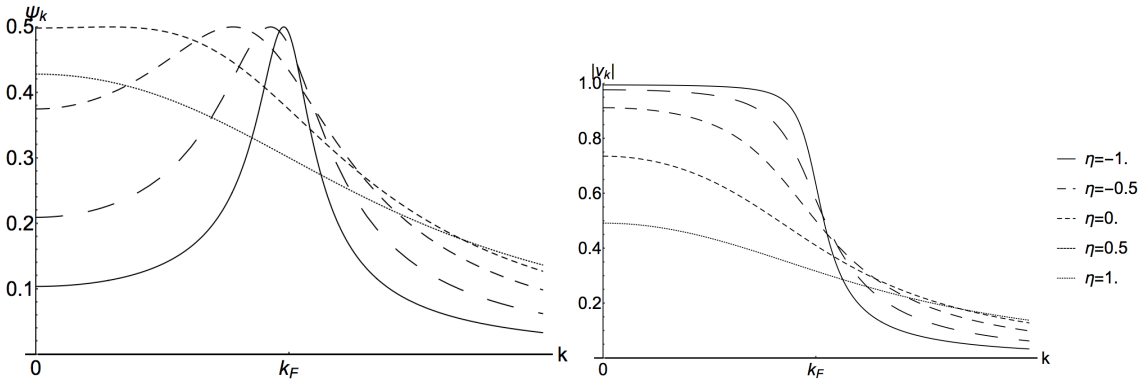

Figure 1.3: Occupancy and pair wave functions for the vanilla theory

BCS limit.

In Figure 1.3 we illustrate the behavior of the pair wave function across the crossover. It is important to distinguish the occupancy of states v_k, which is simply Fermi step function at weak coupling and subsequently broadens, from the interal wave function $\psi_k \sim v_k u_k$ which characterizes the pairing and is restricted to a thin shell around the Fermi surface in the BCS limit, while incorporating more momenta in the BEC limit as the pairs become more tightly bound in real space.

1.3.2 Deviations from Vanilla

As desired, the theory so far interpolates sensibly between a weakly paired BCS state and a Bose-Einstein condensate of tightly bound pairs. Before we develop it further it is worth questioning the approximations we have made to render it tractable.

One assumption relevant to experimental realizations is already present in the contact-interaction (1.5). Encoded in the cutoff Λ is a diluteness assumption: in order for the crossover to be controlled only by the ratio of average interparticle distance to scattering length (or equivalently pair size), neither scale can probe the short-distance behavior of the interaction. Thus if $1/a_S \ll \Lambda$ or $k_F \ll \Lambda$ are violated we must distinguish a "density-driven" crossover controlled by k_F from "interaction-driven" crossover driven by a_S, which correspond to two experimental paths toward its realization.

Cold atoms: an interaction-driven crossover

In the past two decades ultracold atomic atomic gases have opened new experimental frontiers as physicists have gained unprecedented microscopic control over their attributes. Particularly interesting for observing crossover phenomena is a scattering property known as the Feshbach resonance. In these systems, the pairing is between two species of atoms polarized into particular angular momentum and spin states - for instance two hyperfine states

of Lithium - and thus scattering between them is substantially complicated by the presence of additional channels. As shown in Figure 1.4(a), this property is exploited by magnetically tuning the Zeeman energy of the "open channel" scattering atoms with energy E close to a bound state in a "closed channel" (with internal energy exceeding E), producing a field-dependent scattering length $a_S = a_{\rm bg}(1 - \Delta/(B - B_0))$ where B is the magnetic field, B_0 denotes the field at which the bound state is resonant, $a_{\rm bg}$ is a "background" scattering length, and Δ is a resonance width that depends on microscopic parameters (Chin et al. [2010]). Thus one can change η by directly varying a_S at a fixed density of particles. Starting with a BEC and moving to weak coupling, a superfluid has been observed to persist across the crossover by the existence of a vortex lattice induced by rotating the system (Zwierlein et al. [2005]).

Figure 1.4(b) shows the chemical potential as a function of η for fixed density and varying scattering length, for a model Gaussian interaction potential with fixed range $\langle r \rangle$ (Parish et al. [2005]). As the diluteness assumption is violated the crossover point is pushed to stronger interactions. A finite range is not relevant for the current generation of cold atom experiments, but the general lesson holds that corrections to the "universal" mean field theory can shift the crossover point substantially. In two dimensions, mean field theory places the crossover at $\ln(k_F a_S) = 0$ (where this parameter plays the role of η owing to the perpetual presence of a bound state), while a high-temperature strong-coupling expansion sees signatures of Bose-like behavior well beyond this point, and in particular for the parameters accessible to experiment (Ngampruetikorn et al. [2013], Sommer et al. [2012], Levinsen and Parish [2014]). Roughly speaking, capturing these effects in the formalism developed in the first section is akin to adding to the variational wave function "dimer" terms that capture energetically favorable boson-boson correlations.

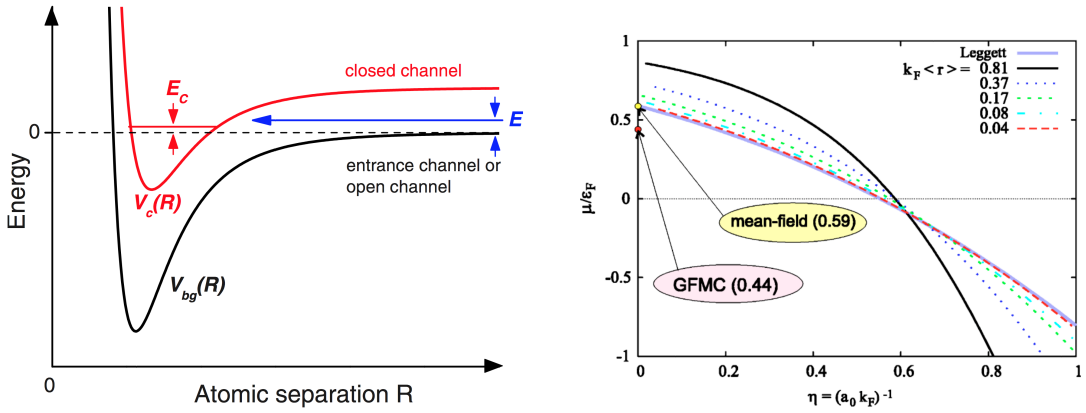

Figure 1.4: Left: Schematic illustration of the Feshbach resonance mechanism, from (Chin et al. [2010]). The bound state with energy E_c is magnetically tuned close to zero energy to resonantly couple to atoms scattering with energy E. Right: Chemical potential in an interaction-driven crossover at fixed density, with finite-range potential, from (Parish et al. [2005]). Notice that the zero crossing is shifted compared to the universal curve (blue) as the zero-range approximation is violated.

Excitons: a density-driven crossover

Electronic systems have of course classically been the province of the BCS state, and a thus natural place to look for the condensation of bosonic pairs as well. Rather than Cooper pairing, we consider here the condensation of excitons, which depends on the screened Coulomb interaction between charge carriers. A key material property is therefore the effective Bohr radius, in analogy to the hydrogen Rydberg: $a_B = 4\pi\epsilon\epsilon_0\hbar^2/(m^*e^2)$ where m^* is the effective (reduced) mass of the charge carriers in question, and ϵ is the dielectric constant. The latter quantity can be orders of magnitude larger than unity, and in particular cause a_B to exceed the lattice spacing substantially so that an interacting gas becomes a reasonable model (Keldysh [1995]). The other parameter relevant to crossover physics is $r_s \propto 1/k_F$, a dimensionless measure of interparticle distance in units of a_B. It is the latter quantity that is experimentally tunable by changing the carrier density.

We begin not with Cooper paris in superconductors, for which the BCS theory was developed, but excitons in semiconductors. These electron-hole pairs do not exhibit the

remarkable electromagnetic response properties of superconductors, but being bound by the Coulomb interaction rather than a more complicated phonon-mediated coupling they are more amenable to discussion in terms of the parameters above.

The Coulomb interaction binds the excitons constituents together while the Pauli repulsion of the latter ensures the stability of the system (Keldysh and Kozlov [1968]). We may incorporate all of these effects within the same formalism as in the first section and ask whether the system can condense (Littlewood and Zhu [1996]).Figure 1.5 shows the chemical potential and order parameter at various densities parameterized by r_s for a one-dimensional model that constrains the electrons and holes to opposite sides of an insulating layer. The hallmarks of a crossover are visible in the growing gap and the chemical potential meeting the binding energy with growing r_S. Lest one worry that these results are an artifact of the geometry, variational Monte Carlo simulations in three dimensions with unrestricted particle positions confirm the crossover scenario, and indeed verify that a pair wave function is energetically favored over a simple plasma of electrons and holes (Zhu et al. [1996]). (As before, the improvement over the vanilla calculation comes from the explicit inclusion of additional pair correlation terms in the variational wave function.)

Excitonic systems were early experimental candidates for observation of BEC. Excitons are easily formed as "preformed pairs" on the BEC side of the crossover, and the experimental challenge to observing condensation comes lies in achieving a sufficiently *high* density that condensation may occur at experimentally accessible temperatures (see the next section for a discussion of the thermodynamics of the crossover) (Hanamura and Haug [1977]). There has been for several decades experimental work aimed at achieving excitonic BEC (recent results include (Alloing et al. [2014], Yoshioka et al. [2013], Stolz et al. [2012], Yoshioka et al. [2011], High et al. [2012])), although the achievement is not yet unambiguous (O'Hara and Wolfe [2000], Jang et al. [2004], Jang and Wolfe [2006, 2005], Wolfe and Jang [2014]).

This is typically attempted by applying a Hertzian contact stress to the host crystal,

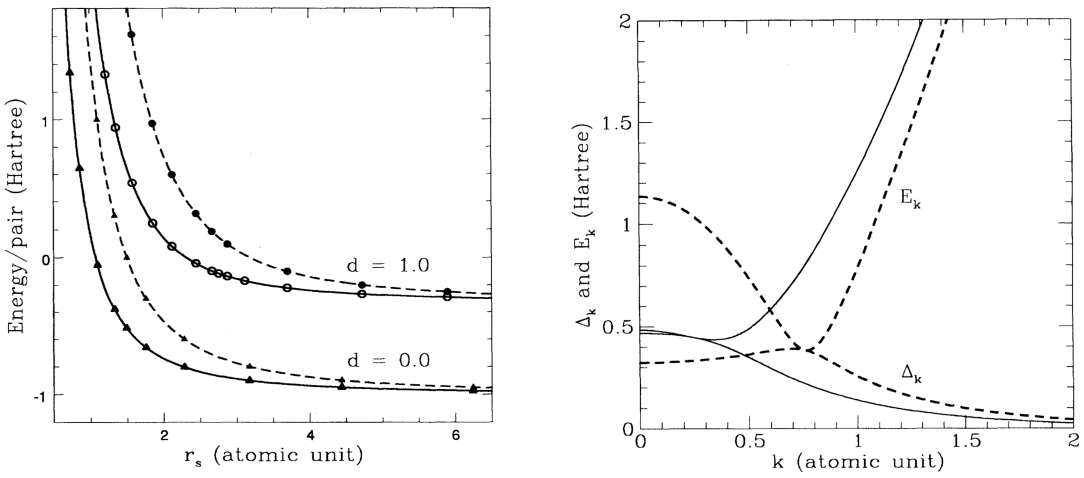

Figure 1.5: Left: Energy per pair (solid) and chemical potential (dashed) as a function of the electron gas parameter r_S in a one-dimensional bilayer structure (see text), for electron-hole separations d. Right: excitation spectrum (upper curve, and see section 1.3.3) and gap function (lower) at $r_S = 2.66, 5.90$ (dashed, solid, respectively). From (Zhu et al. [1995]).

inducing a parabolic spatial strain profile that locally lowers the band gap and thus confines the excitons. Although achievement of exciton BEC has been claimed more than once historically, the signatures of condensation in spectra and spatial distributions that substantiated these reports were not unambiguous, and it now appears that these early efforts were stymied by a two-exciton Auger recombination process which of course becomes more pronounced at higher densities, amidst other phonon-assisted exciton interconversion and decay processes (O'Hara and Wolfe [2000], Jang et al. [2004], Jang and Wolfe [2006]). A further tendency to bind into biexcitonic molecules (which, in contrast to the simple Auger process, is enhanced at low temperatures) continues to limit achievable densities (Jang and Wolfe [2005], Wolfe and Jang [2014]). Thus although recent experiments at millikelvin temperatures, both in stress traps and separated quantum wells, have renewed hope for condensation, a debate as to the interpretation of these results continues to rage (Alloing et al. [2014], Yoshioka et al. [2013], Stolz et al. [2012], Yoshioka et al. [2011]).

Anisotropic Pairing

At face value, some interactions do not admit a crossover scenario: a sufficiently strong short-range repulsive component, for instance, might favor a BCS state with p- or d-wave symmetry, in principle necessitating a phase transition to the isotropic BEC. These cases have been studied in detail and it appears, remarkably, that crossover physics continues to provide a good description (Ohashi [2005]). The key is in recognizing that the order parameter Δ can only be identified with the gap in excitation spectrum in the vanilla theory (see the next section for a discussion of spectral signatures of the crossover) (Randeria et al. [1990]). Thus the order parameter can retain the symmetry favored by the interaction while an isotropic gap opens in the spectrum as the chemical potential is lowered below $\mu = 0$. To the extent that this is a phase transition, it is an unusual one, involving weak singularities that leave first and second derivatives of the free energy continuous. It has been argued these are associated with a change in ground-state topology (Duncan and Sá de Melo [2000]).

The Unitary Gas

It is necessary to distinguish the "universality" of the vanilla theory, which we have seen abundantly violated above, from the area of the phase diagram near which $\eta \to 0^{\pm}$ where the scattering length becomes infinite (assuming that the interaction range remains small), known as the unitarity limit. This is a strongly-interacting limit (in three dimensions) where from dimensional analysis the physics may depend only on η (and a temperature). This truly universal regime, in principle accessible in cold atom experiments, is fertile and active ground for testing new theory (Bloch et al. [2012]). Some results can be interpolated from ϵ expansions in 4 and 2 dimensions, where remarkably the unitary gas maps onto, respectively, a non-interacting Bose gas of infinitely tightly-bound dimers, or a non-interacting Fermi gas at precisely the threshold for the appearance of a bound state (Nishida and Son [2012]). In three dimensions the strong-coupling physics can be described by a number of universal

relations in terms of a quantity known as the contact, which roughly speaking is a measure of pair density that encodes the anomalous scaling behavior induced by the strong correlations between particles (Braaten [2012]). This fact has prompted the development of much new theory for this regime where neither a Cooper pair nor tightly-bound dimer description is appropriate.

1.3.3 Finite Temperature and Excitations

Thermal Physics

The natural generalization of the variational theory is to a functional integral formalism, which is amply reviewed elsewhere (Altland and Simons [2010]). Our approach is to write the thermodynamic partition function as a path integral over configurations of the order parameter Δ,

$$Z = \mathcal{N} \int \mathcal{D}(\Delta, \bar{\Delta})\, e^{-S_{\text{eff}}[\Delta, \bar{\Delta}]} \tag{1.6}$$

where $S_{\text{eff}}[\Delta, \bar{\Delta}]$ is an effective action of the complex order parameter field Δ (and may be obtained by a Hubbard-Stratonovich decoupling and integration over the fermion fields of the full action (1.9)). In principle no approximations have been made at this stage, but in practice S_{eff} must be computed by expanding order by order in some small parameter. Our choice of decoupling field Δ implies that the theory will be valid only with a weak coupling $V_{\mathbf{kk'}}$ favoring Cooper pairing.

Expanding to lowest order, one can find a "mean field" minimum of the free energy by solving

$$\begin{aligned} \frac{\delta S^{(0)}_{\text{eff}}[\Delta, \bar{\Delta}]}{\delta \Delta} &= 0 \\ \frac{\partial S^{(0)}_{\text{eff}}[\Delta, \bar{\Delta}]}{\partial \mu} &= N \end{aligned} \tag{1.7}$$

which again in practice requires physically-motivated assumptions about the form of the order parameter field. At zero temperature these equations reduce to (1.4), and indeed the reparameterization in terms of scattering length remains necessary in this formalism as well (Engelbrecht et al. [1997]). Note that $\Delta = \bar{\Delta} = 0$ is always a solution, and above a temperature $T^* = \frac{8e^{\gamma-2}}{\pi}\epsilon_F \exp(-\pi|\eta|/2)$ (where γ is Euler's constant), $\Delta = 0$ becomes the *only* solution. This prediction, with the transition temperature simply proportional to the zero-temperature gap and growing without bound, simply diagnoses an instability of the uniform Fermi gas to pair formation, which coincides with condensation in the weak-coupling limit. In the opposite limit of a condensing gas of bosonic pre-formed pairs, this treatment is clearly inadequate.

The systematic approach is then to accommodate pairing fluctuations beyond mean field by expanding S_{eff} to second order and applying the prescription once more (Nozières and Schmitt-Rink [1985]). Physically the additional terms incorporate the effects of pair-breaking thermal fluctuations about the mean field; at strong coupling these dephase the condensate into a gas of bosons at the BEC transition temperature $T_c \sim \epsilon_F$ for a gas of bosons of mass $2m$, well before it becomes energetically favorable to dissociate into a Fermi liquid at $T^* \sim \epsilon_F \exp(-\pi|\eta|/2)$ (Engelbrecht et al. [1997]). At weak coupling this distinction is lost. The resulting phase diagram is sketched in Figure 1.6.

This theory, equivalent to the T-matrix approximation (Figure 1.1), becomes that of a free Bose gas in the BEC limit, and an expansion to higher orders produces an effective pair-pair repulsion of scattering length $2a_S$ between bosons of mass $2m$ which stabilizes the condensate (Sá de Melo et al. [1993]). Direct solution of the Schrödinger equation in fact finds a dimer-dimer scattering length $a_{dd} \sim .6a_S$, which repulsion is responsible for the maximum in T_c near the crossover as the transition temperature is modified by $\Delta T_c/T_c \sim n_b^{1/3} a_{dd}$ where n_b is the boson density (Petrov et al. [2005, 2004], Burovski et al. [2008], Baym et al. [1999], Haussmann et al. [2007]). Another important class of corrections arises from including

exchange of spin fluctuations between fermions, which suppresses the transition temperature in the low-density limit (Gorkov and Melikbarkhudarov [1961], Heiselberg et al. [2000]). For mass-imbalanced fermions (relevant to cold-atom experiments where different atomic species take the place of spins) the theory predicts an unphysical double-valued transition temperature and vanishing superfluidity at weak coupling, which has only recently been remedied with a self-consistent approach (Tajima et al. [2014], Hanai and Ohashi [2014]). This calculation, then, should be taken as its original authors advised: an interpolation scheme, albeit one which remains remarkably qualitatively correct for its simplicity.

There is a surprising maximum in the condensation temperature near the crossover point, and one may wonder as to its physical significance and indeed the validity of this calculation. Our expansion in fluctuations about the weak-coupling theory in fact amounts to precisely the same choice of diagrams as the T-matrix approximation (Figure 1.1), and there is no reason to believe these will dominate, particularly in the strong-coupling regime (section 1.3.2). The theory is for one thing self-inconsistent in the sense of using bare fermion propagators to compute the self-energy. This has disastrous consequences for fermions with different masses (relevant to cold-atom experiments where different atomic species take the place of spins), unphysically predicting a double-valued transition temperature and a vanishing superfluid phase at weak coupling, and has only recently been remedied (Tajima et al. [2014], Hanai and Ohashi [2014]). Another important class of corrections arises from including exchange of spin fluctuations between fermions, which suppresses the transition temperature in the low-density limit (Gorkov and Melikbarkhudarov [1961], Heiselberg et al. [2000]). The maximum in T_c itself appears to be real, appearing in Monte Carlo simulations, and has its physical origin in the repulsive interaction between dimers, which can be shown in the strong-coupling limit to shift the transition temperature by $\Delta T_c/T_c \sim n_b^{1/3} a_{dd}$ where n_b is the boson density and a_{dd} is the boson-boson scattering length, this correction falling off at higher η (Burovski et al. [2008], Baym et al. [1999], Haussmann et al. [2007]). (Note that the simple fourth-order

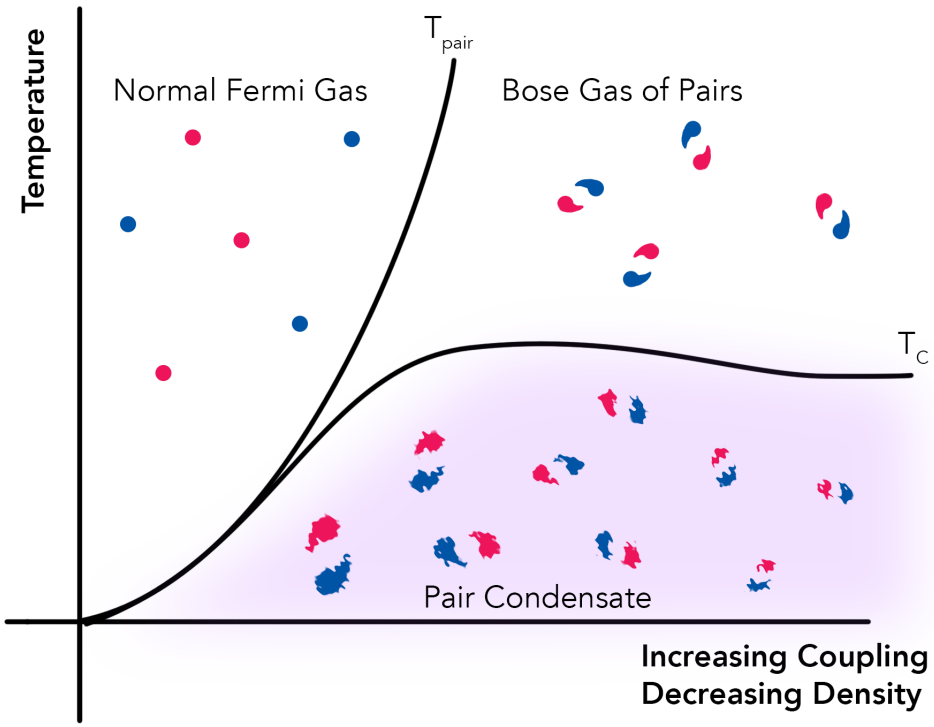

Figure 1.6: Schematic finite-temperature phase diagram of the crossover. T_{pair} is the mean-field weak-coupling result.

expansion giving $a_{dd} = 2a_S$ dramatically overestimates the scattering length, which direct solution of the Schrödinger equation shows to be $a_{dd} \sim .6a_S$ (Petrov et al. [2005, 2004]).)

Excitations

In this section we offer two complementary methods for deriving the excitation spectrum of the vanilla theory, for the separate fermionic (single quasiparticle) and bosonic (collective mode) sectors. Excitations in the BCS mean field theory are described by fermionic quasiparticles defined by the Bogoliubov transformation

First, we construct a mean field theory (equivalent to the trial wave function solution of section 1.3.1 or $S^{(0)}_{\text{eff}}[\Delta, \bar{\Delta}]$ of section 1.3.3) by defining the ground-state expectation value $\Delta = \sum_{\mathbf{k}} \langle c_{-\mathbf{k}\downarrow} c_{\mathbf{k}\uparrow} \rangle$ and inserting it into (1.3). The mean-field approximation consists of

neglecting terms such as $\Delta - \sum_{\mathbf{k}} c_{-\mathbf{k}\downarrow} c_{\mathbf{k}\uparrow}$ under the assumption that fluctuations are small. We obtain, after appropriately rescaling the order parameter,

$$(\hat{H} - \mu \hat{N})^{\text{M.F.}} = \sum_{\mathbf{k}} \begin{pmatrix} c^{\dagger}_{\mathbf{k}\uparrow} \\ c_{-\mathbf{k}\downarrow} \end{pmatrix}^{\mathsf{T}} \begin{pmatrix} \xi_{\mathbf{k}} & -\Delta \\ -\bar{\Delta} & -\xi_{\mathbf{k}} \end{pmatrix} \begin{pmatrix} c_{\mathbf{k}\uparrow} \\ c^{\dagger}_{-\mathbf{k}\downarrow} \end{pmatrix} + \text{const.} \tag{1.8}$$

which can be diagonalized by a Bogoliubov transformation into a theory of noninteracting *fermionic* quasiparticles (which superpose electrons and holes) with spectrum $E_{\mathbf{k}} = \sqrt{\xi^2_{\mathbf{k}} + \Delta^2}$.This function has appeared before in (1.4), and indeed the same equations are obtained by optimizing (1.8) with respect to Δ at fixed particle number.

In the limit $\Delta \to 0$ the quasiparticles become ordinary electrons and holes, with gap 2Δ at the Fermi surface. As Δ grows and the chemical potential crosses zero, the Fermi surface is destroyed and the minimum quasiparticle energy is half the binding energy at $k = 0$ and grows with the chemical potential.

Collective excitations are best derived from the functional integral formalism. We have seen that the leading-order term $S^{(0)}_{\text{eff}}[\Delta, \bar{\Delta}]$ sets the mean-field value of the order parameter, and have interpreted the action to second order $S^{(2)}_{\text{eff}}[\Delta, \bar{\Delta}]$ as incorporating fluctuations. This second-order term can be thought of as a large matrix between Fourier components $\delta\Delta_{\mathbf{k}}$ of the order parameter's fluctuations.

The frequency- and momentum-dependent zero eigenvalues of $S^{(2)}_{\text{eff}}$ define the excitation spectrum of the system.[2] Note that these are fluctuations in the *bosonic* order parameter field and correspond to a collective response of the condensate rather than individual quasiparticles.

This analysis finds two modes: as Goldstone's theorem predicts, the existence of a macroscopic order parameter Δ that breaks the symmetry of (1.3) to global $U(1)$ phase rotations of the fermion operators implies the existence of a sound mode with a dispersion linear in

2. This is nothing more than the statement that the excitations are the poles of the Green function.

k at long wavelengths. This mode, with stiffness $v_F/\sqrt{3}$ where v_F is the Fermi velocity, corresponds to modulations of the order parameter phase, while the second, massive amplitude mode, with spectrum $\omega(k) = 2\Delta + v_F^2 k^2/4\alpha\Delta$ where α is of order unity, reflects modulations in condensate population (Popov [1987]). These spectra are derived without assuming a value of η (except insofar as they come from expanding a weak-coupling theory), yet their quantitative forms yield qualitatively different behavior on different sides of the crossover. (Note, however, that inclusion of other effects, particularly the Coulomb interaction for charged fermions, modifies these results (Côté and Griffin [1993], Belkhir and Randeria [1992]).)

In the BCS limit, the sound mode is quite stiff in the sense that already at low momenta it intersects the quasiparticle continuum (i.e. its energy exceeds 2Δ) where scattering processes are allowed that cause it to quickly decay. (This provides the connection to the BCS/Pippard coherence length $\xi = \hbar v_F/2\Delta$. Hence a restatement of the BCS limit is the condition $k_F\xi \gg 1$.) The amplitude mode likewise quickly decays for the same reason, though note that the precise coincidence $\omega(k = 0) = 2\Delta$ is an artifact of the level of approximation. We conclude therefore that gapped quasiparticle excitations will dominate the observed spectra in the BCS limit.

In the BEC limit, in contrast, where the quasiparticle gap is the binding energy and Δ is large compared to ϵ_F, the superfluid sound mode is soft in comparison, and is the dominant thermally occupied low-energy excitation. Quantitatively this limit is perhaps better described by the Bogoliubov theory of the weakly interacting Bose gas, which predicts a sound velocity that depends sensitively on the boson-boson interaction strength, which can be incorporated directly as a parameter of the theory. As we have seen in section 1.3.3 this differs substantially from the values obtained in our low-order expansion. Note, though, that at finite temperatures pair-breaking excitations that would not exist in a purely bosonic system continue to be important (Kosztin et al. [2000]).

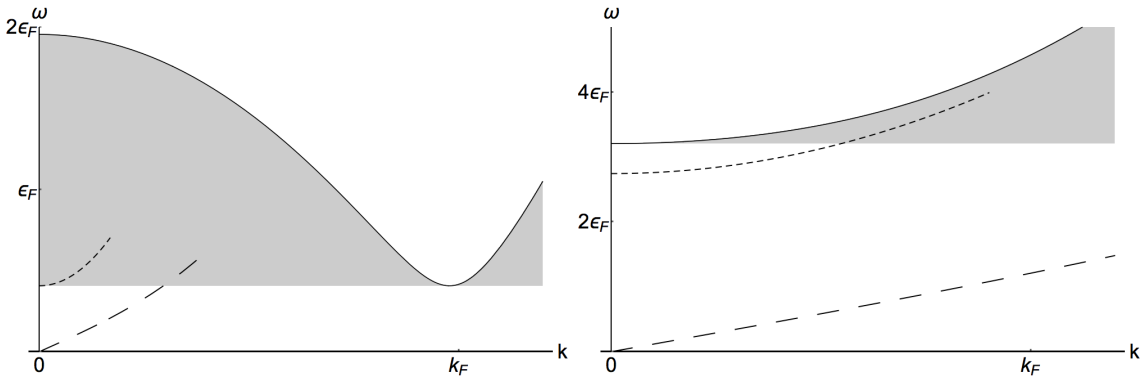

Figure 1.7: Excitation spectra on the BCS ($\eta = -1$, left) and BEC ($\eta = 1$, right) sides of the crossover. Shading below the quasiparticle spectrum $E_{\mathbf{k}}$ indicates the continuum where he collective Higgs (short dashed) and Bogoliubov (long dashed) modes decay.

The spectra in both limits are sketched in Figure 1.7. It appears that in these dynamical signatures we have finally obtained a quantity that differs substantially between the two limits. The experimental implications of these results taken at face value are nevertheless misleading - the remarkable collective response that enables superconductivity occurs in the BCS regime, for instance, where we have claimed that the dynamics are dominated by quasiparticles. We turn to the issue of collective mode dynamics that distinguish the two regimes in the next section.

1.4 Collective Mode Dynamics

1.4.1 Higgs Modes and the Higgs Mechanism

We have seen above that the collective response of the broken-symmetry state consists of a sound-like phase mode, often called the Goldstone mode, and a massive amplitude mode, often called the Higgs mode. First let us clarify some (largely semantic) ambiguity surrounding these terms. In our discussion so far, the symmetry in question has been a global $U(1)$ phase rotation corresponding to charge conservation, $c^\dagger_{\mathbf{k}\sigma} \to e^{i\theta} c^\dagger_{\mathbf{k}\sigma}$, which is broken by the choice of a particular phase for $\Delta \sim \sum_{\mathbf{k}} \langle c_{\mathbf{k}\uparrow} c_{-\mathbf{k}\downarrow} \rangle$ which introduces non-number-conserving

$\Delta c^\dagger c^\dagger$ terms. (One can explicitly compare how (1.8) and (1.3) transform.)

There is a second discussion, particularly relevant to superconductors, concerning the Higgs *mechanism* and gauge symmetries, which is best illustrated by explicitly including the electromagnetic potential $A_\mu = (\phi, \mathbf{A})$ in the model:

$$\begin{aligned} S[A_\mu, c, \bar{c}] = &\int_0^\beta d\tau \int d^d\mathbf{r}\, F^{\mu\nu} F_{\mu\nu} \\ &+ \int_0^\beta d\tau \int d^d\mathbf{r}\, \bar{c}_\sigma(\tau, \mathbf{r}) \left(\partial_\tau + ie\phi + \frac{1}{2m}(-i\nabla - e\mathbf{A})^2 - \mu \right) c_\sigma(\tau, \mathbf{r}) \\ &+ \int_0^\beta d\tau \sum_{\mathbf{k}\mathbf{k}'} \bar{c}_{\mathbf{k}\uparrow}(\tau) \bar{c}_{-\mathbf{k}\downarrow}(\tau) V_{\mathbf{k}\mathbf{k}'} c_{\mathbf{k}'\downarrow}(\tau) c_{-\mathbf{k}'\uparrow}(\tau) \end{aligned} \tag{1.9}$$

where the field strength tensor $F_{\mu\nu} = \partial_\mu A_\nu - \partial_\nu A_\mu$. Under gauge transformations that take the charged fields $c^\dagger_{\mathbf{k}\sigma} \to e^{i\theta(\tau,\mathbf{r})} c^\dagger_{\mathbf{k}\sigma}$ and the gauge field $A_\mu \to A_\mu - \partial_\mu \theta(\tau, \mathbf{r})$ for an arbitrary $\theta(\mathbf{r}, \tau)$, the theory is invariant, whether in the normal or broken-symmetry state, as the order parameter Δ transforms as a matter field with charge $2e$. This invariance, required for any physical theory, simply accounts for the excess degrees of freedom in the field theory compared to physical electromagnetism, and is guaranteed by the electromagnetic coupling in the fermion kinetic term.

Taking (1.9) as a starting point and repeating the procedure of section 1.3.3 to obtain an effective action $S_{\text{eff}}[A_\mu, \Delta, \bar{\Delta}]$, we may further decompose $\Delta = |\Delta| e^{i\theta}$ to isolate the low-energy physics of the phase fluctuations $\delta\theta$. (The massive fluctuations $\delta|\Delta|$ are the Higgs mode.) Two limits are useful: considering only the electric potential ϕ, one finds that the sound mode dispersion acquires a gap $\Omega = \sqrt{4\pi n e^2/m}$, known as the plasma frequency. Physically, our previous analysis had only considered the attractive interaction that promotes pairing, whereas now inclusion of the electric field that mediates the Coulomb interaction has revealed an additional collective response of the charged fluid to density fluctuations. We may also consider a purely magnetic field, $\mathbf{B} = \nabla \times \mathbf{A}^\perp$, whereupon integration over the

phase fluctuations produces

$$S[\mathbf{A}^{\perp}] = \frac{\beta}{2} \sum_{\mathbf{k}} \left(\frac{n_s}{m} + \mathbf{k}^2 \right) \mathbf{A}^{\perp}_{\mathbf{k}} \cdot \mathbf{A}^{\perp}_{-\mathbf{k}} \tag{1.10}$$

where n_s is a measure of the superfluid density. Remarkably, the electromagnetic field carried in vacuum by the massless photon with dispersion $\omega = ck$ has acquired a mass inside the superconductor, which manifests physically as magnetic flux expulsion. This exemplifies the Higgs mechanism: a gauge field coupled to a matter Hamiltonian acquires a mass when the latter enters its broken-symmetry state, at the expense of the massless sound mode that would otherwise be present. We stress the limits of this scenario: the appropriate coupling to a gauge field requires charged particles, and the condensate order parameter must be in the Cooper channel.

1.4.2 Higgs Modes in Charge Density Wave Systems

The physics that enables the Higgs mechanism in superconductors at once vitiates direct observation of the Higgs mode by coupling to an electromagnetic probe. In charge density wave (CDW) systems, in contrast, the order parameter $u \sim \sum_{\mathbf{k}} \langle c^{\dagger}_{\mathbf{k}+\mathbf{Q}} c_{\mathbf{k}} \rangle$ is simply a spatially modulated electronic density, and may be thought of as a frozen phonon mode. As before there is a collective phase mode, associated physically with translations of the CDW, and a Higgs mode corresponding to modulations of $|u|$. Since u controls the gap, it is possible to observe the evolution of its amplitude by time-resolved measurements of the electronic structure. Such experiments have been performed in the rare earth tritellurides, using time- and angle-resolved photoemission spectroscopy (trARPES) to track the evolution of the electronic structure of the CDW material as a function of time after a powerful pump pulse is used to transiently destroy the condensate (Schmitt et al. [2008], Rettig et al. [2014]). Not only do the experimental spectra show oscillations of the Higgs mode, the data for two

successive pump pulses in- or out-of-phase demonstrate that they are coherent, with the collective motion of the electron fluid Rabi flopping like a single spin.

This "quantum quench" response with oscillations in the Higgs mode is typical of the BCS side of the crossover. A quench in the strong-coupling limit is in contrast dominated by interference between the sound modes that dominate the low-energy spectrum leading to the observation of so-called Sakharov oscillations (Hung et al. [2013]). We also note that while all the observed dynamics is damped, the damping cannot be readily interpreted in terms of interaction between quasiparticles and collective modes as in section 1.3.3, since the experimental systems involved in quench experiments are generally highly out of equilibrium and coupled to external sources of dissipation (Rançon et al. [2013]).

The ease of optically coupling to the CDW order parameter also provides an opportunity to observe Higgs mode of the *superconducting* order parameter in materials that exhibit both types of order, such as $NbSe_2$. As we have seen the order parameter Δ depends on the density of particles, or more carefully in the BCS limit, the density of states at the Fermi surface. But the formation of a CDW depletes precisely this quantity, providing a coupling between the two order parameters u and Δ. In particular there is a linear coupling between the phonon and superconducting Higgs mode (which, owing to the phonon interaction, is pushed below the quasiparticle continuum), so that the phonon self-energy depends on Δ and becomes singular in the vicinity of the superconducting gap (Littlewood and Varma [1981], Browne and Levin [1983], Littlewood and Varma [1982]). Raman spectroscopy, which measures this quantity by perturbing the CDW order, shows the development of a second peak in the susceptibility as the material (already CDW ordered) is cooled below the superconducting transition temperature, at the expense of the peak associated with the CDW (Sooryakumar and Klein [1980], Pekker and Varma [2015], Méasson et al. [2014]). In this way, the superconducting Higgs mode which we predicted above should not couple to electromagnetic probes (to linear order) becomes visible in the Raman spectrum: shaking one condensate

at once shakes the other. Of course, at sufficiently high orders of expansion a nonlinear electromagnetic coupling directly to the superconductor Higgs mode appears, and seems to be recently accessible to high-intensity THz experiments (Matsunaga et al. [2013]).

1.4.3 Polaritons

An alternate strategy for observing the dynamics of the order parameter in the Cooper channel with an electromagnetic coupling is to pick a model system around this feature. Polaritons, quasiparticles hybridizing an ensemble of two-level systems with a photonic degree of freedom, were first realized between quantum well excitons and a cavity photon confined by a distributed Bragg reflector, although implementations in cold atoms are currently being attempted as well.

A simple model Hamiltonian will clarify the issue:

$$\begin{aligned}\hat{H} - \mu\hat{N} = &\sum_{\mathbf{q}} \psi^\dagger_{\mathbf{q}}(\omega(\mathbf{q}) - \mu)\psi_{\mathbf{q}} \\ &+ \sum_j \begin{pmatrix} a_j^\dagger \\ b_j^\dagger \end{pmatrix}^\intercal \begin{pmatrix} -(\epsilon-\mu) & g\sum_{\mathbf{q}} e^{i\mathbf{q}\cdot\mathbf{r}_j}\psi^\dagger_{\mathbf{q}} \\ g\sum_{\mathbf{q}} e^{-i\mathbf{q}\cdot\mathbf{r}_j}\psi_{\mathbf{q}} & \epsilon-\mu \end{pmatrix} \begin{pmatrix} a_j \\ b_j \end{pmatrix}\end{aligned} \tag{1.11}$$

Here $a_j^\dagger$, $b_j^\dagger$ are creation operators for the two states of a system at site j, such as the ground and first excited states of an exciton, while $\psi^\dagger_{\mathbf{q}}$ creates a photon of momentum $\mathbf{q}$ with dispersion $\omega(\mathbf{q})$ which is assumed to have a minimum near the energy splitting ϵ of the two-level system. (Confinement of a photon to a cavity causes its dispersion to become quadratic.) The exciton-photon coupling simply encodes the possibility of a transition between states a and b aided by the emission or absorption of the photon, and the whole system may be regarded as simply an ensemble of spins with a dipole coupling, although written to emphasize the dynamics of the photon mediating the interaction. In this form, it is clear

that a photon condensate $\langle\psi\rangle$ would render the Hamiltonian formally similar to and in fact simpler than (1.8), with the two-level systems taking the place of already "preformed" pairs and the photon a dynamic order parameter field. This simple model remarkably provides enough ingredients to facilitate a density-driven crossover: at low excitation densities (compared to the underlying density of spins n), the polaritons are essentially photonic, with a weak repulsive effective interaction mediated by the spins, which are polarized almost completely down. Here the system supports a BEC-like photon condensate, whereas at higher densities comparable to n the degrees of freedom are more democratically hybridized exciton-photon quasiparticles and form a BCS-like condensate. Although by construction there is no separation between pairing and condensation temperatures, the signatures of crossover physics otherwise remain: the chemical potential plunges below the bottom of the band at low densities and the transition temperature deviates from the mean-field BCS value, set by the photon effective mass and density as in a BEC model, as fluctuations of the softening collective sound mode become more important. (There is a second BEC-like regime at much higher density when the exciton band becomes saturated and the degrees of freedom are again photon-like. From the perspective of crossover physics this can be viewed as an artifact of the theory.)

The polariton has a very light mass due to the photonic component, so the Bogoliubov sound mode is about four orders of magnitude stiffer than an excitonic condensate of the same density. Consequently, the dynamical spectrum is dominated by the 'Higgs' mode, to be identified here as the collective oscillation of exciton-polaritons close to the Rabi frequency.

1.5 Concluding Remarks

In this brief survey of the BEC-BCS crossover we began with the observation that a coherent superposition of large and overlapping weakly interacting pairs may be described by the same wave function as a condensate of tightly bound dimers. The simplest version of this theory

is controlled by a single parameter - either the range of the interaction, or the scaled density. Real physical systems can be more complex.

The reliable signatures of crossover are in the dynamics. At strong coupling when the cost of breaking pairs is high, the only low-energy physics remaining is in the collective sound mode. The BCS limit is in contrast the province of "more scales," which are liable to scramble low energies sufficiently that only amplitude mode dynamics emerge unscathed - the only strategy is to shake the condensate and watch.

CHAPTER 2

A POLARITON SUPERSOLID IN A MOIRÉ LATTICE

2.1 Introduction

Polaritons are bosonic quasiparticles that arise when the coupling in a systen of light and matter is sufficiently strong to hybridize the two components. Since the observation of Bose-Einstein condensation in a realization with quantum well excitons coupled to the cavity photons in a distributed Bragg reflector, they have been widely studied as both a platform for exploring condensation phenomena (including at room temperature due to the low effective mass of the cavity photon), as well as a practical photonic nonlinearity for optical computation and quantum simulation (Kasprzak et al. [2006b], Kena-Cohen and Forrest [2010], Su et al. [2020], Schneider et al. [2016], Suarez-Forero et al. [2021]). A recent thrust of experimental efforts has been toward establishing the transition metal dichalcogenides (TMDs) as a polaritonic system (Hu and Fei [2020]). Besides their attractive optical properties, the TMDs naturally exhibit strong interactions that can already realize exotic electronic phases of matter such as Wigner crystals (Zhou et al. [2021], Smolenski et al. [2021]). Stacking multiple layers of TMDs that have been twisted relative to each other generates a Moiré superlattice potential and flattens the low-energy band structure to further exacerbate interaction effects, leading to the observation of more dilute electronic crystals in which charge carriers localized on Moiré lattice sites organize into spatially ordered states (Miao et al. [2021], Xu et al. [2020], Huang et al. [2021], Jin et al. [2021]). Excitons in such structures exhibit strong dipolar interactions and can localize, and a recent experiment has realized strong-coupling polaritons in a Moiré superlattice in a cavity and found evidence of strong nonlinearities associated with the localized excitons saturating at a density of one per Moiré lattice site (Li et al. [2020], Zhang et al. [2021]).

In this work we study a model of polaritons formed from excitons on a lattice coupled to

a planar cavity, taking into account possible strong exciton-exciton interactions. We study the case where the lattice spacing is small compared to the photon wavelength and blockade effects restrict occupancy to one exciton per site; this should be contrasted with previous studies of polariton systems with larger-scale spatial order that can be described in terms of the modulation of some continuous density, leading to polariton band structures (Winkler et al. [2015], Lai et al. [2007], Pickup et al. [2020]).

2.2 Model

The Hamiltonian is $H = H_0 + H_{\text{int}}$, with

$$H_0 = \sum_{\mathbf{q}} \psi^\dagger_{\mathbf{q}} \omega_{\mathbf{q}} \psi_{\mathbf{q}} + \epsilon \sum_j \sigma^z_j + g \sum_{j\mathbf{q}} (e^{i\mathbf{q}\cdot\mathbf{r}_j} \psi^\dagger_{\mathbf{q}} \sigma^-_j + \text{h.c.}) \tag{2.1}$$

and $H_{\text{int}} = \sum_{jj'} U(|\mathbf{r}_j - \mathbf{r}_{j'}|) \mathcal{P}^\uparrow_j \mathcal{P}^\uparrow_{j'}$. H_0 is an extended Dicke model like that studied by (Keeling et al. [2004]), where $\psi_{\mathbf{q}}$ annihilates a photon of in-plane momentum $\mathbf{q}$ and the presence or absence of an exciton on site j with on-site energy ϵ is represented as the up or down eigenstate, respectively, of the spin operator σ^z_j. In what follows we will use the language of spin flips interchagneably with exciton occupancy. The in-plane photon dispersion is $\omega_{\mathbf{q}} = \omega_0 + \mathbf{q}^2/2m^*$ where the fundamental frequency ω_0 and the effective mass m^* are set by the geometry of the cavity. The light-matter term describes an exciton created (annihilated) by absorption (emission) of a photon at site j, and the dipolar coupling strength g can be inferred from the measured Rabi splitting $\Omega = g\sqrt{n}$ where n is the density of lattice sites. $\mathcal{P}^\uparrow_j$ projects onto the spin-up state at site j, so that H_{int} describes a pairwise interaction U between occupied sites.

2.2.1 The Fedotov-Popov Trick

There is a standard steamroller of functional field integral techniques for fermionic systems that will now be convenient to apply. These are nicely introduced for instance in (Altland and Simons [2010]) or (Mahan [2000]) and I do not have any particular insight to add to what can be found there. To apply this steamroller it, however, is necessary to fermionize the model in 2.1, and to do so I will make use of a technique due to (Popov and Fedotov [1988]) which remains under-appreciated, which I will explain in somewhat general terms here.

The basic idea is to introduce fermionic annihilation operators on each site, a_j and b_j, representing the ground and excited states, respectively, so that $\sigma_j^z = \frac{1}{2}(b_j^\dagger b_j - a_j^\dagger a_j)$, $\sigma_j^+ = b_j^\dagger a_j$, and so forth. These can be shown to obey the appropriate spin commutation relations so long as one is dealing with a state with one fermion per site. That is, the states with neither fermion occupying a site or both a and b fermions do not correspond to anything physical in the spin picture, and somehow the constraint $N_j^* = a_j^\dagger a_j + b_j^\dagger b_j = 1$ must be imposed for each site. This could for instance be done with a lagrange multiplier λ_j on each site, so effectively coupling the system to some additional external field, but this approach is cumbersome since the constraint must be carefully enforced at each order in perturbation theory. Instead, the Fedotov-Popov trick accomplishes this exactly and automatically.

Thanks to the fermions, we are now in a much enlarged Hilbert space $\mathcal{H} = \mathcal{H}_{\text{phys}} \otimes \mathcal{H}_{\text{unphys}}$. (The physical subspace is tiny compared to the unphysical one - intuitively, any one site in an unphysical configuration spoils the whole system.) However, we have the important property that the Hamiltonian is "number-conserving" on each site in the sense of the fermion number N_j^*. Therefore in the enlarged Hilbert space the Hamiltonian may be written $H = H_{\text{phys}} \oplus H_{\text{unphys}}$ in the sense of a direct sum rather than a Kronecker sum, i.e. there are no off-diagonal elements driving transitions between the subspaces.

In everything that follows I will be ultimately deriving properties of the system from a

representation of the partition function,

$$Z = \mathrm{tr}(\exp(-\beta H)) = \mathrm{tr}(\exp(-\beta H_{\mathrm{phys}}))) + \mathrm{tr}(\exp(-\beta H_{\mathrm{unphys}}))) = Z_{\mathrm{phys}} + Z_{\mathrm{unphys}} \quad (2.2)$$

which breaks neatly apart into two terms thanks to the block-diagonal Hamiltonian. Therefore the problem is reduced to finding a way to make $Z_{\mathrm{unphys}} = 0$ without altering Z_{phys}. In general we can write $Z_{\mathrm{unphys}} = \sum_{\{\sigma \in \mathrm{unphys}\}} \alpha_\sigma \prod_{j \in \sigma} \mathrm{tr}_j(e^- \beta H)$ where σ labels some unphysical configuration, $\mathrm{tr}_j(e^{-\beta H})$ is a partial trace over the single-site Hilbert space of some site j with an unphysical occupancy, and α_σ is some complicated number from all of the physics beyond single-site going on in a given configuration. So to make $Z_{\mathrm{unphys}} = 0$, it suffices to make the single-site trace of all the unphysical configurations go to zero.

The trick of Fedotov and Popov is to accomplish this by by adding to the Hamiltonian a term $H_* = \sum_j \frac{i\pi T}{2}(N_j^* - 1)$. Notice first that $N_j^* = 1$ in the physical subspace so that H_* does not do anything. Meanwhile, the single-site trace over the $|00\rangle$ and $|11\rangle$ states gives $z_j = \exp(-\beta(0 - i\pi T/2)) + \exp(-\beta(\epsilon - \epsilon + i\pi T/2)) = 0$.

Notice also that H^* amounts to adding a fictitious imaginary temperature-depdendent chemical potential to the system (plus a constant that does not alter the physics). Calculationally, it amounts to a shift of the fermionic Matsubara frequencies $\nu_m = 2\pi T(m + \frac{1}{2}) \to 2\pi T(m + \frac{1}{4})$.

Popov and Fedotov also considered higher-spin Hamiltonians with similar results. I want to remark briefly here that this is not automatically possible for generic many-state Hamiltonians. A salient example is a three-level system in which the photon field only couples to one possible transition between the levels. In this case the direct sum condition is not automatically satisfied and additional constraints must be imposed to enforce it. Assuming this is accomplished somehow, there is an additional inconvenience when the single-site energy levels are not equally spaced. In that case, using the same $\lambda_j(N_j^* - 1)$ construction as above, the condition for z_j to vanish is generically some polynomial in λ_j and does not

necessarily produce a unique solution or one that acts like a Matsubara frequency shift.

2.2.2 Other formal developments

With this fermionization trick we represent the partition function as a functional field integral

$$Z = \int \mathcal{D}[a, b, \psi] \, \exp(-S[a, b, \psi]) \tag{2.3}$$

over coherent states of a complex field ψ for the bosons and Grassmann fields a, b for the fermions. (The Fedotov-Popov trick requires a tweak to the boundary conditions of the fermionic variables but otherwise does not change the rules of Grassmann integration.) The Euclidian-time action $S[a, b, \psi]$ is as usual obtained by going over to the Lagrangian and swapping the operators in the Hamiltonian for fields.

Next, it will be convenient to work in Fourier space. To do that we will assume translation invariance, $U(j, j') = U(|j - j'|)$, to obtain

$$\begin{aligned} S[\psi, a, b] = &\sum_q \psi_q^\dagger(-i\omega_q + \tilde{\omega}_q)\psi_q + \sum_k (-i\nu_k(a_k^\dagger a_k + b_k^\dagger b_k) + \frac{\epsilon}{2}(b_k^\dagger b_k - a_k^\dagger a_k)) \\ &+ g\sum_{kq}(\psi_{-q}^\dagger a_k^\dagger b_{k+q} + \psi_q b_k^\dagger a_{k+q}) \\ &+ \frac{2}{4}\sum_{kk'q}(b_{k+q}^\dagger b_{k'-q}^\dagger - a_{k+q}^\dagger a_{k'-q}^\dagger + 1)U(q)(b_{k'}b_k - a_{k'}a_k + 1) + N(\frac{i\pi T}{2} + \frac{\epsilon}{2}) \end{aligned} \tag{2.4}$$

Here ω_q is a bosonic Matsubara frequency and ν_q is a fermionic one with an extra shift from the Fedotov-Popov trick absorbed into it. Now to deal with the quartic terms we will introduce a bosonic decoupling field $\phi_q \equiv \langle \frac{1}{2}\frac{1}{N}\sum_k (b_k^\dagger b_{k+q} - a_k^\dagger a_{k+q})\rangle$, and after performing a Hubbard-Stratonovich transformation we are left with an action quadratic in the fermion fields, which can be integrated out to finally obtain an effective action

$$
\begin{aligned}
S_{\text{eff}}[\psi,\phi] = &\sum_q \psi_q^\dagger(-i\omega_n + \tilde{\omega}_q)\psi_q - \sum_q \phi_q U(q)\phi_{-q} \\
&- \operatorname{tr}\ln\mathcal{M} \\
\mathcal{M}^{-1}_{kk'} = &\begin{pmatrix} -i\nu_m - \xi_k & 0 \\ 0 & -i\nu_m + \xi_k \end{pmatrix}\delta_{kk'} \\
&+ \sum_q \begin{pmatrix} -|U(q)|\phi_{-q} & g\psi^\dagger_{-q} \\ g\psi_q & |U(q)|\phi_q \end{pmatrix}\delta_{k,k'-q}.
\end{aligned}
\tag{2.5}
$$

Here $\xi_k = (\epsilon - \mu)/2$, μ is the chemical potential, and $\mathcal{M}$ lives in the space of up and down spins $\times$ 4-momenta $k = (m, \mathbf{k})$.

We will consider a number of mean-field Ansätze for $\langle\psi\rangle$ and $\langle\phi\rangle$. Because the Moiré lattice spacing is much smaller than the photon wavelength, for energetic reasons we only consider the possibility of a spatially uniform photon condensate, $\langle\psi_0\rangle = \lambda$. In each case we will minimize the free energy, then expand in fluctuations $\delta\psi$ and $\delta\phi$, as explained later.

2.3 Homogeneous Static Mean-field Theory

First we will study a homogeneous mean-field ansatz with finite expectation values for ψ_0 and ϕ_0 and $(\psi,\phi)_{q\neq 0} = 0$, and consequently diagonal $\mathcal{M} \propto \delta_{kk'}$. The free energy of this state is

$$
f_0 = \tilde{\omega}_0|\psi_0|^2 - U_0\phi_0^2 - T\ln(\cosh\beta E) - \frac{\mu}{2} \tag{2.6}
$$

with $E = \sqrt{(\xi + U_0\phi_0)^2 + g^2|\psi_0|^2}$, subject to the mean-field equations $\partial_{\phi_0} f_0 = \partial_{\psi_0} f_0 = 0$ or

$$
\begin{aligned}
\tilde{\omega}_0\psi_0^\dagger &= \frac{\psi_0^\dagger}{2E}\tanh(\beta E) \\
\phi_0 &= -\frac{\xi + U_0\phi_0}{2E}\tanh(\beta E).
\end{aligned}
\tag{2.7}
$$

which must be supplemented with the occupancy constraint $\phi_0 \in [-\frac{1}{2}, \frac{1}{2}]$. Fig. 2.1 shows the phase boundary as computed by following the line $\psi_0 = 0$. These plots are in some arbitrary energy units to show the effects of turning on the interaction, and then for the rest of time we will work in units of $U_0 = U(0)$. All plots are shown at fixed detuning $\Delta = 2.5$, i.e. with the exciton below the photon. The effect of temperature on this type of plot is clearly just to smear everything out; while it is nice that we can compute this easily, we will ignore it for now. Above the chemical potential $\mu = 0$ it becomes energetically favorable for $|\psi_0|^2$ to grow without bound, and in this regime the theory is a bad model of a photon condensate. Let us first focus on $U = 0$. At lower chemical potential there are two "Mott lobes" centered around $\mu = -\Delta$; it can be shown that $\phi_0 = +(-)1$ in the lower (upper) lobe. Along the $g = 0$ axis, the physics is of spins subject to the external field of μ, which polarizes them around $\mu = -\Delta$. When $U \neq 0$, the homogeneous ϕ_0 field allowed by our mean-field ansatz will attempt to interpolate between one lobe and the other.

At $g \neq 0$, there is a possible energy lowering from the exciton-photon interaction, but the photon acts as a transverse field to the spins and requires them to tilt away from full polarization to realize this effect. Deeper into each Mott lobe, the g required to realize this effect grows, dropping to 0 where the spins are indifferent to their orientation (and near the special $\mu = 0$ point).

The recipe to convert the phase diagram to a more experimentally measurable quantity is in principle simple: the total density $\rho = -\partial_\mu f_0$ is given by

$$\rho = |\psi_0|^2 + \phi_0 + \frac{1}{2}. \tag{2.8}$$

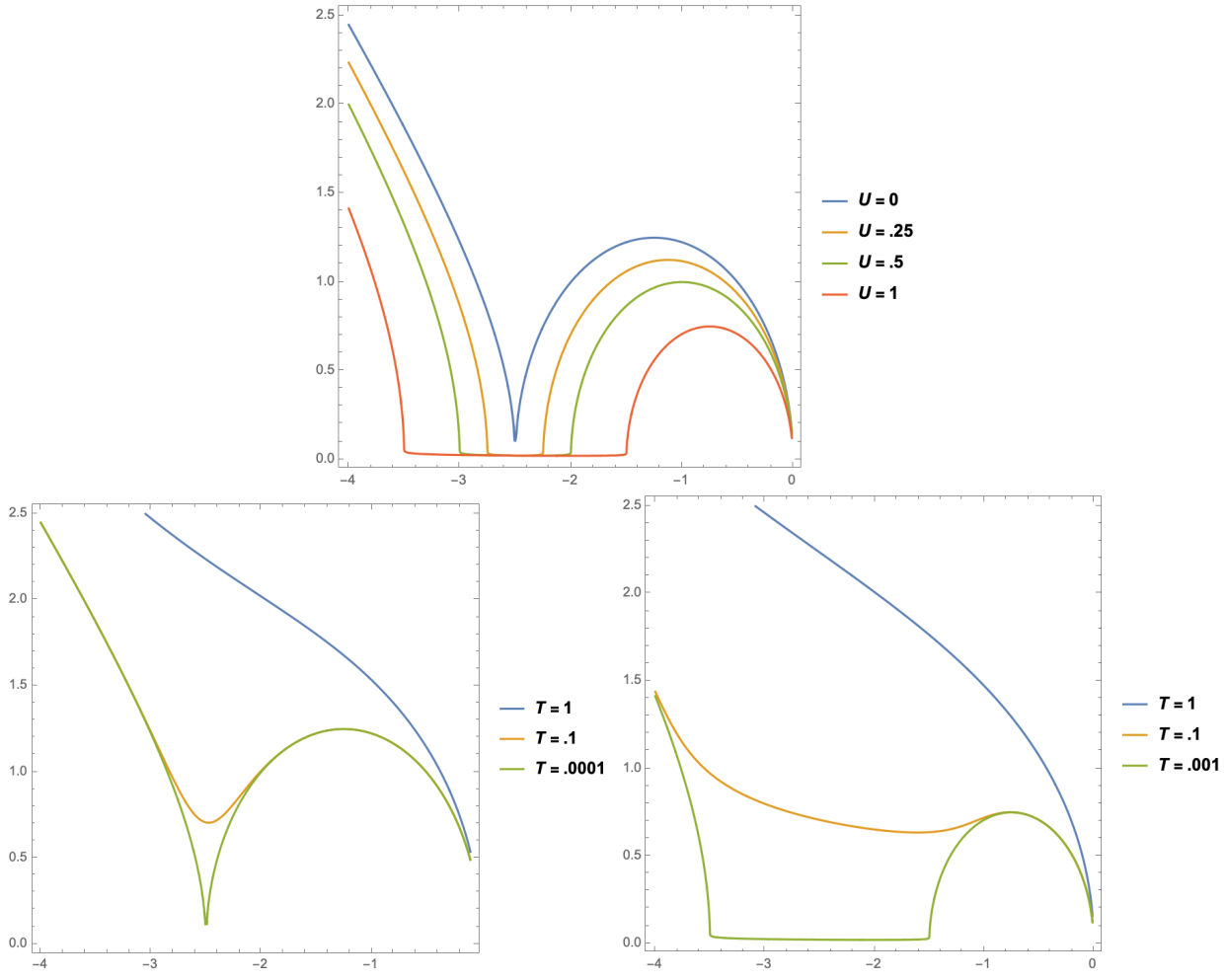

Figure 2.1: Condensate region against μ and g in units of U. Top panel is at $T = 0$, bottom left at $U = 0$, bottom right at $U = 1$.

2.4 Fluctuations of the Uniform States

To compute the fluctuation action to second order we consider:

$$(G_0)_{kk'} = \begin{pmatrix} -i\tilde{\omega}_k - \xi - U_0\phi_0 & g\psi_0^\dagger \\ g\psi_0 & -i\tilde{\omega}_k + \xi + U_0\phi_0 \end{pmatrix}^{-1} \delta_{kk'} \tag{2.9}$$

$$\Delta_{kk'} = \sum_q \begin{pmatrix} -|U(q)|\delta\phi_{-q} & g\delta\psi_{-q}^\dagger \\ g\psi_q & |U(q)|\delta\phi_q \end{pmatrix} \delta_{k,k'-q}$$

$$T\mathrm{tr}(G_0\Delta G_0\Delta) = \begin{pmatrix} \delta\psi_q^\dagger \\ \delta\psi_{-q} \\ \phi_q \end{pmatrix}^T \begin{pmatrix} K_1 & K_2(\psi_0)^2 & K_3\psi_0 \\ K_2^*(\psi_0^\dagger)^2 & K_1^* & K_4\psi_0^\dagger \\ K_3\psi_0^\dagger & K_4\psi_0 & \Pi \end{pmatrix} \begin{pmatrix} \psi_q \\ \psi_{-q}^\dagger \\ \phi_{-q} \end{pmatrix} \tag{2.10}$$

with

$$K_1 = g^2 n(i\omega_q\bar{\xi} - E^2 - \bar{\xi}^2)\frac{\tanh(\beta E)}{E(\omega_q^2 + 4E^2)} \tag{2.11}$$

$$K_2 = g^4 n\frac{\tanh(\beta E)}{E(\omega_q^2 + 4E^2)}$$

$$K_3 = g^2 n|U(q)|(i\omega_q + 2\bar{\xi})\frac{\tanh(\beta E)}{E(\omega_q^2 + 4E^2)}$$

$$K_4 = g^2 n|U(q)|(-i\omega_q + 2\bar{\xi})\frac{\tanh(\beta E)}{E(\omega_q^2 + 4E^2)}$$

$$\Pi = -4g^2 U(q)^2|\psi_0|^2\frac{\tanh(\beta E)}{E(\omega_q^2 + 4E^2)}$$

with $\bar{\xi} = \xi + U_0\phi_0$ and $E = \sqrt{\bar{\xi}^2 + g^2|\psi_0|^2}$. Then the free energy taking into account fluctuations is then $f_2[\delta\psi, \delta\phi] = f_0 + \frac{1}{2}\sum_q \begin{pmatrix} \delta\psi_q^\dagger & \delta\psi_{-q} & \delta\phi_q \end{pmatrix} \cdot Q(\omega_q, q) \cdot \begin{pmatrix} \psi_q & \psi_{-q}^\dagger & \delta\phi_{-q} \end{pmatrix}^T$,

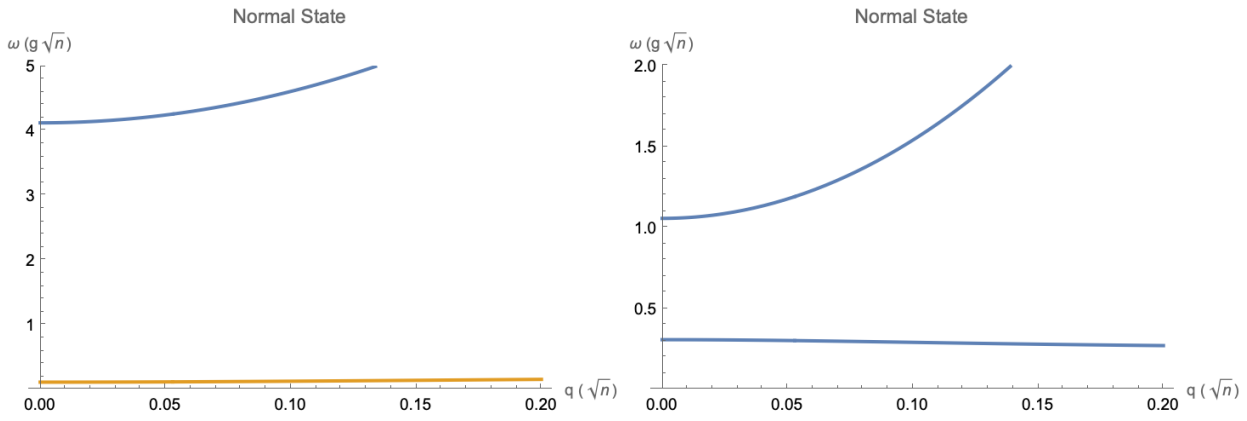

Figure 2.2: Normal state spectrum at $T = 0$ with $\mu = -4$, $g = 1$ (left) and $\mu = -1$, $g = .4$ (right), inside the two Mott lobes.

where

$$Q = \begin{pmatrix} -i\omega_q + \tilde{\omega}_q + K_1 & K_2(\psi_0)^2 & K_3\psi_0 \\ K_2^*(\psi_0^\dagger)^2 & i\omega_q + \tilde{\omega}_q + K_1^* & K_4\psi_0^\dagger \\ K_3\psi_0^\dagger & K_4\psi_0 & -U(q) + \Pi \end{pmatrix} \tag{2.12}$$

The spectrum is got by analytic continuation (substitution) $i\omega_q \to \omega$ and satisfies the condition $\det Q(\omega, q) = 0$.

2.4.1 Normal State

In the normal state where $\psi_0 = 0$, Q becomes diagonal, $\Pi \to 0$, and $E \to \bar{\xi}$, simplifying matters considerably. The spectrum is plotted in Figure 2.2 and it is important to note that the softening that it shows is an entirely mean-field effect, having nothing to do with the form of $U(q)$ which has not yet been specified.

An instability of the normal state can be diagnosed by the condition $\det Q(0, q) = 0$. This turns out to correspond to a softening of the lower polariton mode at $q = 0$, and can be written

$$g^2 = \pm\mu(U_0\phi_0 - \Delta - \mu) \tag{2.13}$$

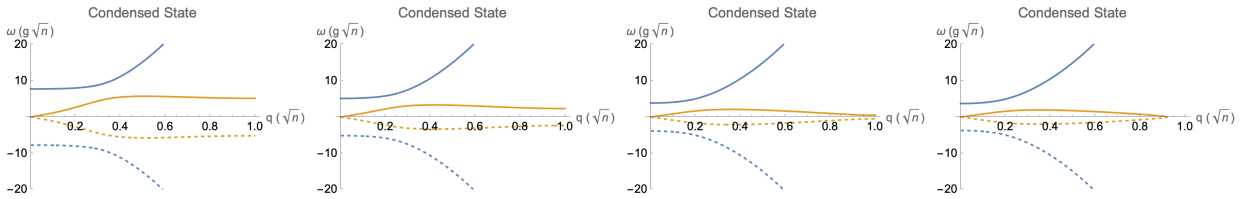

Figure 2.3: Condensed state spectrum at $T = 0$ with $\mu = -2.5$, $g = (4, 3, 2.3, 2.2)$ from left to right.

Evaluated at $\phi_0 = \pm 1/2$ this reproduces the (zero-temperature) phase boundaries of (2.7), it being left as an exercise to the reader to determine which way is more natural or elegant.

2.4.2 Condensed State

Here the modes will inherit some of $U(q)$ so it is necessary to pick something. We will start by considering nearest-neighbor interactions, $U(j, j') = U_0 \delta_{j\pm1,j'}$, in a linear chain, so that $U(q) = U_0 \cos(q\pi/a)$ where a is the lattice spacing. For now we will choose the saturation density $n_s^2 = 1/a^2$. A few sample points are plotted in Figure 2.3, showing a goldstone mode that develops an instability at finite q as the coupling g is lowered.

Once again we can look for instabilities when $\det Q(0, q) = 0$. For the condensed state, this condition turns into

$$U(q) = \frac{-\bar{\omega}_q E^2 - \mu\bar{\xi}^2}{2\bar{\omega}_q |\psi_0|^2 \mu}. \tag{2.14}$$

One can consider a "mean-field" limit that the photon mass $m \to 0$, or perhaps more simply that the q of the instability is much greater than any q where any interesting anti-crossing is happening, and the condition simplifies to $U(q) = -E^2/2\mu|\psi_0|^2$. (That is not necessarily any more transparent - it is certainly not e.g. the energy of the lower polariton in general, and likely reflects the fact that the density polarizability Π is modulated by the condensate amplitude.)

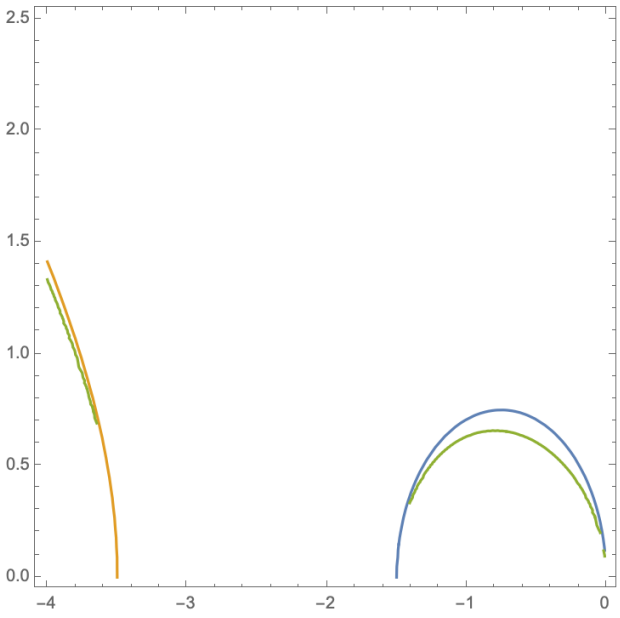

Figure 2.4: Long-wavelength instability of the condensed phase (green), and $q = 0$ instabilities of the normal state lobes (yellow and blue).

In practice one has to make an educated guess about the place where the spectrum goes soft. We begin by trying to reproduce the Mott lobes, which is a $q = 0$ gap-closing phenomenon and therefore actually a little tricky to capture numerically since there are already Goldstone modes with $\omega \to 0$ as $q \to 0$. As a hack we look for a small but finite-momentum instability in the lower polariton that occurs slightly beyond the true phase transition as an artifact. That result is shown in Figure 2.4 alongside the instabilities calculated from (2.13) and we declare the agreement good enough to move on.

Now the real treat: we make another educated guess that the nearest-neighbor interaction will be most destabilizing at $q = 1$ given our choice of parameters, and that boundary is plotted in Figure 2.5. The $m = .0001$ line is negligibly far from the "mean-field" limit above.

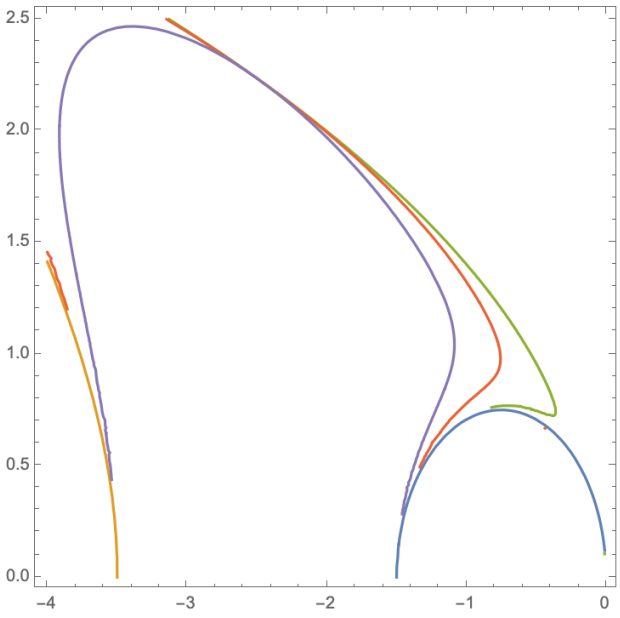

Figure 2.5: $q = 0$ instabilities of the normal state lobes (yellow and blue), and $q = 1$ instability of the uniform condensate for $m = 10$ (green), $m = 1$ (red), and $m = .0001$ (purple)

2.5 Ordered Normal State(s)

2.5.1 Mean Field

I now wish to consider mean fields with some ordering wave vector Q for the matter component. It will be convenient to rewrite the interaction terms in (2.4) as $\sum_{kk'} v_k^\dagger \cdot \mathcal{M}_{kk'} \cdot v_{k'}$ with $v_k^\dagger = \begin{pmatrix} a_k^\dagger & b_k^\dagger & a_{k+Q}^\dagger & b_{k+Q}^\dagger \end{pmatrix}$ so that in this large space the diagonal inverse propagator reads

$$(G_0)^{-1}_{kk'} = \begin{pmatrix} -i\nu_k - \xi & 0 & -|U(Q)|\phi_Q & 0 \\ 0 & -i\nu_k + \xi & 0 & |U(Q)|\phi_Q \\ -|U(Q)|\phi_Q & 0 & -i\nu_k - \xi & 0 \\ 0 & |U(Q)|\phi_Q & 0 & -i\nu_k + \xi \end{pmatrix}. \tag{2.15}$$

The free energy then reads

$$f_Q = -U(Q)\phi_Q^2 - \frac{T}{2}(\ln\cosh(\beta\bar{\xi}_+) + \ln\cosh(\beta\bar{\xi}_-)) + \frac{i\pi T}{2} - \frac{\mu}{2} \tag{2.16}$$

where $\bar{\xi}_\pm = -\frac{\Delta}{2} - \frac{\mu}{2} \pm |U(Q)|\phi_Q$ and the occupancy constraint again restricts $\phi_Q \in [-\frac{1}{2}, \frac{1}{2}]$. Note that in this case opposite signs of ϕ_Q are related by a $\mathbb{Z}_2$ symmetry and degenerate.

2.5.2 Fluctuations

This time we will proceed directly to using the fluctuations to compute the spectrum and the phase boundary. I'm still going to consider only the three types of fluctuations $\delta\psi_q^\dagger, \delta\psi_{-q}, \delta\phi_q$ so that as in (2.12) there will be a 3×3 flucuation matrix Q. That will be computed in the same 4×4 space as (2.15) using

$$\Delta_{kk'} = \sum_q \begin{pmatrix} 0 & g\delta\psi_{-q}^\dagger & -|U(q)|\delta\phi_{-q} & 0 \\ g\delta\psi_q & 0 & 0 & |U(q)|\delta\phi_{-q} \\ -|U(q)|\delta\phi_{-q} & 0 & 0 & g\delta\psi_{-q}^\dagger \\ 0 & |U(q)|\delta\phi_{-q} & g\delta\psi_q & 0 \end{pmatrix} \delta_{k,k'-q} \tag{2.17}$$

to obtain

$$T\mathrm{tr}(G_0\Delta G_0\Delta) = \begin{pmatrix} \delta\psi_q^\dagger \\ \delta\psi_{-q} \\ \phi_q \end{pmatrix}^T \begin{pmatrix} K_Q^- & 0 & 0 \\ 0 & K_Q^+ & 0 \\ 0 & 0 & 0 \end{pmatrix} \begin{pmatrix} \psi_q \\ \psi_{-q}^\dagger \\ \phi_{-q} \end{pmatrix} \tag{2.18}$$

where

$$K_Q^- = g^2 \left(\frac{\tanh(\beta(\xi - |U(Q)|\phi_Q))}{i\omega_q - \xi + |U(Q)|\phi_Q} - \frac{\tanh(\beta(\xi + |U(Q)|\phi_Q))}{-i\omega_q + \xi + |U(Q)|\phi_Q} \right) \tag{2.19}$$

$$K_Q^+ = g^2 \left(-\frac{\tanh(\beta(\xi - |U(Q)|\phi_Q))}{i\omega_q + \xi - |U(Q)|\phi_Q} + \frac{\tanh(\beta(\xi + |U(Q)|\phi_Q))}{-i\omega_q - \xi - |U(Q)|\phi_Q} \right) \tag{2.20}$$

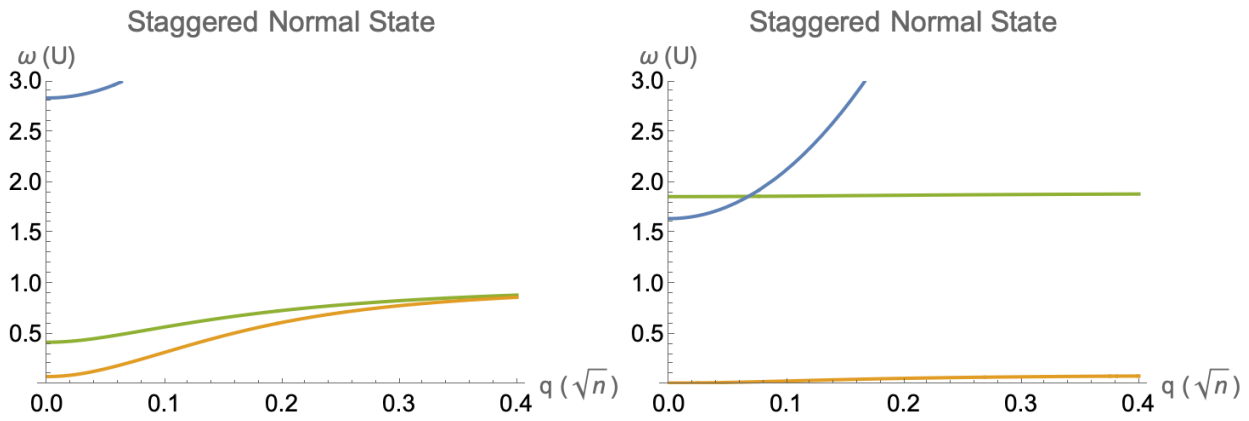

Figure 2.6: Staggered state spectrum at $T = 0$. Left: $\mu = -2.5, g = 1.55$, close to the instability to condensation in the middle of the lobe. Right: $\mu = -1.6, g = .5$, close to the $\phi_0 = 1/2$ state (via a sliver of condensate again).

and in the zero-temperature limit

$$K_Q^{\pm} = \frac{2g^2|U(Q)|\phi_Q}{(i\omega_q \pm 2\xi - 2|U(Q)|\phi_Q)(i\omega_q \pm 2\xi + 2|U(Q)|\phi_Q)}. \tag{2.21}$$

In taking the zero-temperature limit there is one small subtlety in picking the sign of $\tanh(\beta(\xi - |U(Q)|\phi_Q))$. In our units $|U(Q)|\phi_Q = \frac{1}{2}$, and from the phase diagram it is clear that the mott lobe for this state is bounded by $\mu = -\Delta \pm 1$.

So the normal state retains the property that the photon creation and annihilation fluctuations do not mix, as the ground state photon occupancy is zero, and the matter component continues to have no polarizability in the absence of a condensate.

Spectra for this state are shown in Figure 2.6. Now there are two lower polaritons on different sublattices, which in the center of the lobe are nearly degenerate with an excitation energy of U and split as the chemical potential moves. Near the edges of the lobe there is always a $q = 0$ instability to a condensate.

The instability of this state can also be diagnosed by $\det Q(0, q) = 0$ and that is used in Figure 2.7 to fill out the phase diagram so far. The big deal is that the uniform condensate and staggered normal state instability lines are most certainly different, signalling the

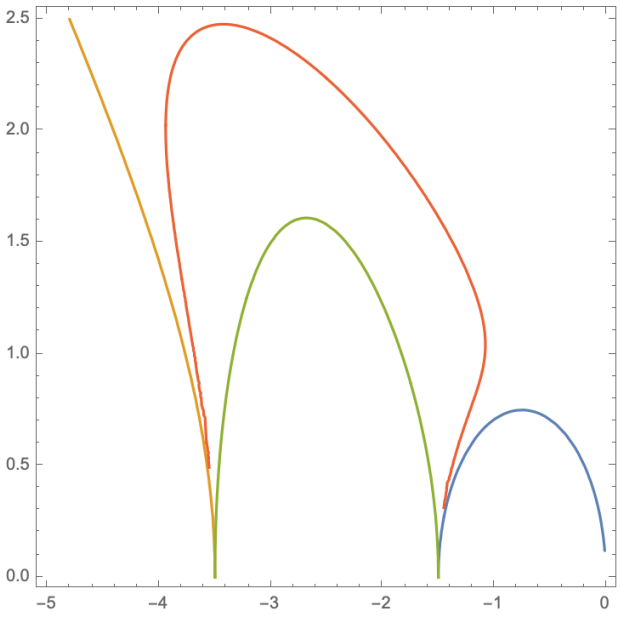

Figure 2.7: Instability lines of the states $\phi_0 = -1/2$ (yellow), $\phi_Q = 1/2$ (green), $\phi_0 = 1/2$ (blue), and the finite $|\psi_0|$ uniform condensate (red) with photon mass $m = .01$.

presence of a supersolid state in the middle.

2.6 Triangular Moiré Lattice

For nearest-neighbor interactions only, the lattice matters only insofar as there is some coordination number that can be absorbed into U and some preferred directions are implicit in the spectra above.

Now, to add in interactions beyond nearest neighbor, I will specialize to the triangular lattice on which the Moiré excitons live. Including next-nearest neighbors, the potential in momentum space can be written

$$\begin{aligned} U(\mathbf{k}) = \; & U\left(\cos(k_x a) + \cos((k_x + \sqrt{3}k_y)a/2) + \cos((k_x - \sqrt{3}k_y)a/2)\right) + \\ & U'\left(\cos(\sqrt{3}k_y a) + \cos((3k_x + \sqrt{3}k_y)a/2) + \cos((3k_x - \sqrt{3}k_y)a/2)\right) \end{aligned} . \tag{2.22}$$

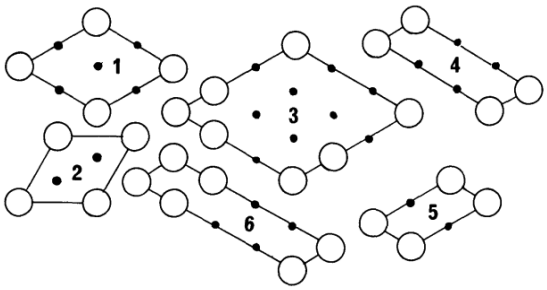

Figure 2.8: Configurations on a triangular lattice with NN+NNN interactions, from Kaburagi and Kanamori. We will be interested in 1, 2, and 5.

I will assume a dipolar exciton-exciton interaction, $U \sim 1/r^3$, so that $U' = U/3\sqrt{3} \approx .19U$. Unfortunately that just barely satisfies the criterion of Kaburagi and Kanamori that for a lattice gas on a triangular lattice with $J_1 > 5J_2 > 0$, there are quarter-, third-, and half-filled structures between filling zero and one, corresponding to the configurations 1, 2, and 5 in Figure 2.8.

2.6.1 Sublattice Formalism

In the special case of half filling it was appropriate to consider the CDW-like order paramater $\phi(Q)$ whose extrema coincide with lattice sites. This is in general not the case, as for instance illustrated in Figure 2.9, which shows a CDW configuration with ordering vectors given by $Q_y = \frac{2}{\sqrt{3}}\pi$ and its two C_3 rotations. Here the empty lattice sites fall in the saddles rather than the minima of the CDW, and higher harmonics would be required to realize the desired state. (As the excitons are dispersionless, there is no gradient term in the CDW and therefore no physical reason to favor longer-wavelength structures.)

Instead I will explicitly construct separate order parameters for the different sublattices in a given configuration, with $1/n$ filling generally requiring n sublattices. For instance, to recapitulate the 1D CDW result in this language we can rewrite the quadratic terms in the decoupled Hamiltonian as $\sum_k kk' v_k^\dagger \cdot \mathcal{M}_{kk'} \cdot v_k^\dagger$ where now $v_k^\dagger = \begin{pmatrix} a_{k1}^\dagger & b_{k1}^\dagger & a_{k2}^\dagger & b_{k2}^\dagger \end{pmatrix}$

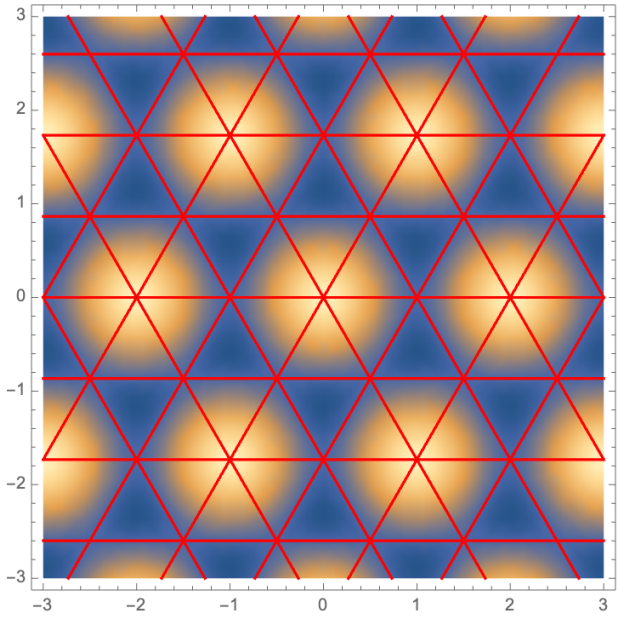

Figure 2.9: Red: planes of superlattice sites. Color: density of simplest 2D CDW with the same symmetry as configuration 1.

and the second label on each operator labeling the sublattices. Then the noninteracting propagator is

$$(G_0)^{-1}_{kk'} = \text{diag}\left(\begin{array}{cccc} -i\nu_k - \xi - U_0\phi_2 & -i\nu_k + \xi + U_0\phi_2 & -i\nu_k - \xi - U_0\phi_1 & -i\nu_k + \xi + U_0\phi_1 \end{array} \right) \tag{2.23}$$

where $\phi_i \equiv \langle \frac{1}{2}\frac{1}{N}\sum_k (b^\dagger_{ki} b_{k+q,i} - a^\dagger_{ki} a_{k+q,i}) \rangle$ is the density order parameter on sublattice i. Compared to (2.15), the interactions become shifts of the on-site energies on each sublattice. To compute fluctuations, I introduce separate fluctuations $\delta\phi_{qi}$ for each order parameter, while the photon fluctuations $\delta\psi_q$ appear on the off-diagonals of a single sublattice and do not couple different sublattice sectors. The same stability analysis reproduces the phase diagram of Figure 2.7.

The generalization to the more complicated states that arise in the case of the triangular Moiré lattice with longer-range interactions is straightforward. $(G_0)^{-1}$ with n sublattices will be enlarged but will remain diagonal, with the effects of longer-range interactions simply incorporated into an appropriate on-site energy shift. Since the photons do not couple sublattices, the fluctuations matrix $\Delta_{kk'}$ will likewise be enlarged but will remain tridiagonal, and in the normal state the contribution of the fluctuations to the free energy will be of the from

$$T\mathrm{tr}(G_0\Delta G_0\Delta) = \begin{pmatrix} \delta\psi_q^\dagger \\ \delta\psi_{-q} \\ \delta\mathbf{\Phi}_q \end{pmatrix}^T \begin{pmatrix} K_n & 0 & 0 \\ 0 & K_n^* & 0 \\ 0 & 0 & \mathbf{\Pi} \end{pmatrix} \begin{pmatrix} \psi_q \\ \psi_{-q}^\dagger \\ \delta\mathbf{\Phi}_{-q} \end{pmatrix} \tag{2.24}$$

where $\delta\mathbf{\Phi}_q$ is a vector of the $\delta\phi_{qi}$ and in the normal state all the elements of the block $\mathbf{\Pi}$ are zero. In the enlarged fluctuation matrix Q there will be some more complicated structure of static interactions between the $\delta\phi$ fields but as before, they will carry no dynamics in the normal state and the stability of the normal state will be determined by K_n, which can be written

$$K_n = \frac{1}{n}\sum_i^n \frac{\tanh(\beta(\xi + U_i(\{\phi\}))}{-i\omega_q + 2(\xi + U_i(\{\phi\}))} \tag{2.25}$$

where $U_i(\{\phi\})$ is the on-site energy shift of sublattice i due to interactions with the other sublattices.

With this recipe (and (2.14) recomputed to use the interaction (2.22) and an appropriate Hartree shift for the uniform state), a phase diagram on the Moiré superlattice can be computed and is shown in Figure 2.10. As before, the unfilled and fully filled Mott lobes give way to a uniform condensed state through second-order transitions, while the condensed state has an instability to supersolidity in the chemical potential region where the interaction splits the Mott lobes. The energy-minimizing symmetry of the supersolid has not been determined

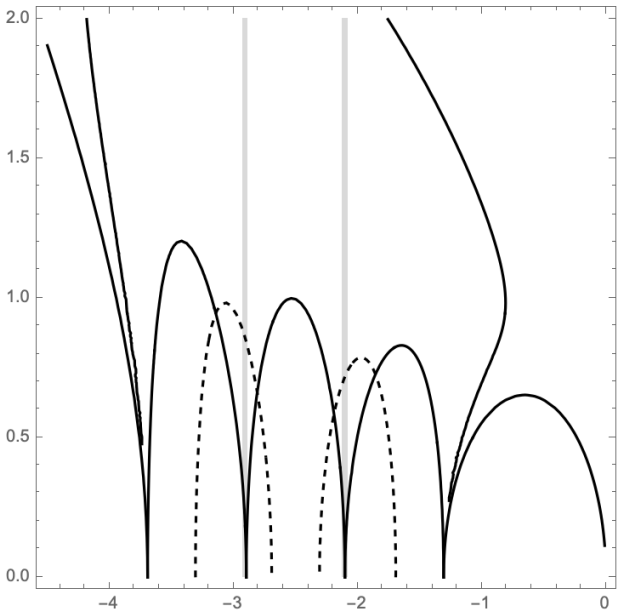

Figure 2.10: Phase diagram for the Moiré superlattice. The solid lobes touching the $g = 0$ axis are, from the left, fillings of 0, 1/4, 1/2, 3/4, and 1. The dashed lobes are at fillings 1/3 and 2/3, and the gray areas mark regions where a $g = 0$ ground state with this symmetry is energetically favored.

here but it is most likely that of the quarter-filled "1" state, with the occupations of the sublattices tuned continuously. At smaller coupling g the supersolid is unstable to states with filling $n/4$. Additionally, as shown with dashed lines, there are two regions of chemical potential at small g where $n/3$-filled states with "2" symmetry are stable, but a transition to these would be first-order. Compared to the other normal states these are only energetically favored in the extremely narrow regions of chemical potential, shaded gray, where the system is nearly indifferent between possible fillings of the other symmetry.

2.7 Discussion and Experimental Signatures

The inclusion of longer-range interactions will stabilize further normal states at intermediate fillings, eventually forming a two-dimensional analog of the devil's staircase (Dublenych [2009]), although given the rapid fall-off of the dipolar interaction and the already narrow

range of chemical potentials that favors the $p/3$ phases, we expect these to be difficult to observe. As seen already with second-neighbor interactions in Figure 2.10, phases with larger regions of stability at $g = 0$ penetrate deeper into the supersolid regime (up to the overall effect of larger chemical potential favoring condensation), and we expect the supersolid to accordingly inherit the symmetry of these phases.

The clearest spectral signature of a spatially ordered phase in our model is the splitting by the interaction of the lower polariton into distinct modes on each sublattice. (We note that the middle polaritons observed in (Lai et al. [2007]) come from the presence of both inter- and intra-layer Moiré excitons, a distinct effect that we have not considered here.) Spectra are computed relative to the chemical potential. Experimentally the density is controlled by pumping the system, and the blue shift of the resulting emission provides a measure of the chemical potential. At $g = 0$, $\mu(\rho)$ (where $\rho = \frac{1}{2} + \phi + |\psi|^2$ is the density) will exhibit a series of jumps as the system transitions between states of different filling. This effect was already predicted in (Eastham and Littlewood [2000]) for the transition between homogeneous fully polarized states. At finite g, the transitions between normal states and regions of the phase diagram with superfluid order will instead be marked by kinks in $\mu(\rho)$, which will then change continuously in the presence of a superfluid.

The visibility of these effects is attenuated by noise sources including inhomogeneous broadening of the excitons, thermal effects, and non-equilibrium physics associated with the driven-dissipative nature of the system. The energy scale on which these signatures appear is set by the nearest-neighbor coupling strength, which in the experiments of (Zhang et al. [2021]) is $U_0 \sim .5\,\mathrm{meV}$, compared to an exciton inhomogeneous broadening of $\sim 8\,\mathrm{meV}$ and cavity linewidth of $\sim 3\,\mathrm{meV}$, and on the same order as the thermal energy at $5\,\mathrm{K}$. To achieve strong coupling the Rabi splitting must be larger than these, and indeed with $\Omega \sim 10\,\mathrm{meV}$ locates the experiment in a region of the phase diagram where only a phase transition from a completely polarized normal state to a uniform condensate is expected. From the measured

cavity dispersion we have extracted $m \sim 10^{-5} m_e$, or $m^* \sim 10^{-6}$, firmly within the mean-field regime. Condensation phenomena are not yet evident in the Moiré polariton system, although they have been achieved in monolayer TMDs (Zhao et al. [2021]).

2.8 Conclusions

We have proposed a simple model that realizes a polariton supersolid phase and may be within reach of present experiments. Our model is closely related to the lattice supersolid phases of hard-core bosons, as realized for instance in an ultracold atomic gas in an optical lattice or helium adsorbed on graphite (Baumann et al. [2010], Choi et al. [2021]). Our model differs in that what would ordinarily be an off-diagonal order parameter in the matter field is here the photon field, imbued with its own dynamics, leading to a reentrant phase diagram. We expect that this would be substantially enriched as the Moiré lattice spacing is increased to become comparable to the photon wavelength, as on the one hand the importance of the exciton-exciton interaction is enhanced by diluteness, and on the other it becomes energetically possible for the light field to condense in a state with a density modulation commensurate with the cavity. In contrast to polariton band structures in which condensation away from $k = 0$ appears as a metastable non-equilibrium effect, the constraint of a single emitter per lattice site would make such supersolids possible in equilibrium. The model is possibly also of relevance to self-organized lattices, for instance due to blockade effects in Rydberg excitons (Kazimierczuk et al. [2014], Bao et al. [2019]).

CHAPTER 3

NORMAL STATE PROPERTIES OF STRONTIUM TITANATE

3.1 Introduction

Strontium titanate, $SrTiO_3$, is a cubic perovskite wide band gap semiconductor which at low temperatures approaches a ferroelectric phase transition but instead saturates at a dielectric constant $\epsilon_0 \sim 2 \times 10^4$, reflecting the presence of an extremely soft transverse optic (TO) phonon (Müller and Burkard [1979], Coak et al. [2018]). Against this background of quantum criticality, when lightly doped the material hosts a plethora of interesting phenomena, including Fermi liquid-like resistivity above the Fermi temperature (Lin et al. [2017]), phonon hydrodynamics (Martelli et al. [2018]), and a superconducting dome spanning electron densities from 10^{17} to 10^{21}cm^{-3} (Schooley et al. [1964], Lin et al. [2013b], Bretz-Sullivan et al. [2019]), with a transition temperature peaking around 300mK, on the order of 1% of the Fermi energy (E_F), comparable to the high-T_C materials. The superconducting state nevertheless appears to be s-wave and weakly coupled, with a BCS-like Δ/T_C ratio (Thiemann et al. [2018], Yoon et al. [2021]).

It has long been known that conventional pairing by acoustic phonons cannot explain the observed behavior, and superconductivity in $SrTiO_3$ has thus spurred great theoretical creativity, both historically and very recently (Koonce et al. [1967], Gastiasoro et al. [2020], Volkov et al. [2021], Kanasugi et al. [2020], Wölfle and Balatsky [2018], Dunnett et al. [2017], Arce-Gamboa and Guzman-Verri [2018], Kedem et al. [2016], Marel et al. [2019]). Here we will focus on a particular class of theories, pioneered by Takada (Takada [1980]), which involve the electron gas coupling to a longitudinal optic (LO) phonon mode (Klimin et al. [2016], Rowley et al. [2018], Ruhman and Lee [2016], Gastiasoro et al. [2019], Gor'kov [2016]). These theories face the difficulty that the coupling to this mode is of the same long-range Coulomb character as the repulsion between the electrons, and the two effects must

therefore be treated on an equal footing. An additional problem as that the LO frequency $\Omega \gg E_F$. As pointed out by (Swartz et al. [2018]), a naive calculation of the BCS coupling constant due to the LO phonon far exceeds the value measured in the superconducting state. Although the elecron-phonon coupling strength in the sense of the Frölich coupling constant $\alpha \sim 2$ (Devreese et al. [2010]) is intermediate at best, both photoemission (Wang et al. [2016]) and tunneling (Yoon et al. [2021], Swartz et al. [2018]) experiments reveal substantial spectral weight in "replica" bands, showing phonon effects beyond a simple quasiparticle mass renormalization.

In this work we attempt to reproduce these observations by studying the normal-state properties of the class of theories discussed above. We treat the Coulombic electron-phonon and electron-electron interactions on equal footing, and employ the cumulant expansion (Kas et al. [2014]) to incorporate the effects of multiple electron-boson interactions. Our main results are illustrated by the spectral function and density of states in Figures 3.1 and 3.2: although our formalism generates replica bands and qualitatively matches the experimental observation that they become weaker and more diffuse as the electron density is increased, we find that they occur at energies corresponding to the *coupled* modes of the LO phonon and the collective response of the electron gas, which evolve with density. This is in glaring contrast to the experiments, which always find them fixed at the bare LO phonon energy.

3.2 Model

We treat the Hamiltonian $H = H_0 + H_{\text{int}}$ with

$$\begin{aligned} H_0 &= \sum_{\mathbf{k}} c^\dagger_{\mathbf{k}} \xi_{\mathbf{k}} c_{\mathbf{k}} + \Omega \sum_{\mathbf{k}} b^\dagger_{\mathbf{k}} b_{\mathbf{k}} \\ H_{\text{int}} &= \sum_{\mathbf{q}} g_{\mathbf{q}} \rho_{\mathbf{q}} (b_{\mathbf{q}} + b^\dagger_{-\mathbf{q}}) + \sum_{\mathbf{q}} V_c(\mathbf{q}) \rho_{\mathbf{q}} \rho_{-\mathbf{q}}. \end{aligned} \tag{3.1}$$

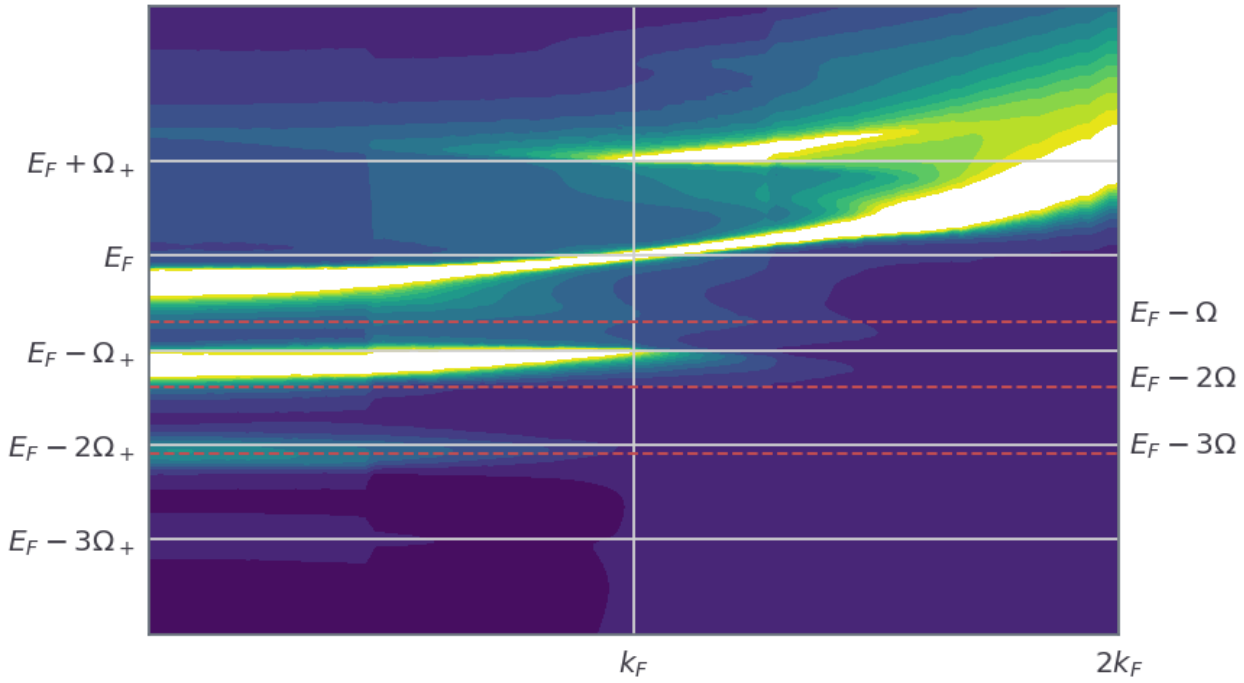

Figure 3.1: Spectral function $A(\mathbf{k}, \omega)$ for $SrTiO_3$ parameters with $n = 5 \times 10^{19}\text{cm}^{-3}$. Solid and dashed horizontal lines are offset from the Fermi surface in multiples of the coupled mode frequency Ω_+ and bare phonon frequency Ω, respectively.

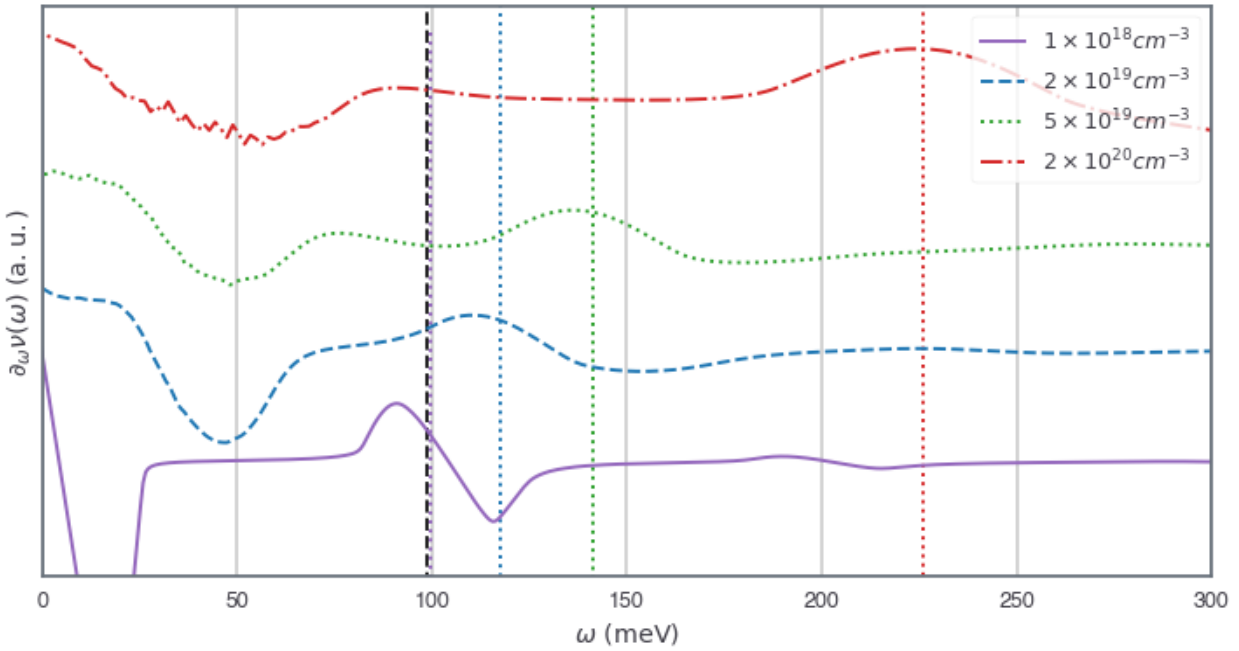

Figure 3.2: First energy derivative of the computed density of states at different carrier densities. The vertical dashed line is the phonon energy, and the vertical dotted lines are Ω_+ at each density

H_0 describes a single band of electrons with isotropic dispersion $\xi_{\mathbf{k}} = k^2/2m - \mu$, where μ is the chemical potential, and an Einstein LO phonon with frequency Ω. Although $SrTiO_3$ has between one and three occupied conduction electron bands at experimentally accessible densities (Marel et al. [2011], Lin et al. [2015b]) and there is possibly some trace of their sequential filling in the superconducting phase diagram, inter-band scattering is large and superconductivity is single-gap (Thiemann et al. [2018]), so we think a single band adequate to model the essential physics. There are likewise multiple phonons but the coupling of electrons to the LO mode near $\Omega = 100$meV is by far the strongest. This coupling is captured in the first, Frölich term of H_{int}, where $\rho_{\mathbf{q}} = \sum_{\mathbf{k}} c^\dagger_{\mathbf{k}} c_{\mathbf{k}+\mathbf{q}}$ is the electron density operator at momentum $\mathbf{q}$ and the coupling $g^2_{\mathbf{q}} = \Omega\gamma\lambda/q^2$ is parameterized in terms of the long-range Coulomb coupling constant $\lambda = 4\pi e^2/\epsilon_\infty$ and a dimensionless parameter γ which characterizes the stiffness of the TO modes that are present but do not couple to the electrons. The second term in H_{int} is the repulsive electron-electron interaction, where $V_c = \lambda/q^2$ is the same long-range Coulomb coupling that appears in the Frölich term. In total this model is controlled by three parameters. The electron gas parameter $r_s = (\frac{4\pi}{3}n)^{-1/3}/a_B$ where n is the density and $a_B = \frac{\hbar^2\epsilon_\infty}{me^2}$ is the effective Bohr radius, which we mean in the sense of the optical dielectric constant $\epsilon_\infty = 5.44$; the large static dielectric constant from the softening TO is an output in this formalism. $SrTiO_3$ in this sense is quite dilute, with $r_s \sim 5$ at optimal doping, $n \sim 10^{20}\text{cm}^{-3}$ and as high as 40 at $n \sim 10^{17}\text{cm}^{-3}$, if such low-density samples are in fact uniform. The phonon frequency $\Omega_{\text{LO4}} = 100$meV enters through an adiabaticity parameter Ω/E_F, where E_F is the Fermi energy; this parameter only drops into the adiabatic regime beyond $n = 1.3 \times 10^{17}\text{cm}^{-3}$. Finally, γ ranges from 0 for an uncoupled system to $\frac{1}{2}$ when the TO mode softens completely and can be thought of as a measure of proximity to ferroelectricity. In an ionic crystal with a rock salt structure, $\gamma = (1/\epsilon_\infty - 1/\epsilon_0)/2$, but it is possible to straightforwardly generalize to the multi-phonon system, where $\sum_s \gamma_s$ plays the same role, and γ_s can readily be extracted from e.g. reflectivity measurements

for each LO mode s (Toyozawa [1972]). We choose to use $\gamma = .4995$ from the measured values of ϵ_0, as if the entirety of $SrTiO_3$'s large permittivity and electron-phonon coupling were attributable to a single LO-TO pair. A different choice does not qualitatively change our conclusions. We would like to emphasize that all of these parameters are in principle experimentally determined, and because the Fröhlich and Coulomb interactions are treated on an equal footing, there is no way within our model to independently tune the electron-phonon coupling strength without side-effects.

For comparison to experiments, we are interested in computing the spectral function at momentum k and energy ω

$$A(\mathbf{k}, \omega) = -\frac{1}{\pi}\mathrm{Im}G^R(\mathbf{k}, \omega) \tag{3.2}$$

where G^R is the retarded Green function. We begin by obtaining the leading-order effective electron-electron interaction,

$$V_{\text{eff}}(\mathbf{q}, \omega) = \frac{V_c(\mathbf{q}) + V_p(\mathbf{q}, \omega)}{1 + \Pi(\mathbf{q}, \omega)(V_c(\mathbf{q}) + V_p(\mathbf{q}, \omega))} \tag{3.3}$$

where $V_p = 2g_{\mathbf{q}}^2\Omega/(\omega^2 - \Omega^2)$ is the phonon-mediated interaction and $\Pi(\mathbf{q}, \omega)$ is the polarizability within the random phase approximation (RPA) (Giuliani and Vignale [2005]). (3.3) can equivalently be obtained by integrating out the phonons and electron density fluctuations to Gaussian order from (3.1), performing a resummation of the bubble-type diagrams, or assuming assuming a dielectric function $\epsilon(\mathbf{q}, \omega) = \epsilon_\infty + \epsilon_{\text{e-ph}} - V_c(\mathbf{q})\Pi(\mathbf{q}, \omega)$ where $\epsilon_{\text{e-ph}} = (\epsilon_0 - \epsilon_\infty)/(1 - \omega^2/\Omega_{\text{TO}}^2)$ is the dieelctric function of a polar crystal with TO frequency determined by the Lyddane-Sachs-Teller relation $\Omega_{\text{LO}}^2/\Omega_{\text{TO}}^2 = \epsilon_0/\epsilon_\infty$ (Mahan [2000], Lyddane et al. [1941]).

We next compute the one-loop "G_0W_0" self-energy,

$$\Sigma_0(\mathbf{k}, \omega) = \sum_{\mathbf{q}} \int \frac{d\omega'}{2\pi} G_0(\omega + \omega', \mathbf{k} + \mathbf{q}) V_{\text{eff}}(\mathbf{q}, \omega') \tag{3.4}$$

where $G_0(\mathbf{k},\omega) = (\omega - \xi_{\mathbf{k}} + i\delta)^{-1}$ is the free electron propagator. All computations are performed with $\delta = .001E_F$. The integrals are split up just as in (Hedin [1965]), and properties of this model for other semiconductors were already studied at this level by (Kim et al. [1978]). We next employ the retarded cumulant expansion of (Kas et al. [2014]) to obtain $G^R(\mathbf{k},\omega)$ by Fourier transforming after computing in the time domain

$$\begin{aligned} G^R(\mathbf{k},t) &= -i\theta(t)\exp(-i\tilde{\xi}_{\mathbf{k}}t)\exp(C^R(\mathbf{k},t)) \\ C^R(\mathbf{k},t) &= \int \frac{d\omega}{\pi}\frac{|\mathrm{Im}\Sigma_0(\mathbf{k},\omega+\epsilon_{\mathbf{k}})|}{\omega^2}(e^{-i\omega t}-1) \end{aligned} \tag{3.5}$$

where $\tilde{\xi}_{\mathbf{k}} = \epsilon_k + \mathrm{Re}\Sigma_0(\mathbf{k},\epsilon_{\mathbf{k}})$ is the modified dispersion obtained from the one-loop calculation of Σ_0. Diagrammatically the cumulant expansion can be thought of as a partial resummation which uses the result of the one-loop self-energy to include rainbow diagrams and some crossing diagrams (Gunnarsson [1994]). Although it is known to differ from more numerically accurate treatments of the electron gas for system sizes where those are available (McClain et al. [2015]), we chose this approximation for its one-shot generation of all replica bands (with spectral weight in each replica matching exact calculations in the limit of momentum-independent coupling to dispersionless bosons), and for its correct placement of those replicas relative to the renormalized bands, at minimal computational effort beyond G_0W_0.

3.2.1 Treating multiple phonon modes

For a material such as STO with non-neglible coupling to multiple phonon modes, there is some ambiguity as to what choices of parameter one should make to compare to a single-phonon model. In brief, the choices I have made amount to absorbing all of the phonon oscillator strength in the material into a single phonon, but here I wish to make slightly more precise how I think about this problem. Much of this discussion I owe to (Toyozawa [1972]), while the coupling to electrons I have found more convenient to do in the language

of functional integrals.

Phonon contribution to the dielectric function

The equations of motion in momentum space for the ions in a crystal are

$$M_\nu \ddot{\mathbf{x}}_\nu + \sum_{\mu=1}^{N} U_{\nu\mu}(\mathbf{q})\mathbf{x}_\mu = Z_\nu \mathbf{E} \tag{3.6}$$

where M_ν and Z_ν are respectively the effective mass and charge of ion ν, $\mathbf{x}_\nu$ is its displacement, $U_{\nu\mu}(\mathbf{q})$ is the dynamical matrix (or very nearly) at wave vector $\mathbf{q}$, and $\mathbf{E}$ is the (total, real) electric field in the unit cell with N ions. Taking first the (possibly fictitious) homogeneous case $\mathbf{E} = 0$ obtains eigenmodes indexed by $s = 1, \ldots, 3N$ with components $(\mathbf{x}_\nu)_i = \xi_{\nu i}^{s\mathbf{q}} e^{-i\Omega_{s\mathbf{q}} t}$ that satisfy

$$-M_\nu \Omega_{s\mathbf{q}}^2 \xi_\nu^{s\mathbf{q}} + \sum_{\mu=1}^{N} U_{\nu\mu}(\mathbf{q})\xi_\nu^{s\mathbf{q}} = 0 \tag{3.7}$$

which defines the eigenfrequencies $\Omega_{s\mathbf{q}}$, and obey

$$\sum_{\nu i} M_\nu \xi_{\nu i}^{s\mathbf{q}} \xi_{\nu i}^{s'\mathbf{q}} = \delta_{ss'} \tag{3.8}$$

and

$$\sum_{s} \sqrt{M_\nu M_\mu}\, \xi_{\nu i}^{s\mathbf{q}} \xi_{\mu j}^{s\mathbf{q}} = \delta_{\nu\mu}\delta_{ij} \tag{3.9}$$

Thus giving us a nice basis. Next we solve the real problem, for a driving field $E_i = E_{0i} e^{i\mathbf{q}\cdot\mathbf{r} - i\omega t}$, and assume solutions

$$x_{\nu i} = e^{i\mathbf{q}\cdot\mathbf{r} - i\omega t} \sum_s c^{s\mathbf{q}\omega} \xi_{\nu i}^{s\mathbf{q}}. \tag{3.10}$$

(Stepping back to count, the $3N$ degrees of freedom are labeled either by ion ν and direction i or by mode index s; $\xi^s_{\nu i}$ is a map between the descriptions; the forced oscillation is described by $3N$ coefficients c labeled by mode.) The c^s then obey

$$(\Omega^2_{s\mathbf{q}} - \omega^2)c^{s\mathbf{q}\omega} = \sum_{\nu i} Z_\nu \xi^{s\mathbf{q}}_{\nu i} E_i \equiv \mathbf{p}^{s\mathbf{q}} \cdot \mathbf{E} \tag{3.11}$$

where we have defined an eigenpolarization $\mathbf{p}^{s\mathbf{q}}$. The total polarization is $\mathbf{P}(\mathbf{q},\omega) = \mathcal{V} c^{s\mathbf{q}\omega} \mathbf{p}^{s\mathbf{q}}$ where $\mathcal{V}$ does the appropriate counting of unit cells, so the dielectric constant defined by $\mathbf{D} = \varepsilon\mathbf{E} = \varepsilon_\infty \mathbf{E} + 4\pi\mathbf{P}$ is

$$\varepsilon(\mathbf{q},\omega) = \varepsilon_\infty(\mathbf{q},\omega) + 4\pi\mathcal{V} \sum_s \frac{\mathbf{p}^{s\mathbf{q}} \otimes \mathbf{p}^{s\mathbf{q}}}{\Omega^2_{s\mathbf{q}} - \omega^2} \tag{3.12}$$

which is the dielectric tensor. Taking the longitudinal component, $\varepsilon_\parallel(\omega) = \mathbf{q} \cdot \varepsilon \cdot \mathbf{q}/q^2$ drags out some number σ of possibly nonzero terms, and taking the limit $q \to 0$ eliminates $\mathbf{q}$:

$$\varepsilon_\parallel = \varepsilon_{\infty\parallel} + \sum_s^\sigma \frac{\alpha^s}{\Omega^2_{s\mathbf{q}} - \omega^2} \tag{3.13}$$

so that by simple algebra this sum can be put together as

$$\frac{\varepsilon_\parallel(\omega)}{\varepsilon_{\infty\parallel}} = \prod_s^\sigma \frac{\omega_s^2 - \omega^2}{\Omega_s^2 - \omega^2} \tag{3.14}$$

This has the obvious interpretation that the transverse modes Ω_s are the fictitious field-free solutions and the poles of the dielectric function, whereas the ω_s are the true zeroes. Furthermore the ω_s are in general completely opaque roots of a high-order polynomial, and pairing them with the Ω_s is at this level of analysis completely arbitrary.

Note that this argument can be repeated at arbitrary q, and as the Ω disperse there is no reason not to expect the eigenpolarizations and thus the ω to disperse as well.

By taking the $\omega \to 0$ limit it is possible to obtain a Lyddane-Sachs-Teller relation,

$$\frac{\varepsilon_0}{\varepsilon_\infty} = \prod_s \frac{\omega_s^2}{\Omega_s^2} \tag{3.15}$$

Diatomic Cubic lattice There are six modes total, and immediately three are acoustic and cannot possibly matter. Of the three remaining optic modes, by symmetry the Ω_s are degenerate, so rearranging the sum can only give

$$\frac{\varepsilon_\parallel}{\varepsilon_{\infty\parallel}} = \frac{\omega_l^2 - \omega^2}{\Omega_t^2 - \omega^2} \tag{3.16}$$

and

$$\frac{\varepsilon_0}{\varepsilon_\infty} = \frac{\omega_l^2}{\Omega_t^2} \tag{3.17}$$

STO Just as a counting exercise, there are 5 atoms per unit cell, for 15 possible phonons. 3 are acoustic, and the cubic symmetry (at room temperature) requires three-fold degeneracy so that there remain 4 candidate LO-TO pairs. These are indeed seen experimentally so we declare victory for the moment.

Coupling to electrons

We will derive the electron-phonon coupling from linear response theory. Consider the action

$$S = \sum_{\mathbf{k}m} \bar{c}_{\mathbf{k}m}(-i\nu_m + \xi_{\mathbf{k}})c_{\mathbf{k}m} + \sum_{\mathbf{q}n} \bar{b}_{\mathbf{q}n}(-i\omega_n + \Omega)b_{\mathbf{q}n} + \sum_{\mathbf{q}mn} g_{\mathbf{q}}\rho_{\mathbf{q}}(b_{\mathbf{q}n} + \bar{b}_{-\mathbf{q}n}) \tag{3.18}$$

Integrating out the phonons generates a retarded electron-electron interaction

$$V_{\text{ph}} = \gamma \frac{\lambda}{q^2} \frac{2\Omega^2}{\omega^2 - \Omega^2} \tag{3.19}$$

from which we read off the dielectric function

$$\epsilon(\omega, \mathbf{q}) = \epsilon_\infty \left(1 + \gamma \frac{2\Omega^2}{\omega^2 - \Omega^2}\right)^{-1} \tag{3.20}$$

As desired, this goes to ϵ_∞ in the high-frequency limit and in the static limit diverges if $2\gamma = \frac{1}{\epsilon_0} - \frac{1}{\epsilon_\infty} = 1$. We can also "experimentally" extract the coupling constant from $\epsilon(\omega)$ using $\frac{\partial \epsilon}{\partial \omega}\Big|_{\omega=\Omega} = \frac{\epsilon_\infty}{\gamma\Omega}$.

In the multi-phonon case these statements generalize. The dielectric function can be written

$$\epsilon = \epsilon_\infty \left(1 + \sum_i \gamma_i \frac{2\Omega_i^2}{\omega^2 - \Omega_i^2}\right)^{-1} \tag{3.21}$$

and the condition for ϵ_0 to diverge is that $\sum_i 2\gamma_i = 1$. Meanwhile it is still true that $\frac{\partial \epsilon}{\partial \omega}\Big|_{\omega=\Omega_i} = \frac{\epsilon_\infty}{\gamma_i \Omega_i}$.

The case of STO

Taking the data compiled by Devreese for $x = .1\%$ Nb-doped STO at 7 K we have $\Omega_{TO} = 2.27,\ 21.8,\ 67.6$ meV, $\Omega_{LO} = 21.2,\ 58.4,\ 98.7$ meV and running through the fitting procedure described above (with $\epsilon_\infty = 5.44$) produces coupling constants $\gamma_i = .00191,\ .0906,\ .407$ for the three modes respectively. It should be noted that according to (3.31) (and using $m* = .81$, also after Devreese), we obtain $\alpha = .016,\ .457,\ 1.58$ which are consistent with the existing literature. Thus we have here a case in which the couplings are weak to moderate in the sense of α but not in the sense of γ. Indeed if we define a $\gamma_{\text{eff}} = \sum \gamma_i$ as a single-mode proxy for proximity to ferroelectricity, in keeping with the condition for a diverging static dielectric constant above, we have $\gamma_{\text{eff}} = .4995$ or one part in a thousand away.

3.2.2 Calculating in the RPA with phonons

Although this calculational technology has been around since the sixties and sits at the heart of many first-principles computations today, some aspects of how to perform these calculations take surprising effort to track down.

Units and quantities

It is difficult to find a civilized collection of these so we begin here. First the parameters to do with the simple coulomb-interacting electron gas. The electron gas parameter is

$$r_s = (\frac{3}{4\pi n})^{1/3}/a_B \tag{3.22}$$

and the Rydberg

$$\mathrm{Ry} = \frac{e^2}{2a_B} = \frac{\hbar^2}{2ma_B^2} \tag{3.23}$$

The Fermi momentum

$$k_F = (\frac{9\pi}{4})^{1/3}\frac{1}{r_s a_B} \tag{3.24}$$

and Fermi energy

$$E_F = (\frac{9\pi}{4})^{2/3}\frac{1}{r_s^2}\,\mathrm{Ry} \tag{3.25}$$

The plasmon is at

$$\omega_p = \sqrt{4\pi n e^2/m} = \frac{\sqrt{12}}{(9\pi/4)^{2/3}}\sqrt{r_s}E_F \tag{3.26}$$

The Thomas-Fermi wave vector is $q_{TF}^2 = \frac{6\pi e^2 n}{E_F}$, or

$$q_{TF} = 3(\frac{4}{9\pi})^{2/3}\sqrt{rs}k_F \tag{3.27}$$

(this should actually make you panic because $q_{\rm TF} \to 0$ at high densities, apparently, but that is only in comparison to k_F). As a bonus it will be useful to know that

$$\lambda k_{\rm F} = 8\pi \frac{e^2}{2a_B}(k_F a_B) = 8\pi(\frac{9\pi}{4})^{1/3}\frac{\rm Ry}{r_S} = 8(\frac{2\pi}{3})^{2/3} r_s E_{\rm F} \tag{3.28}$$

Next, adding the coupling to the LO phonon, its matrix element is

$$g_q^2 = \frac{1}{2}\frac{4\pi e^2}{q^2}\Omega(\frac{1}{\varepsilon_\infty} - \frac{1}{\varepsilon_0}) \tag{3.29}$$

which we nondimensionalize as

$$g_q^2 = \frac{\lambda}{(q/k_F)^2}\gamma\frac{\Omega}{E_F} \tag{3.30}$$

where $\gamma = \frac{1}{2}(1 - \frac{\epsilon_\infty}{\epsilon_0})$ and we have assumed that λ is expressed in units of the optical dielectric constant.

Unfortunately this is not the quantity frequently cited in the literature, which instead considers

$$\alpha = \frac{e^2}{\hbar}\sqrt{\frac{m}{2\hbar\Omega}}(\frac{1}{\epsilon_\infty} - \frac{1}{\epsilon_0}) = \frac{2}{\epsilon_\infty}\frac{e^2}{\hbar}\sqrt{\frac{m_e}{2\,\text{meV}}}\sqrt{\frac{m^*}{\Omega/\,\text{meV}}}\gamma = 42.88\sqrt{\frac{m^*}{\Omega/\,\text{meV}}}\gamma \tag{3.31}$$

where I have used the STO value of $\epsilon_\infty = 5.44$.

The effective electron-electron interaction

At first glance it is not clear what the combined influence of the electron-electron and electron-phonon interactions will be in the RPA. Wiser minds have pointed out that the result must just be the Coulomb interaction divided by a dielectric function that is the sum of the individual dielectric functions due to the phonons, the electrons in the RPA, and high-energy processes (i.e. ϵ_∞). This will indeed turn out to be the case, but I would like to demonstrate that diagramatically for this case and then point out a limitation of this kind

of thinking.

Rewriting the model Hamiltonian as an action,

$$S = \sum_{\mathbf{k}} \bar{c}_{\mathbf{k}}(-i\nu + \xi_{\mathbf{k}})c_{\mathbf{k}} + \sum_{\mathbf{q}} \bar{b}_{\mathbf{q}}(-i\omega + \Omega)b_{\mathbf{q}} + \sum_{\mathbf{kq}} g_{\mathbf{q}}\rho_{\mathbf{q}}(b_{\mathbf{q}} + \bar{b}_{-\mathbf{q}}) + \sum_{\mathbf{q}} \frac{\lambda}{\mathbf{q}^2}\rho_{\mathbf{q}}\rho_{-\mathbf{q}}, \quad (3.32)$$

we consider diagrams to construct an effective electron-electron interaction:

1. A bare interaction line contributes just $\frac{\lambda}{\mathbf{q}^2}$.
2. A phonon line contributes $g_{\mathbf{q}}^2 \frac{2\Omega}{\omega^2 - \Omega^2}$.
3. A polarization bubble contributes $\Pi(\omega, \mathbf{q})$, the Lindhard function.

Diagrams with n polarization bubbles will have $n+1$ lines. The 2^{n+1} different ways to arrange them correspond precisely to the expansion of $((1) + (2))^{n+1}$, so that each such diagram contributes $(3)^n((1) + (2))^{n+1}$. Thus

$$V_{\text{eff}} = \sum_{n=0} (3)^n((1) + (2))^{n+1} = ((1) + (2)) \sum_n ((3)((1) + (2)))^n = \frac{(1) + (2)}{1 - (3)((1) + (2))} \quad (3.33)$$

$$V_{\text{eff}}(\omega, \mathbf{q}) = \frac{\lambda/\mathbf{q}^2 + 2g_{\mathbf{q}}^2\Omega/(\omega^2 - \Omega^2)}{1 - \Pi(\omega, \mathbf{q})(\lambda/\mathbf{q}^2 + 2g_{\mathbf{q}}^2\Omega/(\omega^2 - \Omega^2))}$$

Or the dielectric function is

$$\epsilon(\omega, \mathbf{q}) = \frac{\lambda/\mathbf{q}^2}{\lambda/\mathbf{q}^2 + 2g_{\mathbf{q}}^2\Omega/(\omega^2 - \Omega^2)} - \frac{\lambda}{\mathbf{q}^2}\Pi(\omega, \mathbf{q}) \quad (3.34)$$

An intuitive but misleading transformations Particularly in numerical calculations (but not only), one often encounters a desire to separate out the electron-electron piece from the electron-phonon piece so that different contributions to the self-energy may be calculated by specialized methods, or simply as a way to isolate the effects of different physical processes. For instance, it is very common to see an electron-phonon vertex modified ad-hoc

to incorporate a Thomas-Fermi screening length. Here I wish to remark on the limitations of such a procedure outside of a specific approxmation like that.

One can separate out the screened electronic piece and whatever's left as

$$V_{\text{eff}} = \frac{1}{\epsilon_{\text{RPA}}} \frac{\lambda}{\mathbf{q}^2} + \frac{g_{\mathbf{q}}^2}{\epsilon_{\text{RPA}}^2} D^{\text{eff}} \tag{3.35}$$

where

$$D^{\text{eff}} = \frac{2\Omega}{\omega^2 - \Omega^2 - 2g_{\mathbf{q}}^2 \Omega \Pi / \epsilon_{\text{RPA}}} \tag{3.36}$$

So for a self-energy, one expects something like

$$\Sigma(p) = \Sigma^{\text{RPA}} + i \int \frac{d^4q}{(2\pi)^4} \frac{g_{\mathbf{q}}^2}{\epsilon_{\text{RPA}}^2} G^0(p+q) D^{\text{eff}}(q), \tag{3.37}$$

where

- Σ^{RPA} is the self-energy from just the RPA treatment of the Coulomb interaction,
- D^{eff} is a "bare screened" phonon propagator and does not represent any sort of self-consistent result, and
- $g_{\mathbf{q}}/\epsilon_{\text{RPA}}$ is a "bare screened" electron-phonon vertex which appears twice; the division by ϵ_{RPA} should not be interpreted as any sort of vertex correction to the bare $g_{\mathbf{q}}$.

It is important to note, however, that these two terms inevitably contain bits of different order in e^2 (which is an expansion parameter for better or worse). In practice (at least in some analytic limits we've considered) this leads to unphysical results like double-counted plasmon modes, which a consistent calculation would cancel. Therefore we do not work with this form.

Analytic Limits

The electron self-energy takes on some appealingly simple forms in the extremely dilute or extremely dense limits, which serve both to illuminate the physics and as sanity checks on the numerics.

Plasmon Pole: $r_s \gg 1$ The contribution of the electron gas is dominated by the plasmon at frequency ω_p, so $\Pi_{\text{RPA}} \to \frac{q^2}{\lambda}\frac{\omega_p^2}{\omega^2}$. Doing out the math, one finds

$$V_{\text{eff}} \to \frac{\lambda}{q^2}\frac{\omega^2(\omega^2 + (2\gamma - 1)\Omega^2)}{(\omega^2 - \omega_+^2)(\omega^2 - \omega_-^2)} \tag{3.38}$$

where the hybrid plasmon-phonon mode frequencies are

$$\omega_\pm^2 = \frac{1}{2}(\Omega^2 + \omega_p^2 \pm \sqrt{\Omega^4 + \omega_p^4 + (8\gamma - 2)\Omega^2\omega_p^2}) \tag{3.39}$$

These deserve some comment. In the uncoupled limit $\gamma \to 0$ these decouple as one expects. More interestingly, in the maximally coupled limit $\gamma \to \frac{1}{2}$ (that is $\epsilon_0 \to \infty$ while $\epsilon_\infty = 1$), which STO almost saturates, $\omega_+^2 \to \Omega^2 + \omega_p^2$ and $\omega_-^2 \to 0$.

We calculate in Matsubaras,

$$\Sigma(i\nu_n, \mathbf{k}) = \sum_{\mathbf{q}} T \sum_n V_{\text{eff}}(i\omega_n, \mathbf{q}) G_0(i\nu + i\omega_n, \mathbf{k} + \mathbf{q}) \tag{3.40}$$

For brevity describing the algebra in words:

- The Matsubara sum is done as a contour integral and just picks up the five simple poles
- We take a zero-temperature limit immediately
- We naively continue $i\nu \to \omega + i\epsilon$ and use $\Im \frac{1}{x + i\epsilon} = -\delta(x)$ to find $\Im\Sigma(\omega, \mathbf{k})$.

- We perform the energy and phase space integrals without incident.

The result is

$$\begin{aligned}\Im\Sigma(\omega,p) = \frac{\lambda}{8\pi(\omega_+^2-\omega_-^2)}\,(\\ &F^+(\omega-\omega_+)(1-n_{\rm F}(\omega-\omega_+))\\ &+F^+(\omega+\omega_+)n_{\rm F}(\omega+\omega_+)\\ &+F^-(\omega-\omega_-)(n_{\rm F}(\omega-\omega_-)-1)\\ &-F^-(\omega+\omega_-)n_{\rm F}(\omega+\omega_-)\;)\end{aligned} \tag{3.41}$$

where

$$F^{\pm}(z) = \sqrt{z+\mu}\omega_{\pm}(\omega_{\pm}^2+(2\gamma-1)\Omega^2)\ln(\frac{(k+\sqrt{z})^2}{(k-\sqrt{z})^2})/2k\sqrt{z} \tag{3.42}$$

Thomas-Fermi: $rs \ll 1$ Now $\Pi \to -\nu_0$, and one obtains

$$V_{\rm eff} \to \frac{\lambda}{q^2+q_{\rm TF}^2}\frac{\omega^2+(2\gamma-1)\Omega^2}{\omega^2-\omega_s^2} \tag{3.43}$$

where

$$\omega_s^2 = \Omega^2\frac{q^2+(1-2\gamma)q_{\rm TF}^2}{q^2+q_{\rm TF}^2} \tag{3.44}$$

We immediately set $\omega_s = \Omega$. One can justify this by saying that deep in the Thomas-Fermi limit $q_{\rm TF} \to 0$ in our units of choice. This is a terrible and counterintuitive argument but reflects physically the fact that at extreme high densities the Fermi energy by far dominates all other scales. (At $r_s = 0$ the effective mass is 1.)

We proceed as before.

$$\Sigma(i\nu_n,\mathbf{k}) = \sum_{\mathbf{q}} T\sum_n V_{\rm eff}(i\omega_n,\mathbf{q})G_0(i\nu+i\omega_n,\mathbf{k}+\mathbf{q}) \tag{3.45}$$

The algebra:

- The Matsubara sum is done as a contour integral and picks up three simple poles
- We take a zero-temperature limit immediately
- We naively continue $i\nu \to \omega + i\epsilon$ and use $\Im \frac{1}{x+i\epsilon} = -\delta(x)$ to find $\Im\Sigma(\omega, \mathbf{k})$.
- We perform the energy integral without incident.
- The phase space integral incorporates all the interesting screening effects.

The lengthy result is

$$\Im\Sigma(\omega, p) = \frac{\lambda\gamma\Omega}{8\pi p}(\Theta(\mu+\omega-\Omega)(1-\Theta(\Omega-\omega))F(\mu+\omega-\Omega)+\Theta(\mu+\omega+\Omega)\Theta(-\omega-\Omega)F(\mu+\omega+\Omega)) \tag{3.46}$$

where

$$F(z) = q_{\mathrm{TF}}^2(\frac{1}{q_{\mathrm{TF}}^2 + (p+\sqrt{z})^2} - \frac{1}{q_{\mathrm{TF}}^2 + (p-\sqrt{z})^2}) + \ln(\frac{q_{\mathrm{TF}}^2 + (p+\sqrt{z})^2}{q_{\mathrm{TF}}^2 + (p-\sqrt{z})^2}) \tag{3.47}$$

Numerics

The one-loop self-energy is calculated by following the same transformations used for the electron gas by (Hedin [1965]) and (Lundqvist [1968]). We have defined the self-energy of interest on the Matsubara axis,

$$\Sigma(i\nu_m, \mathbf{k}) = \sum_{\mathbf{q}} T \sum_n V_{\mathrm{eff}}(i\omega_n, \mathbf{q}) G_0(i\nu_m + i\omega_n, \mathbf{k}+\mathbf{q}) \tag{3.48}$$

which in the zero-temperature limit becomes

$$\Sigma(i\nu_m, \mathbf{k}) \to i \sum_{\mathbf{q}} \int \frac{d\omega}{2\pi} V_{\mathrm{eff}}(i\omega, \mathbf{q}) G_0(i\nu_m + i\omega, \mathbf{k}+\mathbf{q}). \tag{3.49}$$

We wish to obtain the retarded self-energy, $\Sigma(i\nu_m \to \nu + \delta)$ and would prefer to compute it directly rather than have to analytically continue after the fact. We also have the subsidiary goal of minimizing the number of difficult function evaluations, which involves separating out terms with no frequency dependence or that can be evaluated as lower-dimensional integrals. To this end we rewrite

$$V_{\text{eff}}(i\omega, \mathbf{q}) = \frac{V_0(\mathbf{q})}{\epsilon(i\omega, \mathbf{q})} = V_0(q) + V_0(\mathbf{q}) \left(\frac{1}{\epsilon(0, \mathbf{q})} - 1 \right) + V_0(\mathbf{q}) \left(\frac{1}{\epsilon(i\omega, \mathbf{q})} - \frac{1}{\epsilon(0, \mathbf{q})} \right) \quad (3.50)$$

Statics The first two terms are independent of energy and only needs to be evaluated once for each momentum grid point. The first term generates the usual exchange contribution Σ_X. We will retain the dynamics in the second piece and take the static limit at the end. First we rewrite it in a spectral representation

$$V_0(\mathbf{q}) \left(\frac{1}{\epsilon(i\omega_n, \mathbf{q})} - 1 \right) \equiv \int_{-\infty}^{\infty} \frac{d\Omega}{2\pi} \frac{B(\Omega, \mathbf{q})}{i\omega_n - \Omega} \quad (3.51)$$

We perform the Matsubara sum:

$$\Sigma_S(i\nu_m, \mathbf{k}) = \Sigma_X + \sum_{\mathbf{q}} \int_{-\infty}^{\infty} \frac{d\Omega}{2\pi} \, B(\Omega, \mathbf{q}) \, T \sum_n \frac{1}{i\omega_n - \Omega} \frac{1}{i\omega_n + i\nu_m - \xi_{\mathbf{k}+\mathbf{q}}} \quad (3.52)$$

$$= \Sigma_X + \sum_{\mathbf{q}} \int_{-\infty}^{\infty} \frac{d\Omega}{2\pi} \, B(\Omega, \mathbf{q}) \, \frac{n_B(\Omega) + n_F(\xi_{\mathbf{k}+\mathbf{q}})}{i\nu_m + \Omega - \xi_{\mathbf{k}+\mathbf{q}}}$$

$$\xrightarrow[i\nu_m \to \omega, \, T \to 0]{} \Sigma_S + \sum_{\mathbf{q}} \int_{-\infty}^{\infty} \frac{d\Omega}{2\pi} \, B(\Omega, \mathbf{q}) \, \frac{-\Theta(-\Omega) + \Theta(\xi_{\mathbf{k}+\mathbf{q}})}{\omega + \Omega - \xi_{\mathbf{k}+\mathbf{q}} + i\delta}$$

$$= \Sigma_X - \sum_{\mathbf{q}} \int_{-\infty}^{0} \frac{d\Omega}{2\pi} \frac{B(\Omega, \mathbf{q})}{\omega - \xi_{\mathbf{k}+\mathbf{q}} + \Omega + i\delta} + \sum_{\mathbf{q}} \int_{-\infty}^{\infty} \frac{d\Omega}{2\pi} \frac{B(\Omega, \mathbf{q})}{\omega - \xi_{\mathbf{k}+\mathbf{q}} + \Omega + i\delta} \, \Theta(\xi_{\mathbf{k}+\mathbf{q}})$$

We use the fact that the dielectric function and therefore B is even to extend the integration in the second term back over the full range to obtain

$$\Sigma_S = \frac{1}{2}\sum_{\mathbf{q}} V_0(\mathbf{q}) \left(\frac{1}{\epsilon(\omega - \xi_{\mathbf{k}+\mathbf{q}}, \mathbf{q})} - 1 \right) - \sum_{\mathbf{q}} V_0(\mathbf{q}) \left(\frac{1}{\epsilon(\omega - \xi_{\mathbf{k}+\mathbf{q}}, \mathbf{q})} - 1 \right) \Theta(\xi_{\mathbf{k}+\mathbf{q}}) + \Sigma_X \tag{3.53}$$

In the static limit there is no frequency dependence. We may also combine the second and third terms to obtain

$$\Sigma_S = \frac{4\pi}{2} \int_0^\infty dq\ q^2 V_0(q) \left(\frac{1}{\epsilon(0,q)} - 1 \right) - 2\pi \int_0^\infty dq\ q^2 V_0(q) \int_{-1}^1 d\cos\theta \frac{\Theta(\xi_{\mathbf{k}+\mathbf{q}})}{\epsilon(0,\mathbf{q})} \tag{3.54}$$

The first term is conventionally called the Coulomb Hole and the second the Screened Exchange term, as it is analogous to Σ_X.

Dynamics At zero temperature we will do the frequency sum as an integral,

$$\Sigma_D(i\nu_m, \mathbf{k}) = \sum_{\mathbf{q}} \int \frac{d\omega'}{2\pi} V_{\text{eff}}(i\omega', \mathbf{q}) G_0(i\nu_m + i\omega', \mathbf{k}+\mathbf{q}) \tag{3.55}$$

where

$$V_{\text{eff}}(i\omega, \mathbf{q}) = V_0(\mathbf{q}) \left(\frac{1}{\epsilon(i\omega, \mathbf{q})} - \frac{1}{\epsilon(0, \mathbf{q})} \right). \tag{3.56}$$

However, we want Σ_D on the real axis. Formally we can obtain it as the sum of a careless analytic continuation before integration and a piece that picks up what we missed:

$$\begin{aligned} \Sigma_D(i\nu_m \to \omega + i\delta, \mathbf{k}) = &\sum_{\mathbf{q}} \int \frac{d\omega'}{2\pi} V_{\text{eff}}(i\omega', \mathbf{q}) \frac{1}{\omega + i\omega' - \xi_{\mathbf{k}+\mathbf{q}}} \\ &+ \sum_{\mathbf{q}} \int \frac{d\omega'}{2\pi} V_{\text{eff}}(i\omega', \mathbf{q}) \left(\frac{1}{\omega + i\omega' - \xi_{\mathbf{k}+\mathbf{q}}} - \frac{1}{i\nu_m + i\omega' - \xi_{\mathbf{k}+\mathbf{q}}} \right) \end{aligned} \tag{3.57}$$

where I have written G_0 explicitly. All of the angular dependence in the first term is in G_0, which can be integrated explicitly to give

$$\Sigma_{D1}(\omega, \mathbf{k}) = 2\pi \int_0^\infty \frac{d\omega'}{2\pi} \int_0^\infty \frac{dq}{(2\pi)^3} \frac{1}{kq} V_{\text{eff}}(i\omega', \mathbf{q}) \log\left(\frac{(\omega')^2 + (\omega - \epsilon_{\mathbf{k}+\mathbf{q}})^2}{(\omega')^2 + (\omega - \epsilon_{\mathbf{k}-\mathbf{q}})^2}\right) \tag{3.58}$$

where we have used that the imaginary part of the integrand is odd in ω' and the real part is even. In particular it should be noted that $V_{\text{eff}}(i\omega, \mathbf{q})$ is pure real, and can be expressed without evaluating any complex numbers.

The second term will be evaluated by closing the ω' contour in the upper half-plane. Suppose that V_{eff} has just a simple pole at ω_j with residue R_j. Then

$$\begin{aligned} &\int \frac{d\omega'}{2\pi} V_{\text{eff}}(i\omega', \mathbf{q}) \left(\frac{1}{\omega + i\omega' - \xi_{\mathbf{k}+\mathbf{q}}} - \frac{1}{i\nu_m + i\omega' - \xi_{\mathbf{k}+\mathbf{q}}}\right) \\ &= \int \frac{d\omega'}{2\pi i} \frac{R_j}{\omega' - \omega_j} \left(\frac{1}{\omega' - i(\omega - \xi_{\mathbf{k}+\mathbf{q}})} - \frac{1}{\nu_m + \omega' + i\xi_{\mathbf{k}+\mathbf{q}}}\right) \end{aligned} \tag{3.59}$$

$$= R_j \left(\frac{1}{\omega_j - i(\omega - \xi_{\mathbf{k}+\mathbf{q}})} - \frac{1}{\omega_j + \nu_m + i\xi_{\mathbf{k}+\mathbf{q}}} + \frac{\Theta(-\xi_{\mathbf{k}+\mathbf{q}})}{\omega_j + \nu_m + i\xi_{\mathbf{k}+\mathbf{q}}} - \frac{\Theta(\omega - \xi_{\mathbf{k}+\mathbf{q}})}{\omega_j - i(\omega - \xi_{\mathbf{k}+\mathbf{q}})}\right)$$

$$\xrightarrow[i\nu_m \to \omega]{} \frac{R_j}{i(\omega - \xi_{\mathbf{k}+\mathbf{q}}) - \omega_j} (\Theta(\omega - \xi_{\mathbf{k}+\mathbf{q}}) - \Theta(\xi_{\mathbf{k}+\mathbf{q}}))$$

So that the contribution from the poles of V_{eff} vanishes, and more generally we can write

$$\begin{aligned} \Sigma_{D2}(\omega, \mathbf{k}) &= \sum_{\mathbf{q}} V_{\text{eff}}(\omega - \xi_{\mathbf{k}+\mathbf{q}}, \mathbf{q}) (\Theta(\omega - \xi_{\mathbf{k}+\mathbf{q}}) - \Theta(-\xi_{\mathbf{k}+\mathbf{q}})) \\ &= 2\pi \int_0^\infty \frac{dq}{(2\pi)^3} \int_{-1}^1 d\cos\theta \; V_{\text{eff}}(\omega - \xi_{\mathbf{k}+\mathbf{q}}, \mathbf{q}) (\Theta(\omega - \xi_{\mathbf{k}+\mathbf{q}}) - \Theta(-\xi_{\mathbf{k}+\mathbf{q}})) \end{aligned} \tag{3.60}$$

Finally, $\Sigma = \Sigma_S + \Sigma_{D1} + \Sigma_{D2}$ and it should be noted that the entire imaginary part of Σ comes from Σ_{D2}. We nondimensionalize and perform these four integrals by Monte Carlo as implemented in (Lepage [2020]).

3.2.3 Cumulant Expansion

The cumulant expansion is a resummation that achieves some desirable properties in the spectral function at the same computational expense as the one-loop calculation. Assuming one believes in perturbation theory, the formal expansion of the Green function in powers of the coupling constant g,

$$G(t,t') = \sum_{n=0}^{\infty} \frac{g^n}{n!} G_n(t,t'), \tag{3.61}$$

can, following (Gunnarsson [1994]), formally be rewritten

$$G(t,t') = G_0(t,t') \exp(\sum_{n=1}^{\infty} \frac{g^n}{n!} C_n(t,t')) \tag{3.62}$$

where C_n is the n^{th}-order cumulant function. We may formally rewrite (3.62)

$$\sum_{n=1}^{\infty} \frac{g^n}{n!} C_n = \ln(G_0^{-1} G) \tag{3.63}$$

and use Dyson's equation to write G in powers of Σ, which we assume to have been computed to lowest order. Then we expand both sides to first order in g. In the case of a Hamiltonian such that the bare coupling constant does not appear to first order, the first-order cumulant also vanishes and the same argument goes through with relabeled n. We obtain

$$gC_1(t,t') = \ln(G_0^{-1}(G_0 + G_0^2\Sigma + \dots)) \approx G_0^{-1}(t,t') \int dt_1 \int dt_2 \; G_0(t,t_1)\Sigma(t_1,t_2)G_0(t_2,t'). \tag{3.64}$$

For our problem of interest, Σ is nothing but the one-loop function we have already computed. The quantity on the left is the lowest-order cumulant function which we will just relabel $C(t,t')$. The integral on the right is just a convolution diagonal in Fourier space. It is

convient to employ yet another spectral representation,

$$\Sigma(\omega, \mathbf{k}) = \Sigma_\infty + \int_{-\infty}^{\infty} \frac{d\Omega}{2\pi} \frac{|-2\Im\Sigma(\Omega, \mathbf{k})|}{\omega - \Omega + i\delta} \tag{3.65}$$

where $|-2\Im\Sigma|$ is just the spectral function of Σ. In fact it is crucial to make this separation Then we obtain

$$C_{\mathbf{k}}(t, t') = ie^{i\xi_{\mathbf{k}}(t'-t} \int \frac{d\omega}{2\pi} \int \frac{d\Omega}{\pi} \frac{|\Im\Sigma(\Omega)|}{\omega - \Omega + i\delta} \frac{1}{(\omega - \xi_{\mathbf{k}} + i\delta)^2} e^{-i\omega(t-t')} \tag{3.66}$$

So that the cumulant depends only on $t - t'$. Closing the ω contour in the upper half-plane,

$$C_{\mathbf{k}}(t) = e^{i\xi_{\mathbf{k}}t} \int \frac{d\Omega}{\pi} \frac{|\Im\Sigma(\Omega)|}{(\Omega - \xi_{\mathbf{k}})^2} (e^{-i\Omega t} - ie^{-i\xi_{\mathbf{k}}t}(-i + (\xi_{\mathbf{k}} - \Omega)t)) \tag{3.67}$$

$$= \int d\Omega \frac{\beta(\Omega)}{(\Omega - \xi_{\mathbf{k}})^2} (e^{-i(\Omega - \xi_{\mathbf{k}})t} + i(\Omega - \xi_{\mathbf{k}})t - 1).$$

It is important to note that $\xi_{\mathbf{k}}$ here comes from the unperturbed G_0 and thus does not reflect any self-energy effects or shifts of the chemical potential. Keeping in mind that the cumulant is re-exponentiated, the physical effects of each term are transparent for a delta-function spectral density $|\Im\Sigma = \delta(\Omega - xi_{\mathbf{k}} - \omega)$: The $e^{i\omega t}$ term generates Poisson-distributed of shake-offs at multiples of the boson frequency, the $i\omega t$ shifts the entire spectrum by the boson energy, and the -1 term reweights the spectrum. As argued in (Nery et al. [2017]), it can also be shown using Kramers-Kronig relations to relate β to $\Re\Sigma$ that in general the $i\omega t$ term produces the on-shell $\Re\Sigma$ quasiparticle shift, while the -1 term produces the $\partial\Re\Sigma/\partial\omega$ quasiparticle weight.

In practice, we begin by constructing an interpolation of $\Im\Sigma$ for each k on a frequency grid whose spacing is an input to the calculation. We choose an initial Fourier grid size as well and from this construct the minimal time grid corresponding to our frequency resolution, and compute $\int d\Omega \frac{\beta(\Omega)}{(\Omega - \xi_{\mathbf{k}})^2} (e^{-i(\Omega - \xi_{\mathbf{k}})t} - 1)$ on this grid from the interpolating function. Notice

that the $i\omega t$ term has been ommitted here. Next, we Fourier transform $C(t)$ to frequency space, and compute

$$G(\omega, \mathbf{k}) = \int d\Omega \frac{C(\Omega)}{(\omega - \Omega) - \xi_{\mathbf{k}} - \Re\Sigma(\xi_{\mathbf{k}}, \mathbf{k})}. \tag{3.68}$$

In other words, we compute (3.62) in frequency space as a convolution, but using a G_0 that has been shifted by the on-shell real self energy. In this way we incorporate both the static piece left over from (3.65) and the $i\omega t$ term in the cumulant expansion in a well-controlled way.

Finally, to check convergence we compute the spectral function $A = -2\Im G$. As this function is positive, we first check that there are no excursions to negative values within a numerical tolerance, and next that A is normalized within a tolerance. If either of these criteria is not met, we double the Fourier transform size and rerun the calculation.

3.3 Results and Discussion

In Figure 3.1 we plot the spectral function for $SrTiO_3$ at $n = 5 \times 10^{19}\text{cm}^{-3}$. All spectral functions are plotted on a logarithmic color scale to enhance the visibility of faint features. Near the Fermi surface, the quasiparticle band is narrow with typical $\text{Im}\Sigma \sim \omega^2$ Fermi-liquid behavior. At a density-dependent momentum away from the Fermi surface, there is a sudden increase in broadening which produces a characteristic kink. Below the quasiparticle band there is a series of replica bands of similar width near the bottom of the band, and vanishing as $k \to k_F$ and more spectral weight is transferred to the quasiparticle. The replicas are spaced by an energy $\Omega_+ \neq \Omega$, which can be understood by considering the large-r_s plasmon pole limit, when $\Pi(\mathbf{q}, \omega) \to \Omega_p^2(\mathbf{q})/(\omega^2 V_c(\mathbf{q}))$ where Ω_p^2 is the plasmon frequency. V_{eff} then has poles at

$$\Omega_\pm^2 = \frac{1}{2}\left(\Omega^2 + \Omega_p^2 \pm \sqrt{\Omega^4 + \Omega_p^4 + (8\gamma - 2)\Omega^2\Omega_p^2}\right). \tag{3.69}$$

We plot these modes at $\mathbf{q} = 0$ alongside the bare phonon and plasmon for $SrTiO_3$ in

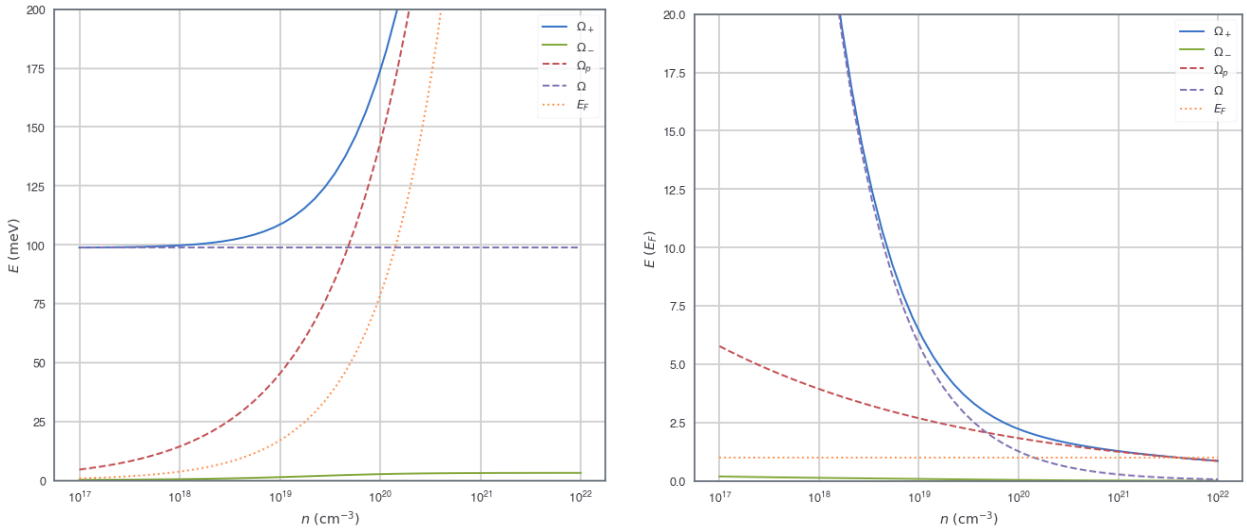

(a) (b)

Figure 3.3: Coupled modes of (3.69) (solid), along with uncoupled modes (dashed) and E_F (dotted), in physical units (left) and in units of E_F (right)

Figure 3.3. For small and intermediate γ the coupled modes largely follow the bare modes except in the vicinity of the anti-crossing, but as γ approaches its maximum value of 1/2, as in the case of $SrTiO_3$, $\Omega_+^2 \to \Omega^2 + \Omega_p^2$ while $\Omega_- \to 0$. In this limit the oscillator strength in the lower mode vanishes as Ω_-^3. The lower coupled mode is therefore too weak for us to observe with $SrTiO_3$ parameters and we only see signatures of Ω_+. This represents a major discrepancy between the model and experimental observations such as the photoemission experiment of (Wang et al. [2016]), which finds replica bands at the phonon frequency at all dopings.

For comparison to the tunneling experiments of (Swartz et al. [2018]), from the spectral function we may also compute the density of states, $\nu(\omega) = \sum_{\mathbf{k}} A(\mathbf{k}, \omega)$. At high densities, ν broadly follows the $\sqrt{\omega}$ free-particle prediction, with small deviations due to the spectral weight in the replica bands, which become increasingly prominent and eventually dominant as the density is decreased. To focus on these features, in Figure 3.2 we plot $d\nu/d\omega$ for densities from $10^{18} - 2 \times 10^{20} \mathrm{cm}^{-3}$. With increasing density these evolve from a sharp peak-dip structure to a broad peak, matching what is seen in experiment, but at all densities they

remain centered at $\omega = \Omega_+$, again at odds with the experimental observation of replicas at the phonon frequencies, independent of density.

A striking feature in the photoemission data is the disappearance of replica bands at high densities, and the development of a quasiparticle band with a kink. Similar phenomenology in TiO_2 was recently explained in terms of Thomas-Fermi screening of the electron-phonon matrix element (Verdi et al. [2017]). In Figure 3.4 we show a cut of $A(k = k_F, \omega)$ with frequencies scaled by Ω_+ for three different densities. The effects of screening are most apparent in the decreased amplitude and greater broadening of the replica peaks with increasing density. The screening wavevector q_{TF} grows with density and enters the electron-boson matrix element as $1/(q^2 + q_{TF}^2)$, increasing the range of momenta around $q = 0$ which contribute significantly and thereby broadening the peak. This effect is insufficient to qualitatively modify the spectrum, however.

A qualitative difference that does emerge at high densities is a broad feature between the quasiparticle and the first replica band. We study this feature as a function of momentum $k > k_F$ in the inset of Figure 3.4, and find that it is nearly non-dispersing and centered around the bare phonon frequency, Ω. (A second feature is seen at $\omega = \Omega_+$, and at all the densities we have studied we observe non-dispersing tails of all replica bands at $k > k_F$. (Kas et al. [2014]) has found a similar effect in the homogeneous electron gas.) At this density, $\Omega/E_F < 1$; this feature disappears as one moves into the anti-adiabatic regime, although it is still faintly present in Figure 3.1, where $\Omega/E_F \sim 2$. The origin of this feature may be understood by examining the structure of the dielectric function $\epsilon(\mathbf{q}, \omega)$. In the q-ω plane, it inherits from the electron gas the well-known electron-hole continuum, bounded by $\omega_\pm(q) = q^2/2m + v_F q$ where $\mathrm{Im}\epsilon \neq 0$ (Giuliani and Vignale [2005]). To the left of ω_-, $\mathrm{Im}\epsilon$ is nonzero along the dispersions of the coupled modes discussed above, but after the plasmon disperses into the continuum, only a single peak at the bare phonon frequency emerges beyond ω_+. We interpret the feature, positioned in a region where $\Im\epsilon = 0$ at the

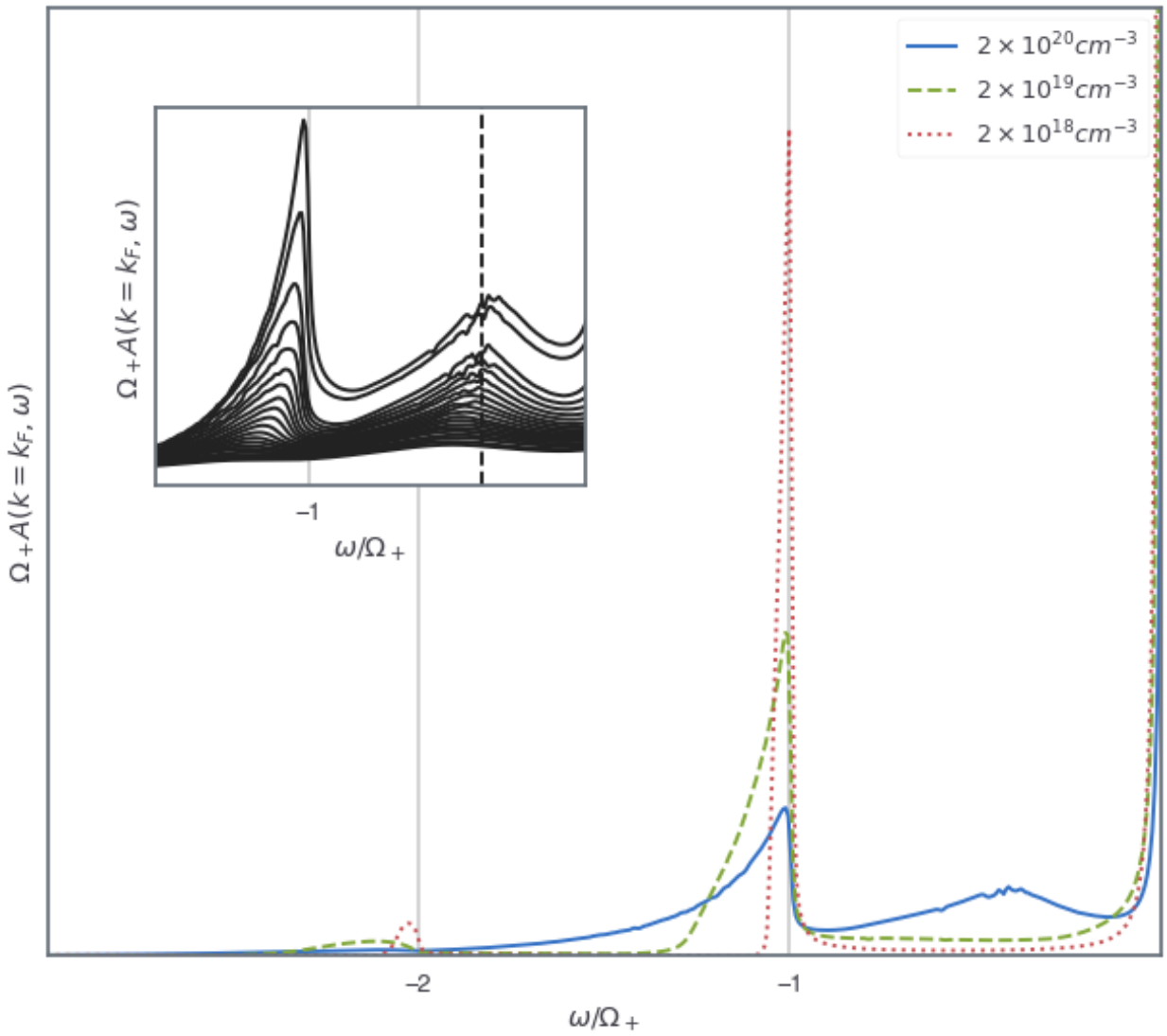

Figure 3.4: Fermi surface spectral function $A(\mathbf{q} = k_F, \omega)$ below E_F at different densities showing the evolution of the replica bands. Inset: $n = 2 \times 10^{20}\text{cm}^{-3}$ spectral functions from $k = k_F$ (top) to $k = 1.4k_F$ (bottom), showing the evolution of dispersionless features at Ω_+ and Ω (dahsed line).

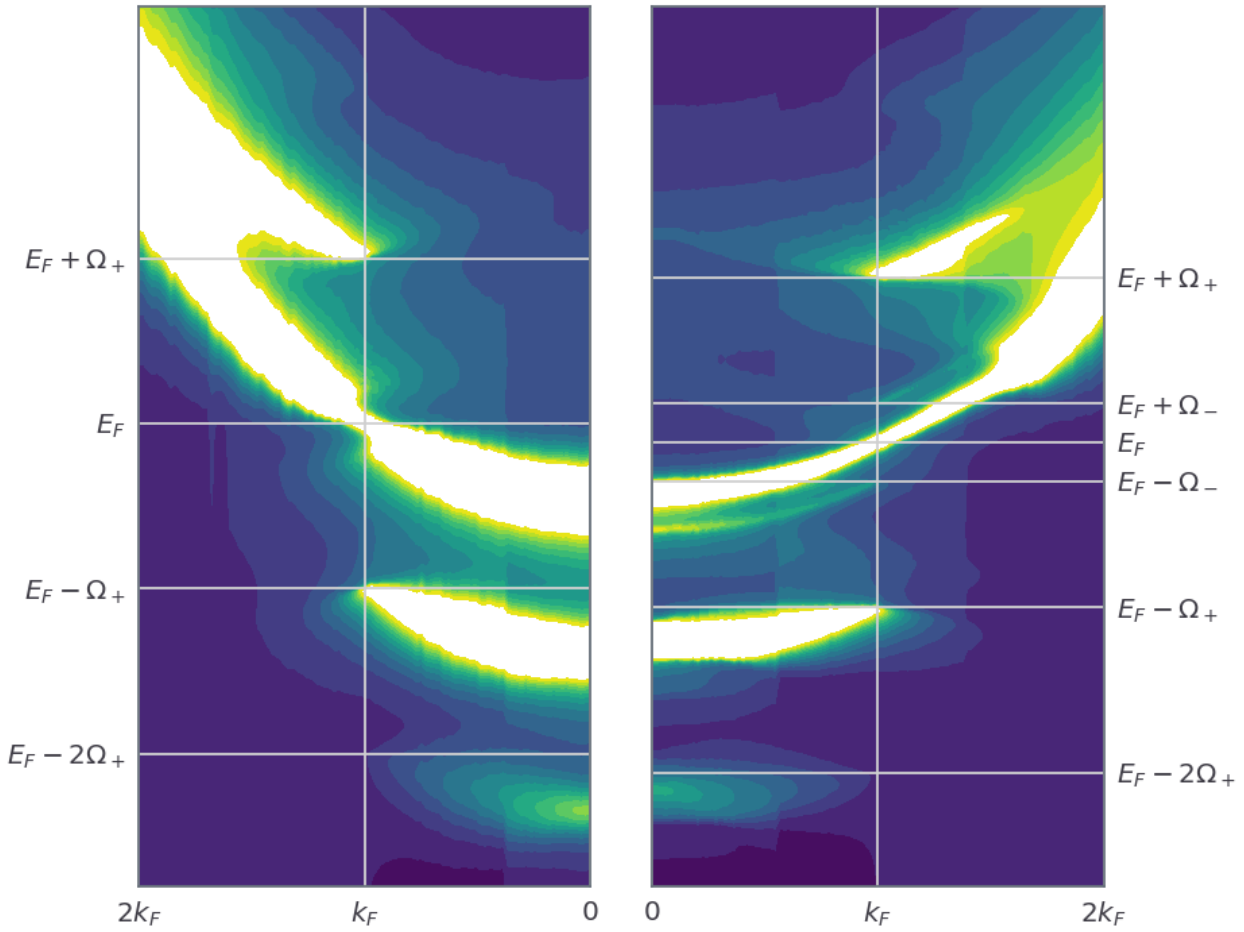

(a) (b)

Figure 3.5: Like Figure 3.1, but with altered parameters a) $\Omega/E_F = .5$, b) $\gamma = .4$.

one-loop level, as a multiple-scattering process involving this mode and the electron-hole continuum.

To further explore the importance of adiabaticity within our model, in Figure 3.5 we artificially vary Ω/E_F and γ away from $SrTiO_3$ parameters while holding the density fixed at $n = 5 \times 10^{19}\text{cm}^{-3}$. In Figure 3.5a the phonon is made adiabatic, $\Omega/E_F = .5$. The quasiparticle and replica bands are substantially broadened, the kink in the quasiparticle moves much closer to the Fermi surface, and the nondispersing feature Ω below E_F becomes much stronger compared to Figure 3.1. In Figure 3.5b, we instead set $\gamma = .4$, substantially increasing the frequency and oscillator strength of Ω_-; note, however, that still $\Omega_- < E_F$

at this density. In this case, an additional, narrow replica band emerges offset from the quasiparticle band, which maintains a modest linewidth with no kinks to the bottom of the band. (A very faint non-dispersing feature at the bare phonon frequency is still detectable, if difficult to resolve by eye.) Here it is worth noting the theory of (Ruhman and Lee [2016]), which suggests that a modest reduction in ϵ_0 is sufficient to impart sufficient strength to the Ω_- mode to mediate pairing while remaining adiabatic. To reproduce the phenomenology of Figure 3.5b, however, with $\Omega_- \approx 25$meV, requires a far greater reduction of $\epsilon_0 \approx 30$, and we note that in this case Ω_+ remains strongly shifted away from Ω.

These results collectively suggest that the transition between replica bands in the spectral function and a broadened quasiparticle with kinks is driven by the interplay of adiabaticity and screening by the electron-hole continuum. The latter imparts some intrinsic width to the quasiparticle band and causes the electron-boson matrix element to deviate from the forward-scattering limit, broadening any replica bands. If the width of the quasiparticle band exceeds the energy difference between it and the replica, the entire structure is absorbed into a broadened quasiparticle. At some point as the intrinsic quasiparticle width decreases as it approaches the Fermi surface, this condition will be violated, causing a kink as the quasiparticle band suddenly narrows. In the case of coupled modes we have studied here, spectral weight at the Fermi surface is not exclusively distributed between the quasiparticle and any remaining replicas, but may also accumulate in a broad feature around the bare phonon frequency.

3.4 Conclusions

Our model neglects many experimentally significant features of $SrTiO_3$, including the occupation of multiple electron bands and the coupling to mulitple optic phonons. While the inclusion of accurate electron and phonon band structures is necessary to obtain quantitative agreement with experiment, we do not believe it would be sufficient to resolve the

major discrepancy we observe here, namely, that the normal-state spectral features within our model are predicted to be unambiguously shifted away from the bare phonon frequencies through hybridization with the plasmon. This presents a challenge to a class of theories of superconductivity which rely on the existence of these hybrid modes, or more broadly plasmon-mediated superconductivity theories dating back to (Grabowski and Sham [1984]).

Equivalently, our results suggest that future work investigate the nature of the plasmon in $SrTiO_3$, which has been indirectly observed in reflectivity data to have a width of the same order as the plasma frequency (Gervais et al. [1993b]). Heuristically, this is consistent with other observations that suggest the electron gas in $SrTiO_3$ behaves as if it were directly screened by ϵ_0 (Rischau et al. [2017]), or equivalently that its diluteness in terms of r_s is unremarkable compared to other semiconductors. If such screening exists, it is a more elusive effect than the multiple-scattering processes we have considered here.

Our theory ultimately suffers from a defect similar to that found in many of the superconducting theories: it is formally an expansion in r_s, which is always substantially greater than unity at the densities we have considered. Paradoxically, as the theory becomes more poorly controlled at low densities, the phenomenology becomes simpler as the response is totally dominated by the plasmon pole physics of (3.69). More sophisticated techniques are needed to understand the interplay of polaron physics and the many-electron fluid.

CHAPTER 4

SUPERCONDUCTING PROPERTIES OF STRONTIUM TITANATE

4.1 Introduction

This chapter presents unpublished work that aims to use the results of the previous chapter to compute superconducting properties. The conventional BCS theory of superconductivity is amply reviewed elsewhere; see, for instance, (Mahan [2000]). By way of introduction I will instead point out that the "BCS approximation" in fact consists of a number of distinct approximations, thereby motivating the approach to STO I take here.

- Weak coupling, in the sense of the BEC-BCS crossover discussed in the introductory chapter. Here it must be noted that STO is peculiar as the dilute normal state appears to be very strongly coupled in the sense of r_s, but with a gap measured at $\sim 40\,\mu$eV by tunneling and Δ/T_c values extracted from critical field or microwave measurements, the superconducting state itself appears to be very much in the weakly-coupled BCS limit.

- Adiabaticity, in the sense that Migdal's theorem asserts the irrelevance of vertex corrections when Ω/E_F is small. STO clearly violates this condition and so the perturbative calculations below are fraught.

- The existence of a cutoff energy scale (also provided by Ω in the conventional theory) such that the pairing interaction is only significant in a thin shell of this scale around the Fermi surface. The calculations below do not rely on this assumption. The inconvenient consequence is that rather than depending only on the density of states at the Fermi surface, the calculations must explicitly run from the bottom of the electron band out to high energies. On the other hand, a favorable consequence is that such a calculation

without a cutoff can naturally incorporate the full Coulomb repulsion on equal footing, without having to employ the pseudo-potentials typically used in BCS-like calculations.

- On-shell approximation, i.e. that the gap function $\Delta(\omega, \mathbf{k}) \propto \delta(\omega - \xi_{\mathbf{k}})$. This arises naturally as a consequence of the other BCS approximations but when those are relaxed, one has the freedom to choose. In the preliminary results shown below we keep this approximation, but the formalism is designed with the idea of being able to relax it.

4.2 Derivation of the gap function

As before, we will be concerned with calculating a self-energy, although this time in an elarged Nambu space where the off-diagonal "anomalous" components describe Cooper pair correlations. This self-energy can be written

$$\mathbf{\Sigma}(i\omega_n, q) = -T \sum_{mk} V_{\text{eff}}(i\nu_m + i\omega_n, k + q)\tau_3 \mathbf{G}(i\nu_m, k)\tau_3 \tag{4.1}$$

which should be regarded as some kind of Hedin equation or self-consistency condition between $\mathbf{\Sigma}$, V_{eff}, and $\mathbf{G}$. Here

$$\mathbf{G} = \begin{pmatrix} G & F \\ F^\dagger & G^\dagger \end{pmatrix} \tag{4.2}$$

in Nambu space, and we can decompose

$$\mathbf{\Sigma} = (1 - Z)i\omega_n + W\tau_1 + \chi\tau_3 \tag{4.3}$$

where the τ_i are Pauli matrices in Nambu space.

Solving Dyson's equation with these substitutions gives

$$G(i\nu,p) = \frac{Z(i\nu,p)i\nu + \tilde{\xi}_p}{(Z(i\nu,p)i\nu)^2 - (\tilde{\xi}_p^2 + W^2(i\nu,p))} \tag{4.4}$$

$$F(i\nu,p) = -\frac{W(i\nu,p)}{(Z(i\nu,p)i\nu)^2 - (\tilde{\xi}_p^2 + W^2(i\nu,p))}$$

where $\tilde{\xi}_p = \epsilon_p - \mu + \chi(i\nu,p)$. In the case that $W = 0$, we have

$$G = \frac{1}{Z(i\nu,p)i\nu - \bar{\xi}(i\nu,p)} = \frac{1}{i\nu - \xi - S(i\nu,p)} \tag{4.5}$$

where S is the normal self-energy. The development of a non-zero W signals the onset of pairing in this formalism.

The functions Z and χ are both even in frequency, and $S = \chi + \omega(1 - Z)$. W is taken to be odd in frequency and therefore so is F.

4.2.1 s-wave approximation

We assume the pairing is isotropic, and to eliminate a further momentum integral we define

$$V_{\text{eff}}(\omega,\epsilon,\epsilon') \equiv \frac{1}{2\pi}\int_{-1}^{1} dx V_{\text{eff}}(\omega, \sqrt{(}\epsilon + \epsilon' + 2\sqrt{\epsilon}\sqrt{\epsilon'}x)) \tag{4.6}$$

and integrate over the density of states $N(\epsilon) = \sqrt{\epsilon}$, which corresponds to the bare band structure and is not modified by self-energy effects. We also use an energy variable in place of the momentum variable, and rewrite the self-energy equation for the two components explicitly:

$$S(i\nu_m,\epsilon) = -\int d\epsilon'\ N(\epsilon')T\sum_n G(i\nu_m + i\omega_n,\epsilon')V_{\text{eff}}(i\omega_n,\epsilon,\epsilon') \tag{4.7}$$

$$W(i\nu_m,\epsilon) = -\int d\epsilon' N(\epsilon')T\sum_n F(i\nu_m + i\omega_n,\epsilon')V_{\text{eff}}(i\omega_n,\epsilon,\epsilon')$$

4.2.2 Spectral representation

As a warm-up we consider the contribution to the gap of the static Coulomb piece $V_0(\epsilon, \epsilon')$:

$$W_c(i\nu_m, \epsilon) = -\int d\epsilon' \; N(\epsilon') T \sum_n F(i\nu_m + i\omega_n, \epsilon') V_0(\epsilon, \epsilon') \tag{4.8}$$

We employ the spectral representation

$$F(i\nu_m + i\omega_n, \epsilon') = \int_{-\infty}^{\infty} \frac{d\eta}{2\pi} \frac{-2\Im F(\eta, \epsilon')}{i\nu_m + i\omega_n - \eta} \tag{4.9}$$

so that

$$\begin{aligned} W_c &= \int d\epsilon' \; N(\epsilon') \int_{-\infty}^{\infty} \frac{d\eta}{\pi} \Im F(\eta, \epsilon') \; T \sum_n \frac{1}{i\nu_m + i\omega_n - \eta} \qquad (4.10) \\ &= \int d\epsilon' \; N(\epsilon') \int_{-\infty}^{\infty} \frac{d\eta}{\pi} \Im F(\eta, \epsilon') \; (-n_B(\eta - i\nu_m)) \\ &= \int d\epsilon' \; N(\epsilon') \int_{-\infty}^{\infty} \frac{d\eta}{\pi} \Im F(\eta, \epsilon') n_F(\eta) \\ &= \int d\epsilon' \; N(\epsilon') \int_0^{\infty} \frac{d\eta}{\pi} \left(\Im F(\eta, \epsilon') n_F(\eta) - \Im F(-\eta, \epsilon') n_F(-\eta) \right) \\ &= -\int d\epsilon' \; N(\epsilon') \int_0^{\infty} \frac{d\eta}{\pi} \Im F(\eta, \epsilon')(1 - 2n_F(\eta)) \end{aligned}$$

using that F is odd in frequency. We take a similar approach for the dynamic part of the interaction, using

$$V(i\omega_n, \epsilon, \epsilon') = V_0(\epsilon, \epsilon') - \int_0^{\infty} \frac{d\Omega}{\pi} \Im V(\Omega, \epsilon, \epsilon') \left(\frac{1}{i\omega_n - \Omega} - \frac{1}{i\omega_n + \Omega} \right) \tag{4.11}$$

where we have defined the retarded function $\Im V$ on the positive (real) energy axis. The dynamic contribution to the gap then becomes

$$W_{\text{dyn}} = \int d\epsilon' \; N(\epsilon') \; T \sum_n F(i\nu_m + i\omega_n, \epsilon') V_{\text{dyn}}(i\omega_n, \epsilon, \epsilon') \tag{4.12}$$

$$= -\int d\epsilon'\ N(\epsilon') \int_0^\infty \frac{d\Omega}{\pi} \Im V(\Omega,\epsilon,\epsilon') \int_{-\infty}^\infty \frac{d\eta}{\pi} \Im F(\eta,\epsilon') \times$$
$$T\sum_n \frac{1}{i\nu_m + i\omega_n - \eta}\left(\frac{1}{i\omega_n - \Omega} - \frac{1}{i\omega_n + \Omega}\right)$$

$$= -\int d\epsilon'\ N(\epsilon') \int_0^\infty \frac{d\Omega}{\pi} \Im V(\Omega,\epsilon,\epsilon') \int_{-\infty}^\infty \frac{d\eta}{\pi} \Im F(\eta,\epsilon') \times$$
$$\left(\frac{n_B(-\Omega) + n_F(\eta)}{i\nu_m - \Omega - \eta} - \frac{n_B(\Omega) + n_F(\eta)}{i\nu_m + \Omega - \eta}\right)$$

$$\xrightarrow[i\nu_m \to \omega]{} -\int d\epsilon'\ N(\epsilon') \int_0^\infty \frac{d\Omega}{\pi} \Im V(\Omega,\epsilon,\epsilon') \int_{-\infty}^\infty \frac{d\eta}{\pi} \Im F(\eta,\epsilon') \times$$
$$\left(\frac{-1 - n_B(\Omega) + n_F(\eta)}{\omega - \Omega - \eta} - \frac{n_B(\Omega) + n_F(\eta)}{\omega + \Omega - \eta}\right)$$

Next we use that F is even in frequency:

$$= \cdots \int_0^\infty \frac{d\eta}{\pi} \Im F(\eta,\epsilon') \left(\frac{-1 - n_B(\Omega) + n_F(\eta)}{\omega - \Omega - \eta} - \frac{n_B(\Omega) + n_F(\eta)}{\omega + \Omega - \eta} \times \right.$$
$$\left. - \frac{-1 - n_B(\Omega) + 1 - n_F(\eta)}{\omega - \Omega + \eta} + \frac{n_B(\Omega) + 1 - n_F(\eta)}{\omega + \Omega + \eta}\ \right)$$

$$= \ldots (1 - 2n_F(\eta))\left(\frac{1}{\eta + \Omega + \omega} + \frac{1}{\eta + \Omega - \omega}\right) +$$
$$(n_B(\Omega) + n_F(\eta))\left(\frac{1}{\eta - \Omega - \omega} + \frac{1}{\eta - \Omega + \omega} + \frac{1}{\eta + \Omega + \omega} + \frac{1}{\eta + \Omega - \omega}\right)$$

We expect to be at low temperatures, where the contributions from the second term are immaterial. Then, adding together the dynamic and static contributions, we get

$$W(\omega,\epsilon) = -\int d\epsilon'\ N(\epsilon') \int_0^\infty \frac{d\eta}{\pi} \Im F(\eta,\epsilon') \tanh(\beta\eta/2) \times$$
$$\left(V_0(\epsilon,\epsilon') + \int_0^\infty \frac{d\Omega}{\pi}\ \Im V(\Omega,\epsilon,\epsilon')\left(\frac{1}{\eta + \Omega + \omega} + \frac{1}{\eta + \Omega - \omega}\right)\right) \tag{4.13}$$

4.2.3 Weak-Coupling approximations

We now follow(Kirzhnits et al. [1973]) to make progress in the case of weak coupling. Making the quasiparticle approximation $G_0 = (iZ\omega - \xi_k)$ and setting $Z = 1$ for now, one can write

the gap equation (4.13) in terms of F:

$$F(\omega,\epsilon) = -\frac{1}{\omega^2-\xi^2}\int d\epsilon'\ N(\epsilon')\ \int_0^\infty \frac{d\eta}{\pi}\Im F(\eta,\epsilon')\tanh(\beta\eta/2)\times \left(V_0(\epsilon,\epsilon') + \int_0^\infty \frac{d\Omega}{\pi}\ \Im V(\Omega,\epsilon,\epsilon')(\frac{1}{\eta+\Omega+\omega}+\frac{1}{\eta+\Omega-\omega})\right) \tag{4.14}$$

Now we use $\Im F = \Im(G_0^2)^{-1}\Re W + \Re(G_0^2)^{-1}\Im W$ with $\Re(G_0^2)^{-1} = \frac{1}{\omega^2-\xi^2}$, $\Im(G_0^2)^{-1} = -\pi\delta(\omega^2-\xi^2)$. $\Re W$ is as written in (4.13), while $\Im W$ comes from restoring the infinitesimal imaginary part in the energy denominators to obtain

$$\Im W = -\int d\epsilon'\ N(\epsilon')\ \int_0^\infty \frac{d\eta}{\pi}\Im F(\eta,\epsilon')\tanh(\beta\eta/2)\times \int_0^\infty \frac{d\Omega}{\pi}\ \Im V(\Omega,\epsilon,\epsilon')(-\pi\delta(\Omega+\eta+\omega)+\pi\delta(\Omega+\eta-\omega)) \tag{4.15}$$

$$= -\int d\epsilon'\ N(\epsilon')\ \int_0^\infty \frac{d\eta}{\pi}\Im F(\eta,\epsilon')\tanh(\beta\eta/2)\Im V(\omega-\eta,\epsilon,\epsilon')\Theta(\omega-\eta))$$

so that in sum,

$$\Im F = -\int d\epsilon'\ N(\epsilon')\ \int_0^\infty \frac{d\eta}{\pi}\Im F(\eta,\epsilon')\tanh(\beta\eta/2)\left[\frac{\delta(\omega-|\xi|)}{2|\xi|}\left(V_0(\epsilon,\epsilon')+ \int_0^\infty \frac{d\Omega}{\pi}\ \Im V(\Omega,\epsilon,\epsilon')(\frac{1}{\eta+\Omega+\omega}+\frac{1}{\eta+\Omega-\omega})\right) - \frac{1}{\omega^2-\xi^2}\Im V(\omega-\eta,\epsilon,\epsilon')\Theta(\omega-\eta)\right] \tag{4.16}$$

Now consider the momentum-dependent gap function

$$\Delta(\epsilon) \equiv 2|\xi|\int_0^\infty d\omega\ \Im F(\omega,\epsilon) \tag{4.17}$$

and apply (4.16). The $1/(\eta+\Omega-|\xi|)$ term arising from $\Re W$ cancels with a term of the opposite sign from $\Im W$, while the $1/(\eta+\Omega+|\xi|)$ terms add. In this way we obtain

$$\Delta(\epsilon)=\int_0^\infty d\epsilon'\ N(\epsilon')\ \int_0^\infty \frac{d\eta}{\pi}\pi\Im F(\eta,\epsilon')\tanh(\beta\eta/2)\left(V_0(\epsilon,\epsilon')+2\int_0^\infty\frac{d\Omega}{\pi}\frac{\Im V(\Omega,\epsilon,\epsilon')}{\eta+|\xi|+\Omega}\right) \tag{4.18}$$

Finally we can make the on-shell approximation

$$\Im F(\omega,\epsilon)=\pi\Delta(\epsilon)\delta(\omega-|\xi|)/2|\xi| \tag{4.19}$$

to obtain

$$\Delta(\xi)=\int_{-\mu}^\infty d\xi'\ N(\xi'+\mu)\frac{\tanh(\beta\xi'/2)}{2\xi'}K(\xi,\xi')\Delta(\xi') \tag{4.20}$$

with

$$K(\xi,\xi')=V_0(\xi+\mu,\xi'+\mu)+2\int_0^\infty\frac{d\Omega}{\pi}\frac{\Im V(\Omega,\xi+\mu,\xi'+\mu)}{|\xi'|+|\xi|+\Omega} \tag{4.21}$$

where we have changed all the momentum variables to be in terms of ξ.

4.2.4 Numerical Calculation of the Kernel

It is generally more convenient to calculate (4.21) on the imaginary frequency axis. This is what is done by (Takada [1978]), for instance. I have insisted on remaining on the real axis because the eventual aim of this program of calculation is to replace the one-loop self-energies derived above with those calculated from the cumulant expansion. There are a two principal calculation difficulties, however:

1. The Coulomb repulsion is naturally included on the imaginary axis, whereas in (4.21) it must be explicitly added to the attractive piece, with the resulting partial cancellation determining the shape of the kernel and the possibility of stabilizing a gap. Near the Fermi surface, both of these terms are logarithmically diverging and must be calculated with sufficient precision.

2. For the STO problem of interest, the dynamical interaction has widely separated energy scales of importance, due to narrow resonances (with widths set by the width of the plasmon, which is very sharp in the dilute limit) at the coupled mode frequencies. These can be close to (or absorbed into) the electron-hole continuum in the case of the lower mode, and at tens of Fermi energies in the case of the upper mode. Physically it is necessary to include both, even if one ends up insignificant to pairing, because excluding any of the interaction's spectral content constitutes a violation of the f sum rule, and in practical terms causes the Coulomb repulsion to overwhelm it.

I will therefore briefly outline the algorithm I have settled on for obtaining adequate results. First I generate logarithmically spaced points ξ, ξ' around the Fermi surface at which to calculate $\Im V(\Omega, \xi, \xi')$. At each point,

1. Generate a uniformly spaced grid of possible angles between the momenta $\sqrt{\xi}$ and $\sqrt{\xi'}$ and from these a grid of possible momentum transfer values q.

2. Calculate the frequency boundaries of the electron-hole continuum for the given momenta and evenly space frequency points between them.

3. Estimate (using an interpolation formula for the plasmon) at what momenta the upper and lower hybrid modes are expected to enter the electron-hole continuum (where they decay) and at what momentum the phonon is expected to exit the continuum, and check if any of these fall in the range of momentum transfer values being sampled.

4. If so, append to the list of frequency points being sampled a tightly spaced grid of points near the possible locations of the resonance, along with logarithmically spaced tails out in frequency.

5. Compute $\Im 1/\epsilon(\Omega, q)$ on the grid.

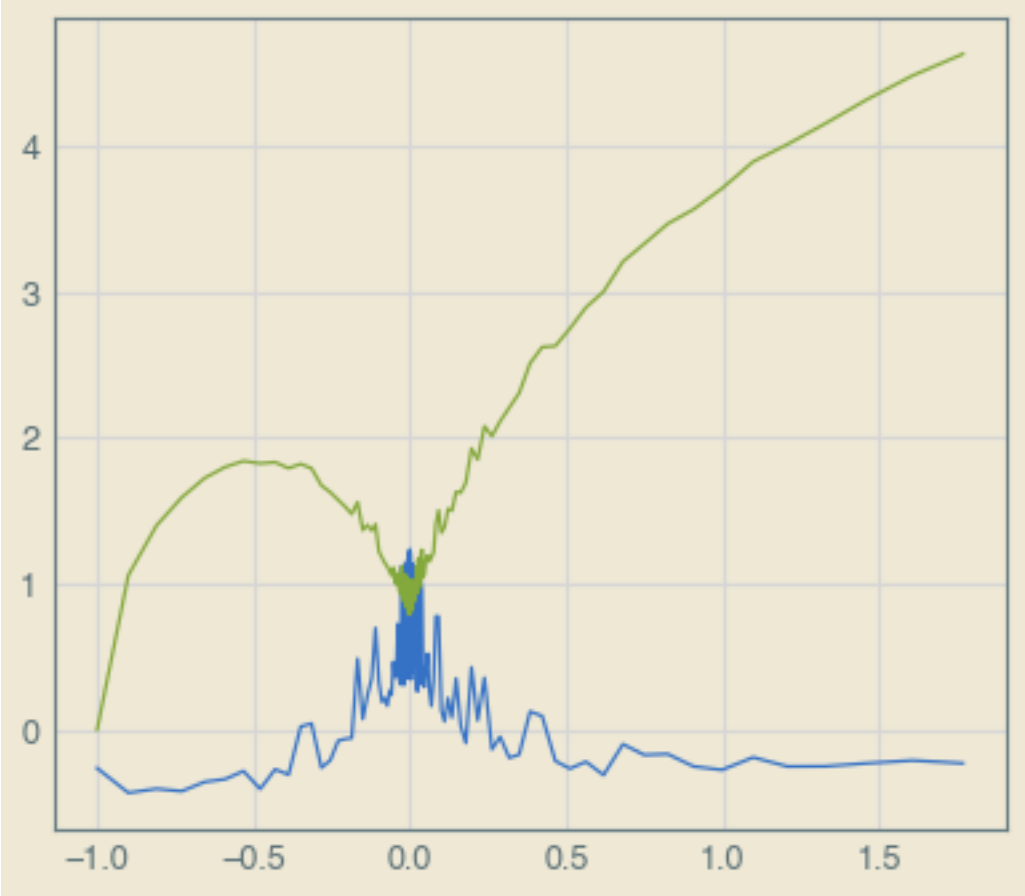

Figure 4.1: Kernel $K(\xi, 0)$ (green) and gap function (blue), both in arbitrary units normalized to their values on the Fermi surface, against energy in units of the Fermi energy. Computed for $r_s = 61$ and $\gamma = 0$.

Finally the energy integration in (4.21) is performed by a simple trapezoid rule. Although this procedure generally works adequately well, in many cases it still suffers from a great deal of noise, as shown for instance for a $\gamma = 0$ (i.e. plasmon-only) calculation at $r_s = 61$ in Figure 4.1.

Already, however, there are some physical insights to emphasize about this type of calculation. The kernel is always positive, i.e. repulsive. The gap in this case is stabilized by a partial cancellation of the Coulomb repulsion by the dynamical attraction which is strongest close to the Fermi surface, producing a dimpled structure. The gap must therefore suffer a sign change some distance from the Fermi surface. This energy scale would be associ-

ated with the Coulomb pseudopotential μ^* in an Eliashberg-type calculation, but arises here naturally due to long-ranged Coulomb nature of both attractive and repulsive interactions.

4.2.5 Plasmon Pole

In the plasmon-pole approximation (or more generally assuming the dynamic part of the interaction comes from Coulomb coupling to single boson), one can write

$$\Im V(\Omega, \mathbf{q}) = -\pi \Omega_0^2 V_0(\mathbf{q}) \delta(\Omega^2 - \tilde{\Omega}^2(\mathbf{q})) \tag{4.22}$$

where V_0 is the Coulomb interaction, Ω_0 is the boson frequency and $\tilde{\Omega}$ is its dispersion. Then we can write

$$2\int_0^\infty \frac{d\Omega}{\pi} \frac{\Im V(\Omega, \mathbf{q})}{|\xi'| + |\xi| + \Omega}) = -V_0(\mathbf{q}) \frac{\Omega_0^2}{|\tilde{\Omega}(\mathbf{q})|} \frac{1}{\tilde{\Omega}(\mathbf{q}) + |\xi'| + |\xi|}. \tag{4.23}$$

Then, in this plasmon pole limit,

$$K(\xi, \xi') = V_0(\xi, \xi')(1 - \sigma \frac{\Omega_0}{\Omega_0 + |\xi| + |\xi'|}) \tag{4.24}$$

where σ is a numerical prefactor obtained from integrating over the boson dispersion. In the case that the boson is dispersionless, $\sigma = 1$. This of course neatly coincides with the formalism of Grabowski and Sham.

This form of kernel is easy to undertand. The Coulomb interaction produces a logarithmic singularity in momentum space, and therefore in energy space on-shell at the Fermi surface. The kernel is always repulsive, and at best the Coulomb interaction is completely cancelled at the Fermi surface. Increasing the boson energy overall weakens the repulsive character of the interaction and generally broadens the features of the kernel. In the case of imperfect screening, $\sigma \neq 1$, there is always a local maximum in the kernel at the Fermi surface due to

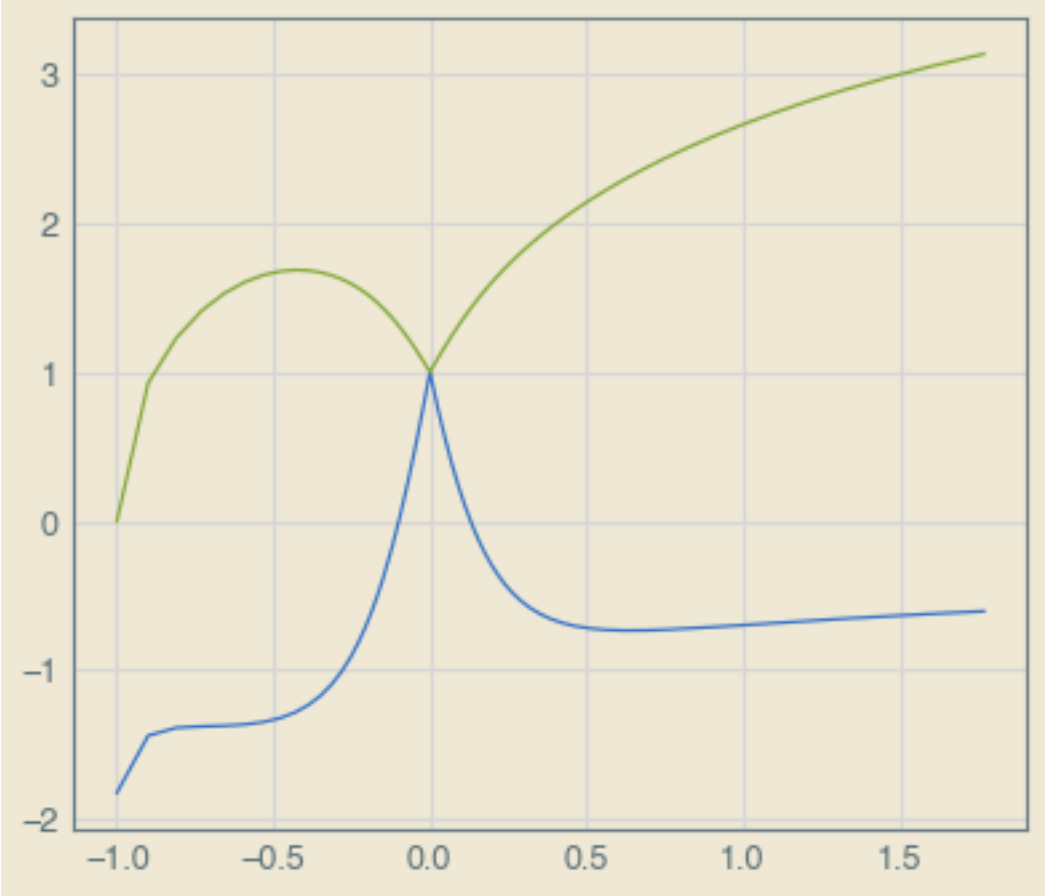

Figure 4.2: Same as Figure 4.1, but smoothed (4.24) as a fitting function.

the Coulomb repulsion, and the existence and depth of a local minimum nearby determine whether a gap forms. In this case, increasing the boson energy makes the repulsive piece more prominent.

It is worth emphasizing that these arguments do not include any Thomas-Fermi screening, which can become important enough to change the qualitative outcome even for r_S substantially greather than unity.

It is also possible to use this plasmon-pole expression (or its natural generalization to multiple bosonic modes) as a simple technique to smooth out the flucutations in the numerically-generated kernels simply fitting Ω_0 and σ. Indeed we have also phenomenologically allowed $V_0(\xi, \xi')$ to be broadened by a Thomas-Fermi-like parameter (which often just reflects nu-

merical broadening rather than real screening). Figure 4.2 shows the results of the procedure applied to the data in Figure 4.1.

4.3 Determining the transition temperature

This method is due to Zubarev and is reproduced by Takada. Define $\phi(x) = W(x)/W(0)$ where $x = \xi/\epsilon_F$. Then the gap equation can be written

$$\phi(x) = -\int_{-1}^{\infty} \frac{dx'}{2x'} \tanh(x'\beta\epsilon_F/2)\phi(x')K(x,x') \tag{4.25}$$

$$\phi(0) = 1 = -\int_{-1}^{\infty} \frac{dx'}{2x'} \tanh(x'\beta\epsilon_F/2)\phi(x')K(0,x') \tag{4.26}$$

Multiplying the latter by $K(0,x)/K(0,0)$ and subtracting from $\phi(x)$, we get

$$\phi(x)-K(x,0)/K(0,0) = -\int_{-1}^{\infty} \frac{dx'}{2x'} \tanh(x'\beta\epsilon_F/2)(K(x,x')-K(0,x')K(x,0)/K(0,0))\phi(x') \tag{4.27}$$

In this form, the singular term at $x' = 0$ is cancelled. Furthermore, provided that $kT \ll \epsilon_F$, it becomes permissible to replace $\tanh(x'\beta\epsilon_F/2)$ by unity. Since we are interested in obtaining the zero-temperature gap function anyway, we readily make this approximation, and solve the gap equation as a matrix inversion problem. With a solution for $\phi(x)$, T_c can be determined from (4.26). It is convenient, however, to break it apart into

$$\begin{aligned} 1 = -K(0,0)\int_{-1}^{1} \frac{dx'}{2x'} \tanh(x'\epsilon_F/2T_c) - \int_{-1}^{1} \frac{dx'}{2x'} \tanh(x'\epsilon_F/2T_c)(K(0,x')\phi(x') - K(0,0)) \\ - \int_{1}^{\infty} \frac{dx'}{2x'} \tanh(x'\epsilon_F/2T_c)K(0,x')\phi(x') \end{aligned} . \tag{4.28}$$

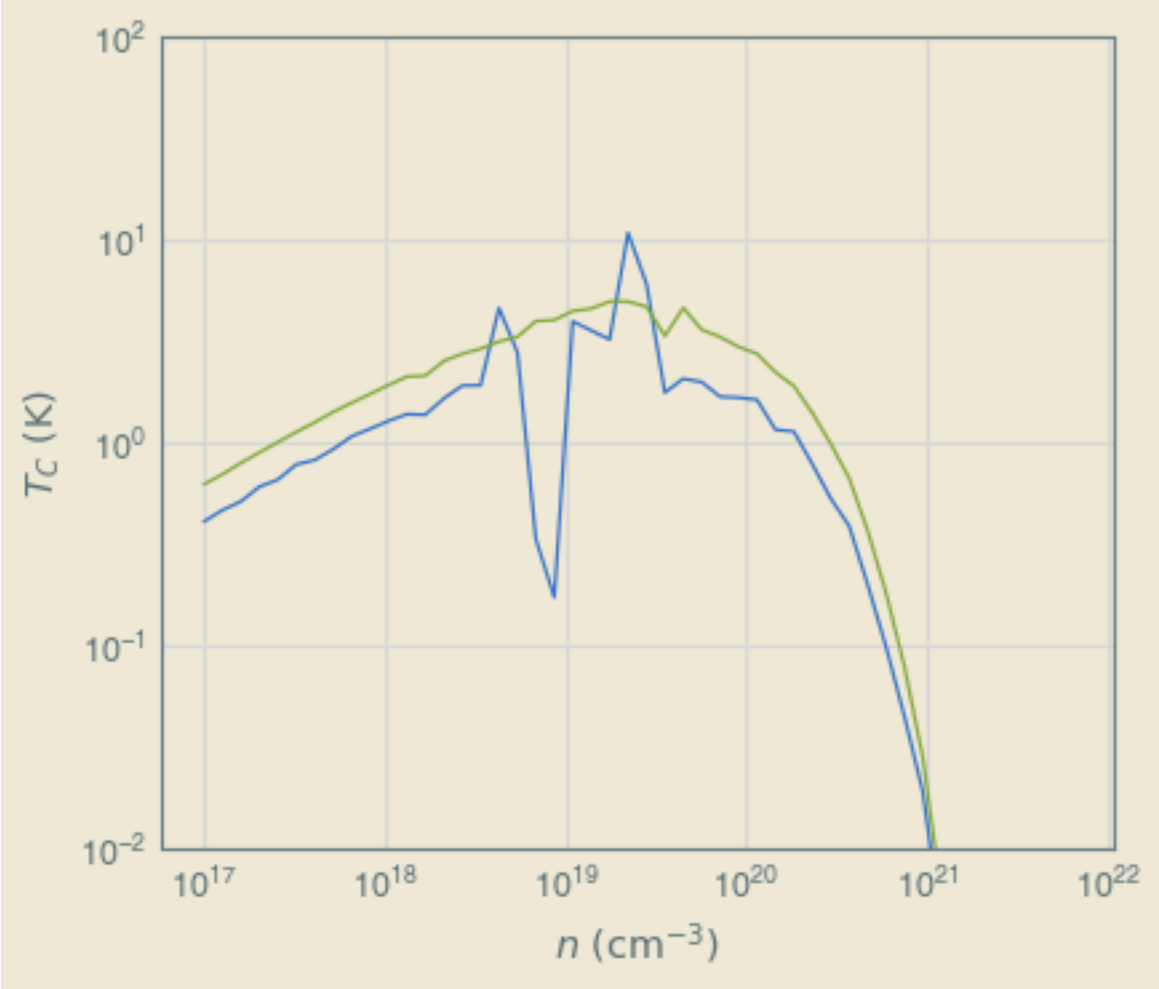

Figure 4.3: Transition temperature of the $\gamma = 0$ plasmon-only model, computed from the raw (blue) and smoothed (green) kernels.

and use that $kT_c \ll \epsilon_F$ to again replace the tanh by unity in the last two terms and move them to the other side. Integrating the first term analytically one obtains

$$T_c = 1.134\epsilon_F \exp\left(\frac{1}{K(0,0)} + \int_{-1}^{\infty} \frac{dx'}{2|x'|}(\phi(x')K(0,x')/K(0,0) - \Theta(1-|x'|))\right) \qquad (4.29)$$

As an illustration of this technique, Figure 4.3 shows T_c for the model with $\gamma = 0$, i.e. only a plasmon mediating the coupling, based both on the raw calculations and those smoothed by fitting to the plasmon pole model. It is also possible to view the same data in

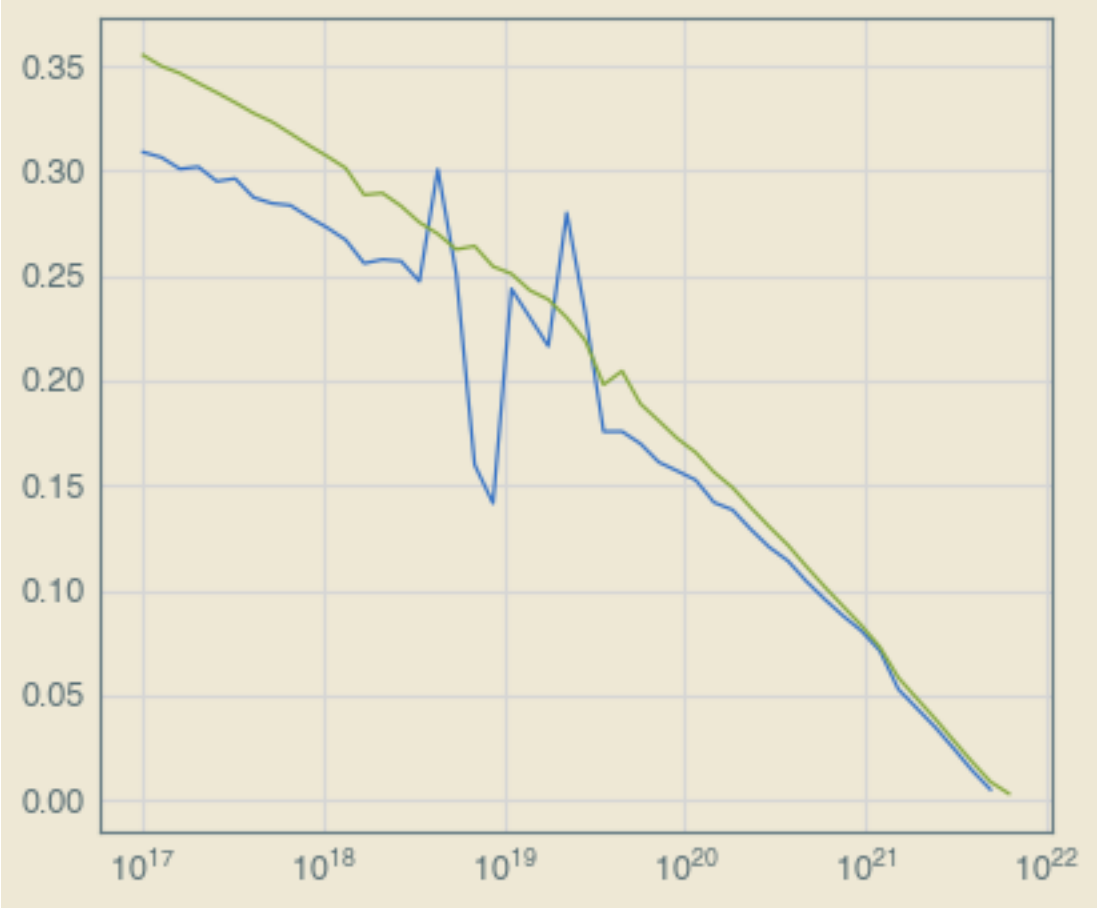

Figure 4.4: As in Figure 4.3, but showing the dimensionless BCS coupling constant

terms of the BCS coupling constant λ, which here is defined by

$$T_c = 1.134\epsilon_F \exp(-1/\lambda). \tag{4.30}$$

Qualitatively, the dome structure in the superconducting phase diagram comes from a competition between too few carriers (and therefore small E_F) in the dilute limit, and a vanishing coupling constant in the dense limit. It is important to note that this vanishing is not associated with the onset of Thomas-Fermi screening, as it also appears in a pure plasmon-pole calculation. Instead it is associated with the approach to the adiabatic limit, where as Ω_0 becomes comparable to the relevant ξ near the Fermi surface, the kernel loses much of the dimpled structure that allows it to stabilize a gap. This observation (within this model at least) is consistent with the peculiar property of STO that it loses its superconductivity just as it becomes adiabatic.

Methodologically, these figures also provide a gauge of the efficacy of the smoothing procedure, particularly in the intermediate-density regions where the calculation particularly struggles.

With these considerations in mind, Figure 4.5 displays the phase diagram for STO under various approximations. What is immediately striking is that plasmon-pole calculations, i.e. those that do not take the RPA structure into account, universally lose their superconductivity near $r_s \sim 10$. As the density is lowered into the dilute limit, models where the oscillator strength is carried in an more anti-adiabatic phonon-like mode lose superconductivity faster than those where the plasmon remains significant, which as (Takada [1992]) has shown, eventually leads to T_c a constant fraction of ϵ_F in the low density limit. At intermediate densities some fine-tuning appears to be possible to trade oscillator strength into the adiabatic modes and quantitatively raise the optimal T_c somewhat, but we expect this to be an extremely model-dependent effect. The most salient feature, however, is the extent of the full-RPA curve to much higher densities than the plasmon-pole curves. This is most likely due to an

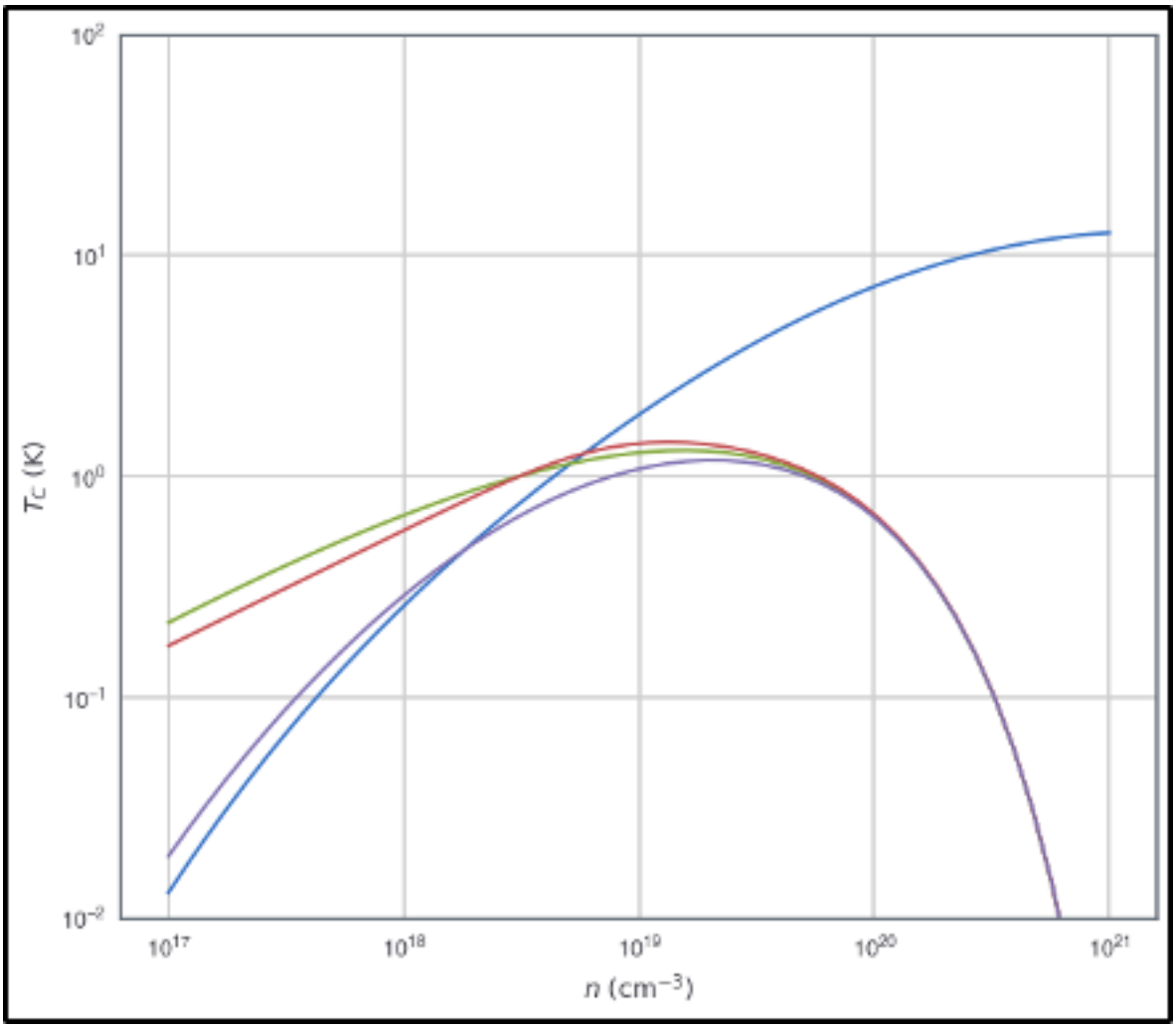

Figure 4.5: Superconducting phase diagram for different models related to STO. Blue: Full RPA calculation with STO parameters. Purple: plasmon-pole calculation with STO parameters. Red: "Paraelectric" $\gamma = .3$ STO, plasmon pole. Green: pure plasmon

unequal effect of Thomas-Fermi screening on the Coulomb repulsion and the electron-ion attraction, but frankly more work is needed to disentangle these effects.

4.4 Extracting a cumulant effective interaction

The final idea to which this work is leading is to regard (4.7) as a generic self-consistency condition and compute it for a numerically generated V_{eff} from the cumulant expansion. Specifically, at T_c where the gap vanishes, the normal-state equation is equivalent to what we have painstakingly computed in the previous chapter, while it should not be a bad approximation to regard the same V_{eff} entering the anomalous self-energy at this level. Nevertheless it should be emphasized that these are completely uncontrolled approximations, and are meant to provide a complementary perspective to the existing observations that the simplest classes of vertex corrections and self-energy corrections that have been considered for models like this tend to vanish in the dilute limit, and the conflicting intuition that it is precisely in that limit that the leading-order calculation is not well-controlled and may be expected to fail.

The problem at hand is then to extract a V_{eff} from what we have already computed, i.e. a spectral function (and therefore, formally, an associated self-energy by Dyson's equation). Starting from (4.7), we can similarly use the spectral decomposition of the interaction to produce an expression for the dynamic part of the self-energy:

$$\begin{aligned} S_{\text{dyn}}(i\nu_m, \epsilon) = \int d\epsilon' \; N(\epsilon') \int_0^\infty \frac{d\Omega}{\pi} \Im V(\Omega, \epsilon, \epsilon') \int_{-\infty}^\infty \frac{d\eta}{2\pi} A(\eta, \epsilon') \times \\ T \sum_n \frac{1}{i\nu_m + i\omega_n - \eta} \left(\frac{1}{i\omega_n - \Omega} - \frac{1}{i\omega_n + \Omega} \right) \end{aligned} \tag{4.31}$$

where $A(\eta, \epsilon)$ is the usual spectral function. The Matsubara sum goes the same way as before

and after analytic continuation we have

$$S_{\mathrm{dyn}}(\omega,\epsilon) = \int d\epsilon'\ N(\epsilon')\ \int_0^\infty \frac{d\Omega}{\pi}\Im V(\Omega,\epsilon,\epsilon')\ \int_{-\infty}^{\infty}\frac{d\eta}{2\pi}A(\eta,\epsilon')\times \left(\frac{-1-n_B(\Omega)+n_F(\eta)}{\omega-\Omega-\eta+i\delta}-\frac{n_B(\Omega)+n_F(\eta)}{\omega+\Omega-\eta+i\delta}\right) \tag{4.32}$$

Taking the imaginary part and integrating over the delta functions one obtains

$$\Im S(\omega,\epsilon) = \int d\epsilon'\ N(\epsilon')\ \int_0^\infty \frac{d\Omega}{\pi}\Im V(\Omega,\epsilon,\epsilon')\times \big(\Theta(-\omega-\Omega)A(\omega+\Omega,\epsilon')+\Theta(\omega-\Omega)A(\omega-\Omega,\epsilon')\big) \tag{4.33}$$

This can be viewed as a sort of self-consistency condition from which $\Im V$ can be determined if $\Im S$ and the spectral function A are known. As a sanity check, using $A(\eta,\epsilon) = 2\pi\delta(\eta-(\epsilon-\mu))$ and $\Im V$ derived from the bare V reproduces the one-loop calculation of $\Im S$.

In practice, this is formulated as a large linear regression problem over all available frequency and momenta simultaneously. It turns out that using a mixed L^1 and L^2 norm for the regression, with the relative weight as an adjustable parameter, seems to produce superior results. The method nevertheless struggles to generate effective potentials that succeed in fitting the input spectral functions. The most salient reason evident to date is that while the spectral functions are originally computed using an integration over all energy and momenta worth sampling, the fit can only make use of the energy and momenta at which the spectral functions have been computed. This gives rise to sharp unphysical features in the imputed $\Im V$ at k_F and $2k_F$, as well as high-energy feature to the extent that $A(\omega,k)$ is still finite in the tails of the input data.

4.5 Conclusions

The history of superconductivity in STO is littered with incorrect theories which produce phase diagrams that match the experimental data. Although the inclusion of physics off

the energy shell and renormalized by the cumulant expansion will no doubt quantitatively change the results presented above, it is already possible to draw a number of conclusions. First, there is a seductive story sometimes told, in which thanks to the hybridization of the phonon with the plasmon there is an adiabatic lower mode that allows for a well-controlled calculation. Unfortunately, in bulk STO, there is simply not enough oscillator strength in the lower mode to mediate pairing, which is in fact almost entirely due to the upper mode.

Second, once one grants the premise of doing such an anti-adiabatic calculation at one-loop order, it turns out that a dome structure is quite generic and the details of the boson spectrum cause only quantitative changes. This is fortunate insofar as it provides a straightforward recipe for extending this calculation to other models or operating on experimental data, as it is quite easy to obtain a dielectric function, compared to for instance the $\alpha^2 F$ and μ^* that are relevant for an Eliashberg-style calculation. The fact that superconductivity is so generic in these models, however, ought to give one pause in assessing the usefulness of the model by its ability to predict T_c. As we argued at length in the introduction to this thesis with respect to the BEC-BCS crossover, in the end T_c is just one number and far less informative than the dynamical signatures of a state of matter.

CHAPTER 5

CONCLUDING REMARKS

5.1 Future Directions

As is nearly always the case in any science, the work presented in this thesis has raised more questions than it has answered. A recurring theme that has emerged in these calculations is the paradoxical impact of diluteness: on the one hand, the generic theoretical expectation is that dilute systems become more strongly-interacting and therefore any type of perturbative calculation becomes less reliable. On the other hand, the calculations presented in this thesis do not suffer from any great divergences or other obvious unphysical results in the dilute limit. If anything, diluteness produces appealing simplifications. Of course many calculations are already performed beginning with strong coupling in mind, and in many cases handle this problem in a well-controlled way by regularizing the problem on some underlying lattice (often the physical crystal lattice). In this way strong electron-electron interactions become a Hubbard U, electron-phonon interactions become Holstein models, and so on. I would like to point out two problems already alluded to in this thesis where this approach is made more difficult by the importance of long-range forces.

5.1.1 Quantum Crystallization

The study of polaritons on a lattice is a first step to understanding the problem when the lattice emerges spontaneously on a length scale set by the exciton-exciton interaction rather than being externally imposed. One can imagine this as merely some very dilute Mott lobe of the supersolid problem described earlier in this thesis, that is stable when interactions are sufficiently strong, and that is somehow favored over simpler states by an interaction-induced detuning from the photon field. This is however a very cumbersome description and misses the details of the low-energy physics except by calculating the high-energy physics in the

same detail. An RPA-like approach is hampered here by the extremely heavy exciton mass and the fact that the resulting exciton dynamics are therefore carried by processes involving photons beyond those that we have already considered.

5.1.2 The Plasmon in STO

The substantial disagreement between the cumulant calculation and the experimental facts of STO can be broadly construed as a puzzle of a missing plasmon. The plasmon can be broadened away to nearly nothing by a large enough quasiparticle scattering rate which at least phenomenologically is an adequate description of some high-temperature superconducting materials. The high-temeprature phase of STO does not appear to be this kind of marginal Fermi liquid (keeping a nearly T^2 resistivity up to room temperature) but does exhibit "bad metallicity" in the sense of scattering rates. Whatever physics can stabilize this high-temperature state may well persist down to low temperatures and account for the absence of a plasmon there as well. Part of the motivation for performing the cumulant expansion was the hope that some of the higher-order crossing diagrams would describe some phonon-mediated mechanism for this effect. Unfortunately it appears that plasmon pole-like coupled modes are all that emerge. An interesting avenue to investigate is some non-perturbative agglomeration of two or more electrons into polaronic objects that may carry the quasiparticle dynamics of the system without much collective response.

5.2 Cavity Physics

I would like to conclude this thesis by situating the calculations described here as examples of cavity physics. In the polariton case this is quite literal, while my use of this term for STO is motivated by the experiments of (Thomas et al. [2019]), where the T_c of a conventional superconductor was raised by embedding it in a physical cavity. The cavity mediates long-ranged electromagnetic interactions that would not be present in the bare material. In STO

a similar effect is accomplished by either the plasmon or the lattice, depending on one's perspective. In either case, the properties of the model are then substantially modified by the emergence of coupled modes at new energy scales.

Whether or not such models are ultimately good descriptions of physical reality, as tools for theory they provide a way to introduce new, tunable emergent energy scales while remaining physically constrained in important ways. On one extreme, the new energy scales emerge naturally (as in the problem of BCS superconductivity) are often difficult to control and widely separated from the existing scales in a given model; this is the classic hallmark of emergence. In a polariton condensate, in contrast, the energy scales are tunable by the properties of the cavity and the strength of the coupling. On the other hand, a cavity is not completely an external field of some kind that is freely tunable. The electron-plasmon-phonon system must still be stable - the phonon coupling strength cannot be manually turned up so high that the system is driven ferroelectric - and must still satisfy the f sum rule. In other words a properly considered cavity forms part of the physical system and is subject to physical constraints.

REFERENCES

Mathieu Alloing, Mussie Beian, Maciej Lewenstein, David Fuster, Yolanda González, Luisa González, Roland Combescot, Monique Combescot, and François Dubin. Evidence for a Bose-Einstein condensate of excitons. *EPL*, 107(1):10012, July 2014.

Alexander Altland and Ben Simons. *Condensed Matter Field Theory*. Cambridge University Press, New York, 2 edition, 2010.

J R Arce-Gamboa and G G Guzman-Verri. Quantum ferroelectric instabilities in superconducting srtio$_3$. Jan 2018. URL `https://arxiv.org/abs/1801.08736`.

Wei Bao, Xiaoze Liu, Fei Xue, Fan Zheng, Renjie Tao, Siqi Wang, Yang Xia, Mervin Zhao, Jeongmin Kim, Sui Yang, Quanwei Li, Ying Wang, Yuan Wang, Lin-Wang Wang, Allan H. MacDonald, and Xiang Zhang. Observation of rydberg exciton polaritons and their condensate in a perovskite cavity. *Proceedings of the National Academy of Sciences*, 116 (41):20274–20279, 2019. ISSN 0027-8424. doi: 10.1073/pnas.1909948116.

R A Barankov, L S Levitov, and B Z Spivak. Collective Rabi Oscillations and Solitons in a Time-Dependent BCS Pairing Problem. *Physical Review Letters*, 93(16):160401, October 2004.

A Bardasis and J R Schrieffer. Excitons and Plasmons in Superconductors. *Phys. Rev.*, 121 (4):1050–1062, February 1961.

Kristian Baumann, Christine Guerlin, Ferdinand Brennecke, and Tilman Esslinger. Dicke quantum phase transition with a superfluid gas in an optical cavity. *Nature*, 464(7293): 1301–1306, 2010. ISSN 0028-0836. doi: 10.1038/nature09009.

Gordon Baym, Jean-Paul Blaizot, Markus Holzmann, Franck Laloë, and Dominique Vautherin. The Transition Temperature of the Dilute Interacting Bose Gas. *Physical Review Letters*, 83(9):1703–1706, August 1999.

Lotfi Belkhir and Mohit Randeria. Collective excitations and the crossover from Cooper pairs to composite bosons in the attractive Hubbard model. *Phys. Rev. B*, 45(9):5087–5090, March 1992.

Immanuel Bloch, Jean Dalibard, and Sylvain Nascimbène. Quantum simulations with ultracold quantum gases. *Nat Phys*, 8(4):267–276, April 2012.

Eric Braaten. Universal relations for fermions with large scattering length. In Wilhelm Zwerger, editor, *The BCS-BEC Crossover and the Unitary Fermi Gas*. Springer, Heidelberg, 2012.

Terence M Bretz-Sullivan, Alexander Edelman, J S Jiang, Alexey Suslov, David Graf, Jianjie Zhang, Gensheng Wang, Clarence Chang, John E Pearson, Alex B Martinson, and et al. Superconductivity in the dilute single band limit in reduced strontium titanate. *arXiv*, 2019.

R T Brierley, P B Littlewood, and P R Eastham. Amplitude-Mode Dynamics of Polariton Condensates. *Physical Review Letters*, 107(4):040401, July 2011.

D A Browne and K Levin. Collective modes in charge-density-wave superconductors. *Phys. Rev. B*, 28(7):4029–4032, October 1983.

Evgeni Burovski, Evgeny Kozik, Nikolay Prokof'ev, Boris Svistunov, and Matthias Troyer. Critical Temperature Curve in BEC-BCS Crossover. *Physical Review Letters*, 101(9): 090402, August 2008.

E W Carlson, V J Emery, S A Kivelson, and D Orgad. Concepts in High Temperature Superconductivity. June 2002.

Cheng Chin, Rudolf Grimm, Paul Julienne, and Eite Tiesinga. Feshbach resonances in ultracold gases. *Rev. Mod. Phys.*, 82(2):1225–1286, April 2010.

Jaewon Choi, Alexey A Zadorozhko, Jeakyung Choi, and Eunseong Kim. Spatially modulated superfluid state in two-dimensional ^{4}he films. *arXiv*, 2021. doi: 10.1103/physrevlett.127.135301.

M J Coak, C R S Haines, C Liu, S E Rowley, G G Lonzarich, and S S Saxena. Emergence of a quantum coherent state at the border of ferroelectricity. Aug 2018. URL `https://arxiv.org/abs/1808.02428`.

Leon N Cooper. Bound Electron Pairs in a Degenerate Fermi Gas. *Physical Review*, 104(4): 1189–1190, November 1956.

R Côté and A Griffin. Cooper-pair-condensate fluctuations and plasmons in layered superconductors. *Phys. Rev. B*, 48(14):10404–10425, October 1993.

J T Devreese, S N Klimin, J L M van Mechelen, and D van der Marel. Many-body large polaron optical conductivity in srti(1-x)nb(x)o3. *Physical Review B*, 81(12):125119, Mar 2010. ISSN 1098-0121. doi: 10.1103/physrevb.81.125119. URL `https://journals.aps.org/prb/abstract/10.1103/PhysRevB.81.125119`.

Yu. I. Dublenych. Ground states of lattice-gas models on the triangular and honeycomb lattices: Devil's step and quasicrystals. *Physical Review E*, 80(1):011123, 2009. ISSN 1539-3755. doi: 10.1103/physreve.80.011123.

R Duncan and C Sá de Melo. Thermodynamic properties in the evolution from BCS to Bose-Einstein condensation for a d-wave superconductor at low temperatures. *Phys. Rev. B*, 62(14):9675–9687, October 2000.

K Dunnett, Awadhesh Narayan, N A Spaldin, and A V Balatsky. Strain and ferroelectric soft mode induced superconductivity in strontium titanate. Dec 2017. doi: 10.1103/physrevb.97.144506. URL `https://arxiv.org/abs/1712.08368`.

M Dzero, E A Yuzbashyan, and B L Altshuler. Cooper pair turbulence in atomic Fermi gases. *EPL*, 85(2):20004, January 2009.

P R Eastham and P B Littlewood. Bose condensation in a model microcavity. *Solid State Communications*, 116(7):357 361, Oct 2000. ISSN 0038-1098. doi: 10.1016/s0038-1098(00)00350-1. URL http://www.sciencedirect.com/science/article/pii/S0038109800003501.

Jan R Engelbrecht, Mohit Randeria, and C A R Sáde Melo. BCS to Bose crossover: Broken-symmetry state. *Phys. Rev. B*, 55(22):15153–15156, June 1997.

Daniel Fisher and P Hohenberg. Dilute Bose gas in two dimensions. *Phys. Rev. B*, 37(10): 4936–4943, April 1988.

J N Fuchs, A Recati, and W Zwerger. Exactly Solvable Model of the BCS-BEC Crossover. *Physical Review Letters*, 93(9):090408, August 2004.

Maria N Gastiasoro, Andrey V Chubukov, and Rafael M Fernandes. Phonon-mediated superconductivity in low carrier-density systems. *Physical Review B*, 99(9):094524, Mar 2019. ISSN 2469-9950. doi: 10.1103/physrevb.99.094524. URL https://journals.aps.org/prb/abstract/10.1103/PhysRevB.99.094524.

Maria N Gastiasoro, Thais V Trevisan, and Rafael M Fernandes. Anisotropic superconductivity mediated by ferroelectric fluctuations in cubic systems with spin-orbit coupling. *arXiv*, 2020. doi: 10.1103/physrevb.101.174501.

François Gervais, Jean-Louis Servoin, Alexis Baratoff, Johannes G Bednorz, and Gerd Binnig. Temperature dependence of plasmons in Nb-doped $SrTiO_3$. *Phys. Rev. B*, 47(13): 8187–8194, April 1993a.

Francois Gervais, Jean-Louis Servoin, Alexis Baratoff, Johannes G Bednorz, and Gerd Binnig. Temperature dependence of plasmons in nb-doped srtio3. *Physical Review B*, 47 (13):8187 8194, Apr 1993b. URL https://journals.aps.org/prb/abstract/10.1103/PhysRevB.47.8187.

Gabriele Giuliani and Giovanni Vignale. *Quantum Theory of the Electron Liquid*. Cambridge University Press, 2005. doi: 10.1017/CBO9780511619915.

L P Gorkov and T K Melikbarkhudarov. Contribution to the Theory of Superfluidity in an Imperfect Fermi Gas. *Soviet Physics Jetp-Ussr*, 13(5):1018–1022, 1961.

Lev P. Gor'kov. Phonon mechanism in the most dilute superconductor n-type srtio3. *Proceedings of the National Academy of Sciences*, 113(17):4646–4651, 2016. ISSN 0027-8424. doi: 10.1073/pnas.1604145113.

M Grabowski and L J Sham. Superconductivity from nonphonon interactions. *Physical Review B*, 29(11):6132 6142, Jun 1984. ISSN 1098-0121. doi: 10.1103/physrevb.29.6132. URL https://journals.aps.org/prb/abstract/10.1103/PhysRevB.29.6132.

O. Gunnarsson. Corrections to migdal's theorem for spectral functions: A cumulant treatment of the time-dependent green's function. *Physical Review B*, 50(15):10462 10473, Oct 1994. ISSN 1098-0121. doi: 10.1103/physrevb.50.10462. URL https://journals.aps.org/prb/abstract/10.1103/PhysRevB.50.10462.

Tom Gustafsson. A simple technique for unstructured mesh generation via adaptive finite elements. *Rakenteiden Mekaniikka*, 54(2):69–79, 2021. doi: 10.23998/rm.99648.

Ryo Hanai and Yoji Ohashi. Heteropairing and component-dependent pseudogap phenomena in an ultracold Fermi gas with different species with different masses. *Phys. Rev. A*, 90 (4):043622, October 2014.

E Hanamura and H Haug. Condensation effects of excitons. *Physics Reports*, 33(4):209–284, October 1977.

R Haussmann, W Rantner, S Cerrito, and W Zwerger. Thermodynamics of the BCS-BEC crossover. *Phys. Rev. A*, 75(2):023610, February 2007.

Lars Hedin. New method for calculating the one-particle green's function with application to the electron-gas problem. *Physical Review*, 139(3A):A796 A823, Aug 1965. ISSN 0031-899X. doi: 10.1103/physrev.139.a796. URL https://journals.aps.org/pr/abstract/10.1103/PhysRev.139.A796.

H Heiselberg, C J Pethick, H Smith, and L Viverit. Influence of Induced Interactions on the Superfluid Transition in Dilute Fermi Gases. *Physical Review Letters*, 85(12):2418–2421, September 2000.

A A High, J R Leonard, A T Hammack, M M Fogler, L V Butov, A V Kavokin, K L Campman, and A C Gossard. Spontaneous coherence in a cold exciton gas. *Nature*, 483(7391):584 588, Mar 2012. ISSN 1476-4687. doi: 10.1038/nature10903. URL http://www.nature.com/nature/journal/v483/n7391/full/nature10903.html.

Fengrui Hu and Zhe Fei. Recent progress on exciton polaritons in layered transition-metal dichalcogenides. *Advanced Optical Materials*, 8(5):1901003, 2020. ISSN 2195-1071. doi: 10.1002/adom.201901003.

Xiong Huang, Tianmeng Wang, Shengnan Miao, Chong Wang, Zhipeng Li, Zhen Lian, Takashi Taniguchi, Kenji Watanabe, Satoshi Okamoto, Di Xiao, Su-Fei Shi, and Yong-Tao Cui. Correlated insulating states at fractional fillings of the ws2/wse2 moire lattice. *Nature Physics*, 17(6):715–719, 2021. ISSN 1745-2473. doi: 10.1038/s41567-021-01171-w.

Chen-Lung Hung, Victor Gurarie, and Cheng Chin. From Cosmology to Cold Atoms: Observation of Sakharov Oscillations in a Quenched Atomic Superfluid. *Science*, 341(6151): 1213–1215, September 2013.

J I Jang and J P Wolfe. Biexcitons in the semiconductor Cu2O: An explanation of the rapid decay of excitons. *Phys. Rev. B*, 72(24):241201, December 2005.

J I Jang and J P Wolfe. Auger recombination and biexcitons in Cu2O: A case for dark excitonic matter. *Phys. Rev. B*, 74(4):045211, July 2006.

J I Jang, K E O'Hara, and J P Wolfe. Spin-exchange kinetics of excitons in Cu2O: Transverse acoustic phonon mechanism. *Phys. Rev. B*, 70(19):195205, November 2004.

Chenhao Jin, Zui Tao, Tingxin Li, Yang Xu, Yanhao Tang, Jiacheng Zhu, Song Liu, Kenji Watanabe, Takashi Taniguchi, James C. Hone, Liang Fu, Jie Shan, and Kin Fai Mak. Stripe phases in wse2/ws2 moire superlattices. *Nature Materials*, 20(7):940–944, 2021. ISSN 1476-1122. doi: 10.1038/s41563-021-00959-8.

Makoto Kaburagi and Junjiro Kanamori. Ordered structure of adatoms in the extended range lattice gas model. *Japanese Journal of Applied Physics*, 13(S2):145, 1974. ISSN 0021-4922. doi: 10.7567/jjaps.2s2.145.

Shota Kanasugi, Dushko Kuzmanovski, Alexander V. Balatsky, and Youichi Yanase. Ferroelectricity-induced multiorbital odd-frequency superconductivity in srtio3. *Physical Review B*, 102(18):184506, 2020. ISSN 2469-9950. doi: 10.1103/physrevb.102.184506.

J J Kas, J J Rehr, and L Reining. Cumulant expansion of the retarded one-electron green function. *Physical Review B*, 90(8):686, Aug 2014. ISSN 1098-0121. doi: 10.1103/physrevb.90.085112.

J Kasprzak, M Richard, S Kundermann, A Baas, P Jeambrun, J M J Keeling, F M Marchetti, M H Szyma nacute, ska, R André, J L Staehli, V Savona, P B Littlewood, B Deveaud, and Le Si Dang. Bose—[ndash]—Einstein condensation of exciton polaritons. *Nature*, 443 (7110):409–414, September 2006a.

J Kasprzak, M Richard, S Kundermann, A Baas, P Jeambrun, J M J Keeling, F M Marchetti, M H Szyma nacute, ska, R Andre, J L Staehli, V Savona, P B Littlewood, B Deveaud, and Le Si Dang. Bose—[ndash]—einstein condensation of exciton polaritons. *Nature*, 443(7110):409 414, Sep 2006b. ISSN 1476-4687. doi: 10.1038/nature05131. URL `http://www.nature.com/nature/journal/v443/n7110/abs/nature05131.html`.

T Kazimierczuk, D Fröhlich, S Scheel, H Stolz, and M Bayer. Giant rydberg excitons in the copper oxide cu2o. *Nature*, 514(7522):343 347, Oct 2014. ISSN 1476-4687. doi: 10.1038/nature13832. URL `http://www.nature.com/nature/journal/v514/n7522/full/nature13832.html`.

Yaron Kedem, Jian-Xin Zhu, and Alexander V Balatsky. Unusual superconducting isotope effect in the presence of a quantum criticality. *Physical Review B*, 93(18):184507, May 2016. ISSN 2469-9950. doi: 10.1103/physrevb.93.184507.

Jonathan Keeling, P Eastham, M Szymanska, and P Littlewood. Polariton condensation with localized excitons and propagating photons. *Physical Review Letters*, 93(22):226403, Nov 2004. ISSN 0031-9007. doi: 10.1103/physrevlett.93.226403. URL `http://prl.aps.org/abstract/PRL/v93/i22/e226403`.

L V Keldysh and A N Kozlov. Collective Properties of Excitons in Semiconductors. *Soviet Physics Jetp-Ussr*, 27(3):521–&, 1968.

L.V. Keldysh. Macroscopic coherent states of excitons in superconductors. In S. Stringari A. Griffin, D.W. Snoke, editor, *Bose-Einstein Condensation*. Cambridge University Press, Cambridge, 1995.

S Kena-Cohen and S R Forrest. Room-temperature polariton lasing in an organic single-crystal microcavity. *Nature Photonics*, 4(6):371 375, Jun 2010. ISSN 1749-4893. doi: 10.1038/nphoton.2010.86. URL `http://www.nature.com/nphoton/journal/v4/n6/full/nphoton.2010.86.html`.

M E Kim, A Das, and S D Senturia. Electron scattering interaction with coupled plasmon-polar-phonon modes in degenerate semiconductors. *Physical Review B*, 18(12):6890 6899, Dec 1978. ISSN 1098-0121. doi: 10.1103/physrevb.18.6890. URL `https://journals.aps.org/prb/abstract/10.1103/PhysRevB.18.6890`.

D. A. Kirzhnits, E. G. Maksimov, and D. I. Khomskii. The description of superconductivity in terms of dielectric response function. *Journal of Low Temperature Physics*, 10(1-2):79–93, 1973. ISSN 0022-2291. doi: 10.1007/bf00655243.

S N Klimin, J Tempere, J T Devreese, and D van der Marel. Multiband superconductivity due to the electron-lo-phonon interaction in strontium titanate and on a srtio3/laalo3 interface. *Journal of Superconductivity and Novel Magnetism*, 30(3):757–761, 2016. ISSN 1557-1939. doi: 10.1007/s10948-016-3664-2.

C. S. Koonce, Marvin L. Cohen, J. F. Schooley, W. R. Hosler, and E. R. Pfeiffer. Superconducting transition temperatures of semiconducting srtio3. *Physical Review*, 163(2):380–390, 1967. ISSN 0031-899X. doi: 10.1103/physrev.163.380.

Ioan Kosztin, Qijin Chen, Ying-Jer Kao, and K Levin. Pair excitations, collective modes, and gauge invariance in the BCS–Bose-Einstein crossover scenario. *Phys. Rev. B*, 61(17):11662–11675, May 2000.

C. W. Lai, N. Y. Kim, S. Utsunomiya, G. Roumpos, H. Deng, M. D. Fraser, T. Byrnes, P. Recher, N. Kumada, T. Fujisawa, and Y. Yamamoto. Coherent zero-state and π-state in an exciton-polariton condensate array. *Nature*, 450(7169):529–532, 2007. ISSN 0028-0836. doi: 10.1038/nature06334.

Victor Lakhno. Cooper pairs and bipolarons. *Modern Physics Letters B*, 30(31):1650365, November 2016.

T D Lee, F E Low, and D Pines. The Motion of Slow Electrons in a Polar Crystal. *Physical Review*, 90(2):297–302, April 1953.

A.J. Leggett. Diatomic molecules and cooper pairs. In J.A. Przystawa A. Pękalski, editor, *Modern Trends in the Theory of Condensed Matter, Proceedings of the XVI Karpacz Winter School*. Springer, Berlin Heidelberg New York, 1980.

Peter Lepage. gplepage/vegas: vegas version 3.4.2, February 2020. URL https://doi.org/10.5281/zenodo.3647546.

Jesper Levinsen and Meera M Parish. Strongly interacting two-dimensional Fermi gases. August 2014.

Weijie Li, Xin Lu, Sudipta Dubey, Luka Devenica, and Ajit Srivastava. Dipolar interactions between localized interlayer excitons in van der waals heterostructures. *Nature Materials*, 19(6):624–629, 2020. ISSN 1476-1122. doi: 10.1038/s41563-020-0661-4.

Xiao Lin, Zengwei Zhu, Benoît Fauqué, and Kamran Behnia. Fermi Surface of the Most Dilute Superconductor. *Phys. Rev. X*, 3(2):021002, April 2013a.

Xiao Lin, Zengwei Zhu, Benoit Fauque, and Kamran Behnia. Fermi surface of the most dilute superconductor. *Physical Review X*, 3(2):021002, Apr 2013b. doi: 10.1103/physrevx.3.021002. URL https://journals.aps.org/prx/abstract/10.1103/PhysRevX.3.021002.

Xiao Lin, German Bridoux, Adrien Gourgout, Gabriel Seyfarth, Steffen Krämer, Marc Nardone, Benoît Fauqué, and Kamran Behnia. Critical Doping for the Onset of a Two-Band Superconducting Ground State in $SrTiO_3$. *Physical Review Letters*, 112(20):207002, May 2014.

Xiao Lin, Benoît Fauqué, and Kamran Behnia. Scalable T2 resistivity in a small single-component Fermi surface. *Science*, 349(6251):945–948, August 2015a.

Xiao Lin, Benoit Fauque, and Kamran Behnia. Scalable t2 resistivity in a small single-component fermi surface. *Science*, 349(6251):945 948, Aug 2015b. ISSN 0036-8075. doi: 10.1126/science.aaa8655. URL http://science.sciencemag.org/content/349/6251/945.

Xiao Lin, Carl Willem Rischau, Lisa Buchauer, Alexandre Jaoui, Benoit Fauque, and Kamran Behnia. Metallicity without quasi-particles in room-temperature strontium titanate. *npj Quantum Materials*, 2(1):2847, Jul 2017. doi: 10.1038/s41535-017-0044-5.

P Littlewood and C Varma. Gauge-Invariant Theory of the Dynamical Interaction of Charge Density Waves and Superconductivity. *Physical Review Letters*, 47(11):811–814, September 1981.

P Littlewood and C Varma. Amplitude collective modes in superconductors and their coupling to charge-density waves. *Phys. Rev. B*, 26(9):4883–4893, November 1982.

P B Littlewood and Xuejun Zhu. Possibilities for exciton condensation in semiconductor quantum-well structures. *Phys. Scr.*, 1996(T68):56–67, January 1996.

B I Lundqvist. Single-particle spectrum of the degenerate electron gas. *Physik der kondensierten Materie*, 7(2):117 123, Mar 1968. ISSN 0031-9236. doi: 10.1007/bf02422898. URL https://link.springer.com/article/10.1007/BF02422898.

R H Lyddane, R G Sachs, and E Teller. On the polar vibrations of alkali halides. *Physical Review*, 59(8):673 676, Apr 1941. ISSN 0031-899X. doi: 10.1103/physrev.59.673. URL https://journals.aps.org/pr/abstract/10.1103/PhysRev.59.673.

Gerald Mahan. *Many-Particle Physics*. Springer, Boston, 3 edition, 2000.

D van der Marel, J L M van Mechelen, and I I Mazin. Common fermi-liquid origin of t^2 resistivity and superconductivity in n-type srtio3. *Physical Review B*, 84(20):205111, Nov 2011. ISSN 1098-0121. doi: 10.1103/physrevb.84.205111. URL https://journals.aps.org/prb/abstract/10.1103/PhysRevB.84.205111.

D van der Marel, F Barantani, and C W Rischau. Possible mechanism for superconductivity in doped srtio 3. *Physical Review Research*, 1(1), 2019. doi: 10.1103/physrevresearch.1.013003.

Valentina Martelli, Julio Larrea Jimenez, Mucio Continentino, Elisa Baggio-Saitovitch, and Kamran Behnia. Thermal transport and phonon hydrodynamics in strontium titanate. *Physical Review Letters*, 120(12):125901, 2018. ISSN 0031-9007. doi: 10.1103/physrevlett.120.125901.

Ryusuke Matsunaga, Yuki I Hamada, Kazumasa Makise, Yoshinori Uzawa, Hirotaka Terai, Zhen Wang, and Ryo Shimano. Higgs Amplitude Mode in the BCS Superconductors Nb1−xTixNInduced by Terahertz Pulse Excitation. *Physical Review Letters*, 111(5):057002, July 2013.

James McClain, Johannes Lischner, Thomas Watson, Devin A Matthews, Enrico Ronca, Steven G Louie, Timothy C Berkelbach, and Garnet Kin-Lic Chan. Spectral functions of the uniform electron gas via coupled-cluster theory and comparison to the *gw* and related approximations. *Physical Review B*, 93(23):201, Dec 2015. ISSN 2469-9950. doi: 10.1103/physrevb.93.235139. URL http://arxiv.org/abs/1512.04556.

M A Méasson, Y Gallais, M Cazayous, B Clair, P Rodière, L Cario, and A Sacuto. Amplitude Higgs mode in the 2H−NbSe2superconductor. *Phys. Rev. B*, 89(6):060503, February 2014.

Shengnan Miao, Tianmeng Wang, Xiong Huang, Dongxue Chen, Zhen Lian, Chong Wang, Mark Blei, Takashi Taniguchi, Kenji Watanabe, Sefaattin Tongay, Zenghui Wang, Di Xiao, Yong-Tao Cui, and Su-Fei Shi. Strong interaction between interlayer excitons and correlated electrons in wse2/ws2 moire superlattice. *Nature Communications*, 12(1):3608, 2021. doi: 10.1038/s41467-021-23732-6.

K A Müller and H Burkard. SrTi O3: An intrinsic quantum paraelectric below 4 K. *Phys. Rev. B*, 19(7):3593–3602, April 1979.

D W Snoke N Proukakis and P B Littlewood, editors. *Universal themes of Bose-Einstein condensation*. Cambridge University Press, Cambridge, 2017.

Jean Paul Nery, Philip B Allen, Gabriel Antonius, Lucia Reining, Anna Miglio, and Xavier Gonze. Quasiparticles and phonon satellites in spectral functions of semiconductors and insulators: Cumulants applied to full first principles theory and fröhlich polaron. *Physical Review B*, 97(11):920, Oct 2017. ISSN 2469-9950. doi: 10.1103/physrevb.97.115145. URL `https://arxiv.org/abs/1710.07594`.

Vudtiwat Ngampruetikorn, Jesper Levinsen, and Meera M Parish. Pair Correlations in the Two-Dimensional Fermi Gas. *Physical Review Letters*, 111(26):265301, December 2013.

Yusuke Nishida and Dam Thanh Son. Unitary fermi gas, ϵ expansion, and nonrelativistic conformal field theories. In Wilhelm Zwerger, editor, *The BCS-BEC Crossover and the Unitary Fermi Gas*. Springer-Verlag, Heidelberg, 2012.

P Nozières and S Schmitt-Rink. Bose condensation in an attractive fermion gas: From weak to strong coupling superconductivity. *J Low Temp Phys*, 59(3-4):195–211, May 1985.

K E O'Hara and J P Wolfe. Relaxation kinetics of excitons in cuprous oxide. *Phys. Rev. B*, 62(19):12909–12922, November 2000.

Y Ohashi. BCS-BEC Crossover in a Gas of Fermi Atoms with a p-Wave Feshbach Resonance. *Physical Review Letters*, 94(5):050403, February 2005.

Meera M Parish. The BCS-BEC Crossover. February 2014.

Meera M Parish, Bogdan Mihaila, Eddy M Timmermans, Krastan B Blagoev, and Peter B Littlewood. BCS-BEC crossover with a finite-range interaction. *Phys. Rev. B*, 71(6): 064513, February 2005.

David Pekker and C M Varma. Amplitude/Higgs Modes in Condensed Matter Physics. *Annu. Rev. Condens. Matter Phys.*, 6(1):269–297, March 2015.

L Perfetti, B Sciolla, G Biroli, C J van der Beek, C Piovera, M Wolf, and T Kampfrath. Ultrafast Dynamics of Fluctuations in High-Temperature Superconductors Far from Equilibrium. *Physical Review Letters*, 114(6):067003, February 2015.

D S Petrov, C Salomon, and G V Shlyapnikov. Weakly Bound Dimers of Fermionic Atoms. *Physical Review Letters*, 93(9):090404, August 2004.

D S Petrov, C Salomon, and G V Shlyapnikov. Scattering properties of weakly bound dimers of fermionic atoms. *Phys. Rev. A*, 71(1):012708, January 2005.

L. Pickup, H. Sigurdsson, J. Ruostekoski, and P. G. Lagoudakis. Synthetic band-structure engineering in polariton crystals with non-hermitian topological phases. *Nature Communications*, 11(1):4431, 2020. doi: 10.1038/s41467-020-18213-1.

Popov and Fedotov. The functional-integration method and diagram technique for spin systems. *JETP*, 67:535, 1988.

V.N. Popov. *Functional Integrals and Collective Excitations*. Cambridge University Press, Cambridge, 1987.

A Rançon, Chen-Lung Hung, Cheng Chin, and K Levin. Quench dynamics in Bose-Einstein condensates in the presence of a bath: Theory and experiment. *Phys. Rev. A*, 88(3): 031601, September 2013.

Mohit Randeria. Crossover from bcs theory to bose-einstein condensation. In S. Stringari A. Griffin, D.W. Snoke, editor, *Bose-Einstein Condensation*. Cambridge University Press, Cambridge, 1995.

Mohit Randeria, Ji-Min Duan, and Lih-Yir Shieh. Bound states, Cooper pairing, and Bose condensation in two dimensions. *Physical Review Letters*, 62(9):981–984, February 1989.

Mohit Randeria, Ji-Min Duan, and Lih-Yir Shieh. Superconductivity in a two-dimensional Fermi gas: Evolution from Cooper pairing to Bose condensation. *Phys. Rev. B*, 41(1): 327–343, January 1990.

L Rettig, J H Chu, I R Fisher, U Bovensiepen, and M Wolf. Coherent dynamics of the charge density wave gap in tritellurides. *Faraday Discuss.*, 171(0):299–310, November 2014.

Carl Willem Rischau, Xiao Lin, Christoph P. Grams, Dennis Finck, Steffen Harms, Johannes Engelmayer, Thomas Lorenz, Yann Gallais, Benoit Fauque, Joachim Hemberger, and et al. A ferroelectric quantum phase transition inside the superconducting dome of sr1xcaxtio3δ. *Nature Physics*, 13(7):643–648, 2017. ISSN 1745-2473. doi: 10.1038/nphys4085.

S E Rowley, C Enderlein, J Ferreira de Oliveira, D A Tompsett, E Baggio Saitovitch, S S Saxena, and G G Lonzarich. Superconductivity in the vicinity of a ferroelectric quantum phase transition. Jan 2018. URL `https://arxiv.org/abs/1801.08121`.

Jonathan Ruhman and Patrick A Lee. Superconductivity at very low density: the case of strontium titanate. May 2016. doi: 10.1103/physrevb.94.224515. URL `https://arxiv.org/abs/1605.01737`.

C Sá de Melo, Mohit Randeria, and Jan Engelbrecht. Crossover from BCS to Bose superconductivity: Transition temperature and time-dependent Ginzburg-Landau theory. *Physical Review Letters*, 71(19):3202–3205, November 1993.

F Schmitt, P S Kirchmann, U Bovensiepen, R G Moore, L Rettig, M Krenz, J H Chu, N Ru, L Perfetti, D H Lu, M Wolf, I R Fisher, and Z X Shen. Transient Electronic Structure and Melting of a Charge Density Wave in TbTe3. *Science*, 321(5896):1649–1652, September 2008.

C Schneider, K Winkler, M D Fraser, M Kamp, Y Yamamoto, E A Ostrovskaya, and S Höfling. Exciton-polariton trapping and potential landscape engineering. *Reports on Progress in Physics*, 80(1):016503, 2016. ISSN 0034-4885. doi: 10.1088/0034-4885/80/1/016503.

J. F. Schooley, W. R. Hosler, and Marvin L. Cohen. Superconductivity in semiconducting srtio3. *Physical Review Letters*, 12(17):474–475, 1964. ISSN 0031-9007. doi: 10.1103/physrevlett.12.474.

Daniel E Sheehy and Leo Radzihovsky. BEC–BCS crossover, phase transitions and phase separation in polarized resonantly-paired superfluids. *Annals of Physics*, 322(8):1790–1924, August 2007.

Tomasz Smolenski, Pavel E. Dolgirev, Clemens Kuhlenkamp, Alexander Popert, Yuya Shimazaki, Patrick Back, Xiaobo Lu, Martin Kroner, Kenji Watanabe, Takashi Taniguchi, Ilya Esterlis, Eugene Demler, and Atac Imamoglu. Signatures of wigner crystal of electrons in a monolayer semiconductor. *Nature*, 595(7865):53–57, 2021. ISSN 0028-0836. doi: 10.1038/s41586-021-03590-4.

Ariel T Sommer, Lawrence W Cheuk, Mark J H Ku, Waseem S Bakr, and Martin W Zwierlein. Evolution of Fermion Pairing from Three to Two Dimensions. *Physical Review Letters*, 108(4):045302, January 2012.

R Sooryakumar and M V Klein. Raman Scattering by Superconducting-Gap Excitations and Their Coupling to Charge-Density Waves. *Physical Review Letters*, 45(8):660–662, August 1980.

Heinrich Stolz, Rico Schwartz, Frank Kieseling, Sunipa Som, Maria Kaupsch, Siegfried Sobkowiak, Dirk Semkat, Nobuko Naka, Thomas Koch, and Holger Fehske. Condensation of excitons in Cu2O at ultracold temperatures: experiment and theory. *New J. Phys.*, 14 (10):105007, October 2012.

Rui Su, Sanjib Ghosh, Jun Wang, Sheng Liu, Carole Diederichs, Timothy C. H. Liew, and Qihua Xiong. Observation of exciton polariton condensation in a perovskite lattice at room temperature. *Nature Physics*, 16(3):301–306, 2020. ISSN 1745-2473. doi: 10.1038/s41567-019-0764-5.

D G Suarez-Forero, F Riminucci, V Ardizzone, A Gianfrate, F Todisco, M De Giorgi, D Ballarini, G Gigli, K Baldwin, L Pfeiffer, and D Sanvitto. Ultrafast, low-energy, all-optical switch in polariton waveguides. *arXiv*, 2021.

Adrian G Swartz, Hisashi Inoue, Tyler A Merz, Yasuyuki Hikita, Srinivas Raghu, Thomas P Devereaux, Steven Johnston, and Harold Y Hwang. Polaronic behavior in a weak-coupling superconductor. *Proceedings of the National Academy of Sciences*, 115(7):1475 1480, Feb 2018. ISSN 0027-8424. doi: 10.1073/pnas.1713916115. URL `http://www.pnas.org/content/early/2018/01/29/1713916115.short`.

Hiroyuki Tajima, Takashi Kashimura, Ryo Hanai, Ryota Watanabe, and Yoji Ohashi. Uniform spin susceptibility and spin-gap phenomenon in the BCS-BEC-crossover regime of an ultracold Fermi gas. *Phys. Rev. A*, 89(3):033617, March 2014.

Yasutami Takada. Plasmon mechanism of superconductivity in two- and three-dimensional electron systems. *Journal of the Physical Society of Japan*, 45(3):786 794, Sep 1978. ISSN 0031-9015. doi: 10.1143/jpsj.45.786. URL https://journals.jps.jp/doi/10.1143/JPSJ.45.786.

Yasutami Takada. Theory of superconductivity in polar semiconductors and its application to n-type semiconducting srtio3. *Journal of the Physical Society of Japan*, 49(4):1267 1275, Oct 1980. ISSN 0031-9015. doi: 10.1143/jpsj.49.1267. URL https://www.jstage.jst.go.jp/article/jpsj1946/49/4/49_4_1267/_article.

Yasutami Takada. Insignificance of vertex corrections in the plasmon mechanism of superconductivity at low electron concentration: Migdal's theorem in the antiadiabatic region. *Journal of the Physical Society of Japan*, 61(11):3849 3852, Nov 1992. ISSN 0031-9015. doi: 10.1143/jpsj.61.3849. URL https://journals.jps.jp/doi/abs/10.1143/JPSJ.61.3849.

Markus Thiemann, Manfred H Beutel, Martin Dressel, Nicholas R Lee-Hone, David M Broun, Evangelos Fillis-Tsirakis, Hans Boschker, Jochen Mannhart, and Marc Scheffler. Single-gap superconductivity and dome of superfluid density in nb-doped srtio3. *Physical Review Letters*, 120(23):237002, Jun 2018. ISSN 0031-9007. doi: 10.1103/physrevlett.120.237002.

Anoop Thomas, Eloïse Devaux, Kalaivanan Nagarajan, Thibault Chervy, Marcus Seidel, David Hagenmüller, Stefan Schütz, Johannes Schachenmayer, Cyriaque Genet, Guido Pupillo, and Thomas W Ebbesen. Exploring superconductivity under strong coupling with the vacuum electromagnetic field. 2019.

I V Tokatly. Dilute Fermi Gas in Quasi-One-Dimensional Traps: From Weakly Interacting Fermions via Hard Core Bosons to a Weakly Interacting Bose Gas. *Physical Review Letters*, 93(9):090405, August 2004.

Yutaka Toyozawa. Dynamical properties of charge carriers in dielectrics. In Jozef T Devreese, editor, *Polarons in Ionic Crystals and Semiconductors*. 1972.

D van der Marel, J L M van Mechelen, and I I Mazin. Common fermi-liquid origin of t^2 resistivity and superconductivity in n-type $srtio_3$. *Phys. Rev. B*, 84(20):205111, November 2011.

Carla Verdi, Fabio Caruso, and Feliciano Giustino. Origin of the crossover from polarons to fermi liquids in transition metal oxides. *Nature Communications*, 8(1):1 7, May 2017. ISSN 2041-1723. doi: 10.1038/ncomms15769.

Pavel A Volkov, Premala Chandra, and Piers Coleman. Superconductivity from energy fluctuations in dilute quantum critical polar metals. *arXiv*, 2021.

Z Wang, S McKeown Walker, A Tamai, Y Wang, Z Ristic, F Y Bruno, A de la Torre, S Ricco, N C Plumb, M Shi, and et al. Tailoring the nature and strength of electron-phonon interactions in the srtio3(001) 2d electron liquid. *Nature Materials*, Apr 2016. doi: 10.

1038/nmat4623. URL http://www.nature.com/nmat/journal/vaop/ncurrent/full/nmat4623.html?WT.feed_name=subjects_surfaces-interfaces-and-thin-films.

Karol Winkler, Julian Fischer, Anne Schade, Matthias Amthor, Robert Dall, Jonas Geeler, Monika Emmerling, Elena A Ostrovskaya, Martin Kamp, Christian Schneider, and Sven Hofling. A polariton condensate in a photonic crystal potential landscape. *New Journal of Physics*, 17(2):023001, 2015. ISSN 1367-2630. doi: 10.1088/1367-2630/17/2/023001.

James P Wolfe and Joon I Jang. The search for Bose–Einstein condensation of excitons in Cu2O: exciton-Auger recombination versus biexciton formation. *New J. Phys.*, 16(12): 123048, December 2014.

Peter Wölfle and Alexander V Balatsky. Superconductivity at low density near a ferroelectric quantum critical point: Doped srtio. *Physical Review B*, 98(10):104505, Sep 2018. ISSN 2469-9950. doi: 10.1103/physrevb.98.104505. URL https://journals.aps.org/prb/abstract/10.1103/PhysRevB.98.104505.

Yang Xu, Song Liu, Daniel A. Rhodes, Kenji Watanabe, Takashi Taniguchi, James Hone, Veit Elser, Kin Fai Mak, and Jie Shan. Correlated insulating states at fractional fillings of moire superlattices. *Nature*, 587(7833):214–218, 2020. ISSN 0028-0836. doi: 10.1038/s41586-020-2868-6.

Hyeok Yoon, Adrian G Swartz, Shannon P Harvey, Hisashi Inoue, Yasuyuki Hikita, Yue Yu, Suk Bum Chung, Srinivas Raghu, and Harold Y Hwang. Low-density superconductivity in srtio$_3$ bounded by the adiabatic criterion. *arXiv*, 2021.

Kosuke Yoshioka, Eunmi Chae, and Makoto Kuwata-Gonokami. Transition to a Bose-Einstein condensate and relaxation explosion of excitons at sub-Kelvin temperatures. *Nat Comms*, 2:328, May 2011.

Kosuke Yoshioka, Yusuke Morita, Kenta Fukuoka, and Makoto Kuwata-Gonokami. Generation of ultracold paraexcitons in cuprous oxide: A path toward a stable Bose-Einstein condensate. *Phys. Rev. B*, 88(4):041201, July 2013.

Long Zhang, Fengcheng Wu, Shaocong Hou, Zhe Zhang, Yu-Hsun Chou, Kenji Watanabe, Takashi Taniguchi, Stephen R. Forrest, and Hui Deng. Van der waals heterostructure polaritons with moire-induced nonlinearity. *Nature*, 591(7848):61–65, 2021. ISSN 0028-0836. doi: 10.1038/s41586-021-03228-5.

Jiaxin Zhao, Rui Su, Antonio Fieramosca, Weijie Zhao, Wei Du, Xue Liu, Carole Diederichs, Daniele Sanvitto, Timothy C. H. Liew, and Qihua Xiong. Ultralow threshold polariton condensate in a monolayer semiconductor microcavity at room temperature. *Nano Letters*, 21(7):3331–3339, 2021. ISSN 1530-6984. doi: 10.1021/acs.nanolett.1c01162.

You Zhou, Jiho Sung, Elise Brutschea, Ilya Esterlis, Yao Wang, Giovanni Scuri, Ryan J. Gelly, Hoseok Heo, Takashi Taniguchi, Kenji Watanabe, Gergely Zarand, Mikhail D. Lukin, Philip Kim, Eugene Demler, and Hongkun Park. Bilayer wigner crystals in a

transition metal dichalcogenide heterostructure. *Nature*, 595(7865):48–52, 2021. ISSN 0028-0836. doi: 10.1038/s41586-021-03560-w.

Xuejun Zhu, P B Littlewood, Mark S Hybertsen, and T M Rice. Exciton Condensate in Semiconductor Quantum Well Structures. *Physical Review Letters*, 74(9):1633–1636, February 1995.

Xuejun Zhu, Mark S Hybertsen, and P B Littlewood. Electron-hole system revisited: A variational quantum Monte Carlo study. *Phys. Rev. B*, 54(19):13575–13580, November 1996.

M W Zwierlein, J R Abo-Shaeer, A Schirotzek, C H Schunck, and W Ketterle. Vortices and superfluidity in a strongly interacting Fermi gas. *Nature*, 435(7045):1047–1051, June 2005.